VNIVERSIDAD NACIONAL AVTNOMA DE MEXICO

UNIVERSIDAD NACIONAL AUTÓNOMA DE MÉXICO

PROGRAMA DE MAESTRÍA Y DOCTORADO EN INGENIERÍA

Comparación de una Simulación Neutrónica / Termohidráulica con Datos Reales de Planta de un Transitorio de Reactividad en un Reactor de Agua en Ebullición

Comparison of a Neutronics / Thermal-Hydraulic Simulation with Real Plant Data from a Reactivity Transient in a Boiling Water Reactor

T E S I S

QUE PARA OPTAR POR EL GRADO DE**:**

MAESTRO EN INGENIERÍA

ENERGÍA – SISTEMAS ENERGÉTICOS

P R E S E N T A :

RODRIGO GUADARRAMA LARA

DIRECTORA:
DRA. CECILIA MARTÍN DEL CAMPO MÁRQUEZ

CO-DIRECTOR:
DR. VÍCTOR HUGO SÁNCHEZ ESPINOZA

2012

JURADO ASIGNADO:

Presidente:	Dr. Juan Luis François Lacouture
Secretario:	Dra. Cecilia Martín del Campo Márquez
Vocal:	Dr. Arturo Guillermo Reinking Cejudo
1er. Suplente:	Dr. Armando Miguel Gómez Torres
2º. Suplente:	M. en C. Gabriel Calleros Micheland

Lugares donde se realizó la tesis:

Universidad Nacional Autónoma de México, Facultad de Ingeniería. Ciudad de México.

Karlsruhe Institute of Technology, Campus Nord. Karlsruhe, Alemania.

DIRECTORA DE TESIS:

DRA. CECILIA MARTÍN DEL CAMPO MÁRQUEZ

_____

FIRMA

Acknowledgments

Thanks to Dr. Victor Sanchez-Espinoza

For giving me the opportunity to go to KIT and letting me be part of this interesting and important project, also for helping me from the very beginning staying in communication and sending the necessary documents for all the paper work; for teaching me, for the time and patience.

Thanks to Dr. Armando Gomez-Torres

For helping me explaining some theory, concepts and with Python programming. For the talks and for telling me many things about Germany.

Thanks to Dr. Wadim Jaeger and Dipl. Eng. Christoph Hartmann

For listening to me, for the file scripts and the advices; for their time and the answers.

Thanks to the National Autonomous University of Mexico

For being my home and embracing me. For all the knowledge, the people, the support and the opportunities.

Thanks to Dr. Cecilia Martin-del-Campo

Who plays an important role in my career. Thanks for believe in me, for all the support and help, for all the pushing, the encouragement, and the relief words.

Thanks to Dr. Ignacio Torres-Alvarado (R.I.P.)

For his kind personality and his unconditional willingness to help.

Thanks to the members of the Jury

For their contribution and advices made on this work.

Thanks to CONACYT

For the support with the *National Program of High Quality Graduate* fellowship number 52978.

Thanks to my mom Irma, my dad Enrique, and my sisters Ana and Monica for their support.

Thanks to the family being there and sending me all their love and blessings.

Specially, thanks to the most important person in my life, Su, for being unconditional, for the long waiting and being amazingly strong, helpful, supportive…*najlepša hvala za vse. Ljubim te zelo močno za vedno moj taman.*

Thank God for the chances, for the life, for the people I have met and the path I have walked.

Resumen

El presente trabajo muestra los resultados obtenidos durante la participación en el marco de los estudios realizados sobre el *Benchmark de Estabilidad de un Reactor de Agua en Ebullición Basado en el Evento Transitorio de Agua de Alimentación en Oskarshamn-2*, el cual es parte de una serie de investigaciones que tienen por objetivo definir, encaminar y resumir los diferentes Benchmarks de la Agencia de Energía Nuclear de la Organización para la Cooperación y el Desarrollo Económico, para el análisis de incertidumbre en los cálculos de mejor estimación de códigos acoplados empleados para el diseño, operación y análisis de seguridad en reactores de agua ligera.

El objetivo principal fue reproducir el evento transitorio ocurrido en la unidad 2 de la planta nuclear Oskarshamn, el cual fue originado por el flujo de refrigerante hacia el reactor a menor temperatura que la establecida en condiciones normales. Esto causó una mayor moderación de neutrones incrementando la potencia del reactor, misma que fue controlada y reducida por la acción automática de las bombas de recirculación. Esta situación se repitió en dos ocasiones, mostrando oscilaciones de potencia dentro del límite permitido. Los operadores del reactor tomaron la decisión de realizar un *scram* parcial introduciendo dos bancos de barras de control, acción que no fue suficiente para mitigar las oscilaciones de potencia que fueron aumentando su amplitud con una razón de decaimiento de oscilación mayor a uno, alcanzando así el límite máximo de potencia permitido, evento que finalizó con la introducción automática de todas la barras de control para apagar el reactor, es decir, un *scram*.

Para la simulación del evento descrito, se usaron los códigos TRACE y PARCS de manera acoplada para realizar las simulaciones de la parte termohidráulica y neutrónica respectivamente. Se realizó una extensión del modelo inicial, el cual define dos ensambles combustibles representados por un solo canal termohidráulico, por lo que se tenían inicialmente 222 canales termohidráulicos representando los 444 ensambles combustibles en el núcleo del reactor. El modelo desarrollado permite un mapeo uno a uno mediante la representación de cada ensamble combustible asociado a un canal termohidráulico, teniendo finalmente 444 canales termohidráulicos en el nuevo modelo.

Los resultados obtenidos muestran buena concordancia con la referencia desde el inicio del evento transitorio hasta la simulación del *scram* parcial. Posteriormente la curva de potencia muestra oscilaciones de menor amplitud comparadas con el comportamiento medido, para dar paso después a oscilaciones que cruzan el límite máximo de potencia permitido lo que debió simular un *scram* y dar fin a estas oscilaciones pero en la simulación no sucedió así. Por ello, deben realizarse análisis futuros más profundos para identificar la razón por la cual no fue posible simular el scram. Sin embargo, el modelo desarrollado permite una mayor precisión en los resultados, requiriendo por consiguiente, de un tiempo de simulación mayor.

Palabras clave: Reactor de agua en ebullición, evento transitorio, temperatura de agua de alimentación, oscilación de potencia.

Abstract

The present work shows the results obtained during the participation on the frame of studies on the *BWR Stability Event Benchmark Based on Oskarshamn-2 1999 Feedwater Transient*, which is part of an investigation series aiming to define, direct and summarize the different Benchmarks of the Nuclear Energy Agency of the Organisation for Economic Co-operation and Development, for uncertainty analysis in best estimate coupled code calculations used for design, operation and safety analysis of Light Water Reactors.

The main goal was to reproduce the transient event on the unit 2 in the Nuclear Power Plant Oskarshamn, which was originated by the low temperature coolant flow into the core. This situation caused a higher neutron moderation increasing the reactor power, which in turn was controlled and reduced by the automatic action of the recirculation pumps. This situation happened again two more times, showing a power oscillation within the permitted limit. The operators decided to perform a partial scram inserting two control rod banks, but it was not enough to mitigate the power oscillations, which increased the amplitude with a decay ratio greater than one, reaching thereby, the maximum power limit allowed, event finalized with the insertion of all the control rods to shut down the reactor, i.e. a scram.

For the simulation of the event described, the codes TRACE and PARCS were used as coupled system to perform the neutronics and thermal-hydraulics calculations, respectively. An extension to the initial model, which considers two fuel assemblies associated to one thermal-hydraulic channel, was made considering a one-to-one mapping in which the total 444 fuel assemblies in the core are coupled to 444 thermal-hydraulic channels.

The results obtained show a good agreement with the reference from the beginning of the transient event until the simulation of the partial scram. Subsequently, the power curve shows oscillations with lower amplitude compared with the measured behavior and incidentally, the oscillations crossed the maximum power limit allowed. However, the expected scram did not happen during the simulation. For this reason, profound analyses are required in the future to identify the cause for which it was not possible to simulate the scram. However, the model developed allows a higher precision in the results, requiring consequently, of more time for the simulation.

Keywords: Boiling water reactor, transient event, feedwater temperature, power oscillation.

List of abbreviations and acronyms

AOO	Anticipated Operational Occurrences
APRM	Average Power Range Monitor
ATWS	Anticipated Transient Without Scram
BOC	Beginning Of Cycle
BWR	Boiling Water Reactor
CMFD	Coarse Mesh Finite Difference
CNTH	Coupled Neutronics / Thermal-Hydraulics
DR	Decay Ratio
ECC	Emergency Core Coolant
FA	Fuel Assembly
GE	General Electric
GenPMAXS	Generation of the Purdue Macroscopic Cross Sections
HTC	Heat Transfer Coefficient
LPRM	Local Power Range Monitor
LWR	Light Water Reactor
MOC	Medium Of Cycle
NEA	Nuclear Energy Agency
NF	Natural Frequency
NK	Neutron-Kinetics
NPP	Nuclear Power Plant
O2	Oskarshamn unit 2
OECD	Organisation for Economic Co-operation and Development
PARCS	Purdue Advanced Reactor Core Simulator
RPV	Reactor Pressure Vessel
SNAP	Symbolic Nuclear Analysis Package
SA	Stand-Alone
SI	Semi-Implicit Method
SETS	Stability Enhanced Two Step Method
SS	Steady-State
TH	Thermal-Hydraulic
TR	Transient
TRACE	TRAC / RELAP Advance Computational Engine
XS	Cross Section

Table of Content

List of Figures

List of Tables

1 Introduction

Nuclear power plants are sophisticated technology and their design, licensing and operation requires profound knowledge of all involved engineering fields like mechanical, electrical, chemical, nuclear, material science, etc. On the other hand, the safe operation of the nuclear power plant is of highest priority to avoid any danger for the operators, the society, the environment, and of the plant itself.

The instability of Boiling Water Reactors (BWR) is one of the most complex phenomena that need an extensive investigation since the root causes for it are not yet fully understood. Instabilities in BWR may happen when the reactor is operated at high power and low mass flow rate conditions. The cause for it can be of thermal-hydraulic nature reinforced by core neutronics via the feedback mechanisms.

BWR instability events can be simulated using best-estimate coupled Neutron-Kinetics (NK) and Thermal-Hydraulics (TH) codes based on three dimensional models of the reactor core.

Instability events have occurred in many BWR plants especially at the beginning of their operation period. The evaluation of these events is very important in order to acquire proper knowledge and understanding about the instability phenomena. In addition, several experimental investigations were performed in some nuclear power plants. Both, the data of the events and that of the experimental investigations, are very important for the validation of the prediction capability of the coupled codes.

1.1 Motivation

There are two important activities in the nuclear energy field that get along due to the sophisticated technology and the safety issues involved, in one hand the needs and the concerns regarding the design of a nuclear power plant, the licensing, operation and other implications that all together result in a complex analysis; on the other hand, it exists the necessity to assess and guarantee the safety of the operators, the society, the environment, and the plant itself.

To perform studies with a high approach to the real systems developing simple theoretical models is not enough for understanding the responses of some real or proposed perturbations in the nuclear reactors.

The efforts of the industry, energy companies, foreign organizations and research institutions are focused in the development of advanced computational tools for simulating reactor system behaviors during real and hypothetical transient scenarios. The lessons learned from simulations using these tools help to form the basis for decision making in regards to plant design, operation procedures, and safety systems.

In one particular case, the stability of a Boiling Water Reactor brings concerns regarding the two-phase flow present in the core. Instabilities may occur when a parameter of the

system changes affecting the operating conditions of the reactor. This situation may cause additional changes and oscillations in other parameters which could increase the amplitude of the initial instability.

Simulations of complex scenarios in Nuclear Power Plants (NPP) have been improved by the utilization of coupled neutron-kinetics and thermal-hydraulics codes. This technique consists in incorporating three dimensional neutron model of the reactor core into system codes to simulate transient events that involve asymmetric core spatial power distribution, local reactivity changes and strong feedback effects between neutronics and thermal-hydraulics.

Therefore, it is very important to acquire proper knowledge and understanding about the instability phenomena through both experimental and computational activities with the aim of simulating and predicting the possible behavior of the reactor under instable conditions and also to verify and validate the capabilities of the codes.

1.2 Objectives of the investigations and tasks to perform

The main objective of the current work was to analyze and to propose improvements to the Exercise 1 in the model studied for the BWR Stability Event Benchmark based on Oskarshamn-2 1999 Feedwater Transient [1] in order to obtain the qualification of the coupled Neutron-Kinetics (NK) and Thermal-Hydraulics (TH) codes PARCS [2] and TRACE [3].

The intention was to reproduce the transient event representing the total of 444 thermal-hydraulic channels involved in the system to simulate the behavior of different parameters, such as reactor power, and to evaluate the impact of a finer model in the results, in order to obtain a more precise calculation and more accurate results that come closer to the reference. Therefore, it will be possible to verify and validate the capabilities of the codes used.

The investigations performed in the frame of the internship at the Institute of Neutron Physics and Reactor Technology (INR) of KIT were focused on the analysis of the Exercise 1 of the international BWR Stability Oskarshamn-2 Benchmark. The instability event to be analyzed is initiated by a feedwater transient occurred in 1999, as described in section 3.2.

The investigations included the following tasks:

- Literature review about BWR analysis methodologies, simulation codes and involved physical phenomena.

- Familiarization with the coupled neutronics/thermal-hydraulics code system PARCS/TRACE as well as the pre and post-processor SNAP [4] and AptPlot [5] programs.

- Review of the Oskarshamn-2 stability benchmark specifications regarding the BWR plant data (geometrical, material, operation conditions) and the exercises to be investigated.

- Systematic preparation of the Oskarshamn-2 plant data for the simulation of the stability events.

- Extension of a simplified TRACE model of the Oskarshamn-2 plant using one CHAN component per fuel assembly.

- Testing of the detailed TRACE model for the stationary plant conditions just before the stability event and comparison with the reference data given in the benchmark.

- Development of a TRACE input model for a coupled TRACE / PARCS simulation.

- Development of a PARCS core model for a one-to-one mapping between the neutronics and the thermal-hydraulics.

- Testing of the coupled TRACE / PARCS plant model performing a steady-state coupled simulation and comparing the predicted parameters with the reference data.

- Simulation of the transient event with the coupling TRACE / PARCS.

- Detailed documentation of the performed work.

2 Literature Review – State of the Art

2.1 Role of Benchmarks for Code Validation

The improvement of the efficiency on nuclear power plants, while keeping high safety standards, is a continuous effort of the nuclear industry. The assessment of the performance and safety characteristics of nuclear power plants is based on numerical simulation tools. The application of coupled codes and recently the development of multi-physics and multi-scale codes (taking advantage of the new computational power) are getting increased attention and gaining importance.

In addition to the improvement of the physical models of the coupled codes such as PARCS/RELAP5 [6], PARCS/TRACE, ATHLET [7]/DYN3D [8], CATHARE [9]/CRONOS2 [10], the validation of these numerical tools is very important. International organizations such as the OECD/NEA have initiated different Benchmarks dedicated to Light Water Reactors (LWRs).

Among the main goals of having international standard benchmark problems, the following can be listed:

- Increase confidence in the use of different tools assessing the safety in nuclear facilities,
- Better understanding of postulated events and NPP behavior,
- Comparison and evaluation of best-estimate code capabilities,
- Improvements, recommendations and guidelines, and
- Enhancement of the code user ability.

Hence, the development of efficient and reliable analysis methodologies and codes to analyze complex problems of LWRs is necessary. Although the use of plant data is the most appropriate for code validation, sometimes it is difficult to obtain due to the scarcity of publicly available data. Experimental data or even a code-to-code comparison in the frame of benchmarks is acceptable.

2.2 Instability in Boiling Water Reactors

The concern about controlling the power in a reactor is closely related to the effects on the reactivity due to changes in the temperature distribution of the different materials present in the core of the reactor. In particular in a BWR, a two-phase flow is present in the core which may lead to unstable behavior under certain conditions, thereby causing periodic oscillations which, in some cases, could present a tendency to very large amplitudes [11].

From a physical point of view, the removal of thermal power by boiling water in the core vertical channels may cause instability in the operation due to density changes and the related thermal-hydraulics mechanisms. In a BWR plant the water cooling is also the moderator, so, an oscillation in the core void content results in a variation of the neutron

flux and in the generated power that, in turn, affects the void, which affects the neutron moderation.

Changes in the reactor power involve changes in fuel and coolant/moderator temperatures, and in the content of voids in the core. If the feedwater temperature decreases, it creates a potential for reduction of the steam volume into the core and a consequent increase in moderation and in fission power.

A reactivity change due to the action of the reactor control system that results in a power level change will cause a temperature and voids change which will then alter the reactivity of the core; similarly the reactivity changes due to temperature and voids take the form of a reactivity feedback effect.

It is a fact that an increment of voids in the core means a reduction in the density of the moderator, and in BWRs the reactivity coefficient of void is negative, consequently there is a negative reactivity feedback; with less moderation of neutrons the reactor power will decrease. The capability of steam to remove heat is lower than the one of the water; consequently there is less heat removing and it causes the fuel temperature to increase but there is a negative feedback on the reactivity because the fuel temperature coefficient of reactivity in BWRs is negative. Then there is a total auto-control feedback mechanism very important in BWRs.

On the other hand, an increase in the fuel temperature will increase the energy of U-238 causing a wider region of resonance for the capture of neutrons despite the reduction of the resonance peak, having as a consequence that neutrons with a wider range of energies may be absorbed by U-238 atoms. This is known as the Doppler Broadening Effect and may lead to decrease the reactivity due to the major capture of neutrons if the fuel temperature increases [12].

Figure 2-1 shows a block map containing the interaction of the neutronics and thermal-hydraulics feedback effects.

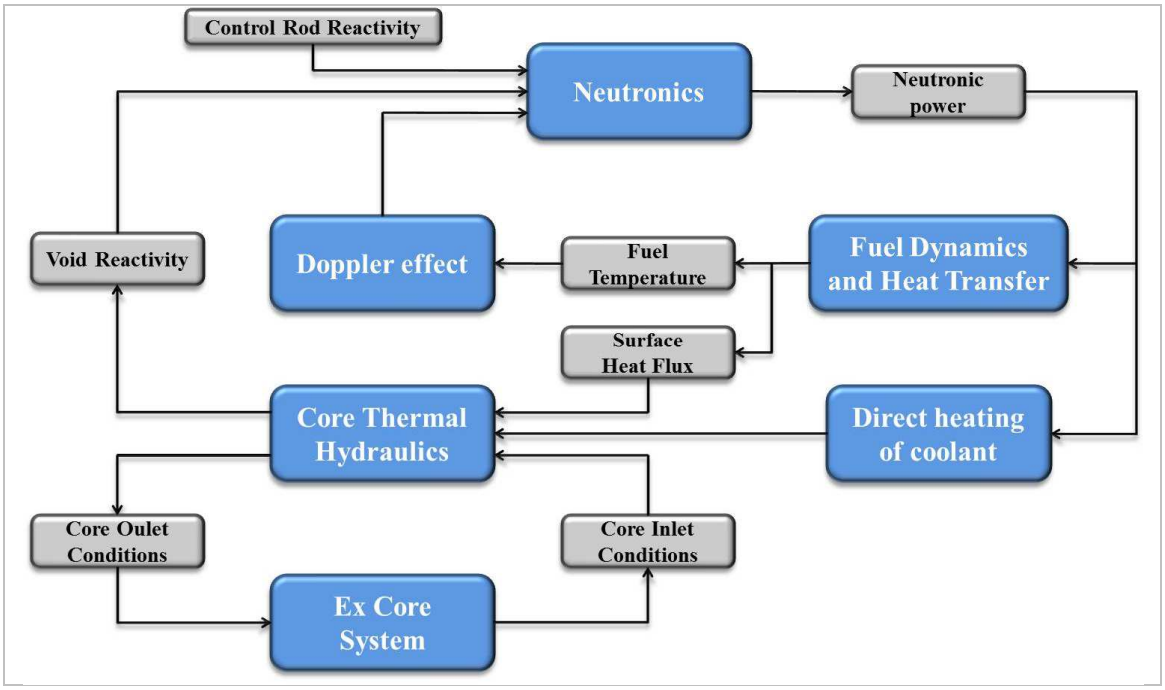

Figure 2-1. Neutronics / Thermal-Hydraulics feedbacks

Another reactivity feedback present in a BWR is described with the following example. If the mass flow rate at the inlet of the core is increased, the void fraction will be reduced. This reduction can be interpreted as a wave moving with the water flow which travels along the channel in few seconds accompanied of a low pressure that is smaller than the total pressure drop in the channel. In this way, the channel pressure drop will be delayed. A decrease in pressure drop increases the channel flow due to the reduction in the resistance for the water to flow in. This brings as a result a feedback loop between inlet flow and pressure drop in the channel, which occurs with a time delay causing oscillations in time. This wave oscillation of density is a thermal-hydraulic phenomenon reinforced by neutronic feedback.

The oscillations are characterized by a decay ratio and a natural frequency. The decay ratio (DR) can be explained as the ratio of two successive peaks in the wave. When the value is greater than one, it means that the wave tends to increase the peak every second leading to a greater instability. The natural frequency is the number of oscillations per second [13].

Two types of instability by reactivity have been characterized [14]:

- In-phase. In this case, the variables such as power, mass flow, and pressure oscillate in phase determining a limit cycle. From the point of view of safety, this type of instability has relatively small relevance, unless it is associated with an Anticipated Transient Without Scram (ATWS).

- Out-of-phase. In this case, the instabilities occur when a neutronic azimuthal mode is excited by thermal-hydraulic mechanisms causing asymmetric power oscillations

at a given time, while half part of the reactor operates at high-mass flow and low-power level, in the other half the opposite situation happens; this behavior must be studied in detail because of safety implications. For large amplitudes, power oscillations may have an undesirable influence on the fuel integrity.

The decay ratio and the natural frequency (NF) of the power oscillations signals are parameters used to evaluate the instabilities. The DR gives a measure of the inherent damping properties of the system. Parametric or non-parametric methods can be used to evaluate the DR. For non-parametric methods, the DR is evaluated from the autocorrelation function (ACF) of the signal. For parametric methods, it is evaluated from the impulse response of the system or from its effective transfer function. For the same time series signal, DR can have significant variation on its result depending on the method selected for its calculation [15].

2.3 Best-estimate Neutron-Kinetics / Thermal-Hydraulics Codes

In the last decades many coupled neutron-kinetics / thermal-hydraulics codes have been developed and validated worldwide. To the most widespread codes are for example: PARCS/RELAP5, CATHARE/CRONOS2, ATHLET/DYN3D, PARCS/TRACE, etc.

In the next subchapters the PARCS and TRACE codes will be described in more detail.

2.3.1 The Neutron-Kinetics Code PARCS

PARCS [2] is a three-dimensional (3D) reactor core simulator which solves the steady-state and time-dependent, multi-group neutron diffusion and SP3 transport equations in orthogonal and non-orthogonal geometries. PARCS is coupled directly to the thermal-hydraulics system code TRACE which provides the temperature and flow field information to PARCS during the transient calculations via the few group cross sections.

The major calculation features in PARCS for predicting the global and local response of the reactor in steady-state and transient conditions include the ability to perform *eigenvalue* calculations, *transient (kinetics)* calculations, *Xenon/Samarium transient* calculations, *decay heat* calculations, *pin power* calculations and *adjoint* calculations for commercial Light Water Reactors. The primary use of PARCS involves a 3D calculation model for the realistic representation of the physical reactor. However, various one-dimensional (1D) modeling features are available in PARCS to support faster simulations for a group of transients in which the dominant variation of the flux is in the axial direction, as for example in several BWR applications.

A card name based input system is employed in PARCS such that the use of default input parameters is maximized while the amount of the input data is minimized. A restart feature is available to continue the transient calculation from the point where the restart file was written.

Advanced numerical solution methods are used in PARCS in order to minimize the computational burden. The solution of the Coarse Mesh Finite Difference (CMFD) linear system is obtained using a Krylov subspace method. The eigenvalue calculation to establish the initial steady-state is performed using the Wielandt eigenvalue shift method. When using the two group nodal methods, a pin power reconstruction method is available in which predefined heterogeneous power form functions are combined with a homogeneous intranodal flux distribution.

For 1D calculations, two modes are available in PARCS: normal 1D and quasistatic 1D. The normal 1D mode uses a 1D geometry and pre-collapsed 1D group constants, while the quasistatic 1D keeps the 3D geometry and cross sections but performs the neutronic calculation in the 1D mode using group constants which are collapsed during the transient. The group constants to be used in PARCS 1D calculation can be generated through a set of 3D PARCS calculations. During the 1D group constant generation, "current conservation" factors are employed in the PARCS 1D calculations to preserve the 3D planar averaged currents in the subsequent 1D calculations.

PARCS is also capable of performing core depletion analysis. Burnup dependent macroscopic cross sections are read from the PMAXS file prepared by the code GenPMAXS, and the PARCS node-wise power is used to calculate the region-wise burnup increment for time advancing the macroscopic cross sections.

2.3.2 The Thermal-Hydraulics Code TRACE

TRACE [3] has been developed to perform best-estimate analyses of Loss of Coolant Accidents (LOCAs), operational transients and other accident scenarios in LWRs. It can also model phenomena occurring in experimental facilities designed to simulate transients in reactor systems. Models used in TRACE include multidimensional two-phase flow, non-equilibrium thermo-dynamics, generalized heat transfer, reflood, level tracking and reactor point kinetics.

TRACE takes a component-based approach to model a reactor system. Each physical piece of equipment in a flow loop can be represented by a hydraulic component type, and each component can be further nodalized into some number of physical volumes or cells over which the fluid, conduction and kinetics equations are averaged. There is no built-in limit for the number of components or volumes that can be modeled; the size of a problem is theoretically only limited by the available computer memory. Some of the hydraulic components in TRACE are PIPEs, CHANs (BWR fuel channels), TEEs, PUMPs, SEPDs (separators), TURBs (turbines), VESSELs, HTSTR (heat structure). FILL and BREAK components are used to apply the desired coolant-flow and pressure boundary conditions, respectively, in the reactor system in order to perform steady-state and transient calculations.

TRACE allows the user to model the power generation in the reactor core in several ways: constant power, power specified from a table, point-reactor kinetics with reactivity feedback, or full 3D transient neutronics calculation when TRACE is coupled to PARCS.

The point kinetics cases can be run with the reactor core at a constant with a user-specified trip power until a user specified trip occurs. The core model defines the local, volumetric heat-generation rate in the heat-conduction equation. The geometry of the heat structure is defined in the HTSTR (for PWR) or CHAN (for BWR) component input. The radial and axial power distributions and total power is defined via the POWER component input, except for BWR applications where the CHAN component includes fuel pin radial power distribution, rod-to-rod power distribution, and CHAN-to-CHAN power distributions. TRACE cannot be used for asymmetric core transients, such as control rod ejection, because it is only capable of point kinetics. In order to take into account the reactivity feedback in which three-dimensional effects are important, it is necessary to couple TRACE with a spatial kinetics code such as PARCS.

The partial differential equations that describe two-phase flow and heat transfer are solved by using finite volume numerical methods. The heat-transfer equations are evaluated by using a semi-implicit time-differencing technique. The fluid-dynamics equations in the spatial one-dimensional (1D) and three-dimensional (3D) components use a multi-step time-differencing procedure that allows the material Courant-limit condition to be exceeded. A more straightforward semi-implicit time-differencing method is also available. The finite-difference equations for hydrodynamic phenomena form a system of coupled, nonlinear equations that are solved by the Newton-Raphson iteration method. The resulting linearized equations are solved by direct matrix inversion. For the 1D network matrix, this is done by a direct full-matrix solver; for the multiple-vessel matrix, this is done by the capacitance-matrix method by means of a direct banded-matrix solver.

The code's computer execution time is highly problem dependent and is a function of the total number of mesh cells, the maximum allowable time step size, and the rate of change of the neutronic and TH phenomena being evaluated.

Some of the main characteristics of TRACE are summarized below.

- ***Multi-Dimensional Fluid Dynamics***

A 3D (x, y, z) Cartesian and/or (r, θ, z) cylindrical geometry flow calculation can be simulated within the reactor vessel or other reactor components where 3D phenomena take place. Flows within a coolant loop are usually modeled in one dimension using PIPE and TEE components.

The combination of 1D and 3D components allows an accurate modeling of complex flow networks as well as local multidimensional flows. This is important in determining emergency core coolant (ECC) downcomer penetration during blowdown, refill and reflood periods of a LOCA.

- ***Non-homogeneous, Non-equilibrium Modeling***

A full two-fluid (six-equation) hydrodynamics model evaluates gas-liquid flow, thereby allowing important phenomena such as countercurrent flow to be simulated explicitly. A

stratified-flow regime has been added to the 1D hydrodynamics; a seventh field equation (mass balance) describes a non-condensable gas field; and an eighth field equation tracks dissolved solute in the liquid field that can plated out on surfaces when solubility in the liquid is exceeded.

- ***Flow-Regime-Dependent Constitutive Equation Package***

The thermal-hydraulic equations describe the transfer of mass, energy, and momentum between the steam-liquid phases and the interaction of these phases with heat flow from the modeled structures. Because these interactions are dependent on the flow topology, a flow-regime dependent constitutive-equation package is used by the code.

- ***Comprehensive Heat Transfer Capability***

TRACE can perform detailed heat-transfer analyses of the vessel and the loop components. Heat transfer from the fuel rods and other structures is calculated by using flow-regime-dependent heat transfer coefficients (HTC) obtained from a generalized boiling curve based on a combination of local conditions and history effects. Inner and/or outer surface convection heat-transfer and tabular or point-reactor kinetics with reactivity feedback volumetric power source can be modeled. 1D or 3D reactor kinetics capabilities are possible through coupling with PARCS.

2.4 Methodology of Analysis

In this work the thermal-hydraulic system code TRACE was used coupled with the 3D neutron-kinetics code PARCS to perform the steady-state and transient simulation. PARCS considers parameters coming from TRACE, like the moderator temperature and density, and fuel temperature, in order to evaluate the appropriate feedback effects in the neutron cross sections. On the other hand, TRACE uses the space-dependent power calculated in PARCS as a heat source and solves the heat conduction in the core heat structures.

The coupling process and mapping between the channels are described in detail in sections 6-3 and 6-4.

One of the objectives of the present work was to create an input file for TRACE with all the 444 channels represented in an individual way and to perform the coupled steady-state and transient calculations with PARCS. The PARCS mapping file presents a symmetric core of 444 channels in total. In order to obtain the one to one representation, a previous available TRACE model was modified, which contained 222 channels, each one grouping two fuel assemblies of the same type, to relate each one of the 444 channels to one unique position in the core.

The geometry of the channels and the physical characteristics remained the same for the both cases with 222 channels and 444 channels.

Previous work in stability analysis was performed in [16], where the application and validation of TRACE and PARCS for BWR stability analysis was described. It is based on the stability test points of Ringhals-1 benchmark [17] and [18].

For Ringhals-1 benchmark, two temporal difference methods were applied to three different mesh sizes in heated channels with series of time step sizes, the Semi-Implicit method (SI) and the Stability Enhanced Two Step (SETS) method. When applying the SI method with adjusted mesh and Courant time step sizes (the largest time step size under the Courant limit), the numerical damping was minimized and the predicted Decay Ratio agrees well with the reference values which were obtained from the measured noise signal. The SI method with adjusted mesh and Courant time step size was then applied to all test points of cycle 14 with three types of initiating perturbations, control rod, pressure perturbation and noise simulation. There was a good agreement between the decay ratios and frequencies predicted by TRACE/PARCS and those from the plant measurements.

The steady-state results showed good agreement with the plant data and were also consistent with SIMULATE-3 solutions.

In [19], a coupling between TRACE and PARCS for the transient event in Oskarshamn-2 was performed. The methodology was based on the 1994 Ringhals-1 event. A half-core symmetric model was defined with 222 channels with 25 axial nodes.

The power level calculated was under predicted from the first pump run-down during the transient. Results were compared with the RAMONA5 [20] code, which showed the same behavior, and it was found that the power level drops more than expected.

The reason found was a time delay in the resistance temperature detector (RTD) response at the moment of measuring the feedwater temperature due to the time required for the heat convection and conduction between the feedwater and the RTD, which is located in a well inside the feedwater pipe. Since the characteristics of the RTD were not available, the proposed solution was to assume that temperature would drop twice faster.

The adjustment in the feedwater temperature boundary condition resulted in an increment of the power matching the APRM data. The results obtained were compared with available data from SIMULATE showing a good agreement with the results for both steady-state and transient calculations.

3 The Oskarshamn-2 Stability Benchmark

As described in [7], the assessment of Coupled Neutronics / Thermal-Hydraulics (CNTH) codes has been enhanced since the middle of '90s by a series of coupled code benchmarks based on operating reactor data, conducted by the Organisation for Economic Co-operation and Development/Nuclear Energy Agency (OECD/NEA), including:

- OECD PWR Main Steam Line Break Benchmark (based on TMI) [21].
- OECD BWR Turbine Trip Benchmark (based on Peach Bottom) [22].
- OECD VVER1000 Coolant Transient Benchmark (based on Kozloduy) [23].

There are two existing OECD/NEA benchmarks related to BWR stability. Both related to linear stability:

- Ringhals-1.

  - Stability tests at the beginning of cycles BOC14, BOC15, BOC16, BOC17, and the medium of cycle MOC16.
  - Both time domain and frequency domain solutions are possible.

- Forsmark-1 and -2.

  - Measured APRM and LPRM data.
  - Analysis of time series data by noise analysis techniques in the time domain.

The previous OECD benchmarks for CNTH codes have confirmed their capability to model and simulate anticipated operational occurrences (AOOs). The primary objective of the benchmark is to establish confidence in extending code applications from its original intended use, AOOs, to more challenging events like unstable power oscillations without scram, when modeling non-linear effects becomes relevant.

Previous BWR stability benchmarks are based on noise measurements of a stable reactor, where a DR less than 1.0 was measured for all conditions and linear models could be used successfully. The BWR stability benchmark considering the transient event in Oskarshamn-2 would be the first benchmark based on measured plant data for a stability event with a DR greater than one, where nonlinear models are required.

The main goal of the Oskarshamn-2 (O2) BWR Stability Benchmark is to provide experimental data, obtained from a real operating BWR, for the validation of the best-estimate coupled codes such as TRACE / PARCS. The BWR O2 is the first benchmark based on measured plant data for a stability event with a DR greater than one. Hence, it is a very challenging type of instability for coupled NK/TH codes due to the following facts:

- Events with both large amplitude nonlinear power oscillations and challenging plant transients including sub-cooling changes at the core entrance and partial control rod insertions;

- Accuracy of the TH solution: numerical methods, model discretization, constitutive relations, flow regime maps;

- Accuracy of the NK solution: coolant temperature and density feedback, neutronics and kinetics data; accuracy of TH / NK coupling, tightly coupled transient, oscillatory conditions with feedback, fast multi-physics and a strongly coupled problem.

In addition, this benchmark will identify code's weaknesses, modelling limitations and provide guidelines for code improvement.

3.1 Scope of the Benchmark

To increase confidence in the different developed codes performance, stability measurements before and after the event are included in the benchmark but these are not part of the evaluation in the current exercise.

The stability benchmark based on Oskarshamn-2 consists of three exercises:

- Feedwater transient (stability event) from 25.02.1999.
- Five stability tests performed on 12.12.1998, 10 weeks before the event.
- Five stability tests performed on 13.03.1999, 3 weeks after the event.

The tests were performed at various flow and power conditions, providing data on DR and NF. Instead of using a control rod or pressure perturbation to excite the oscillations, noise analysis was performed on the power signal.

These tests are important for the validation and verification in order to show that the codes are able to reproduce in a right manner the oscillations intended and then continue with further work to simulate more complicated transient events with confidence.

The exercise selected for the current work is the feedwater transient following the recommendations performing the event with the vessel and core in the model and defining the feedwater flow and temperature as the inlet boundary condition, and the steam line pressure as the outlet boundary condition.

The thermal-hydraulic data to set the boundary conditions, such as feedwater flow, feedwater temperature, steam line pressure and pump speed were provided for the simulation transient event.

3.2 Description of the Exercise 1

3.2.1 Description of the Transient Event

Oskarshamn-2 experienced an instability event on February 25, 1999. A loss of feedwater pre-heaters and control system logic failure resulted in a condition with high feedwater flow and low feedwater temperature without reactor scram. In addition to the initiating event, an interaction of the automatic power and flow control system caused the plant to move into the low flow – high power regime. The combination of these events culminated in diverging power oscillations which triggered an automatic scram at high power. The power evolution for the event is shown in Figure 3-1.

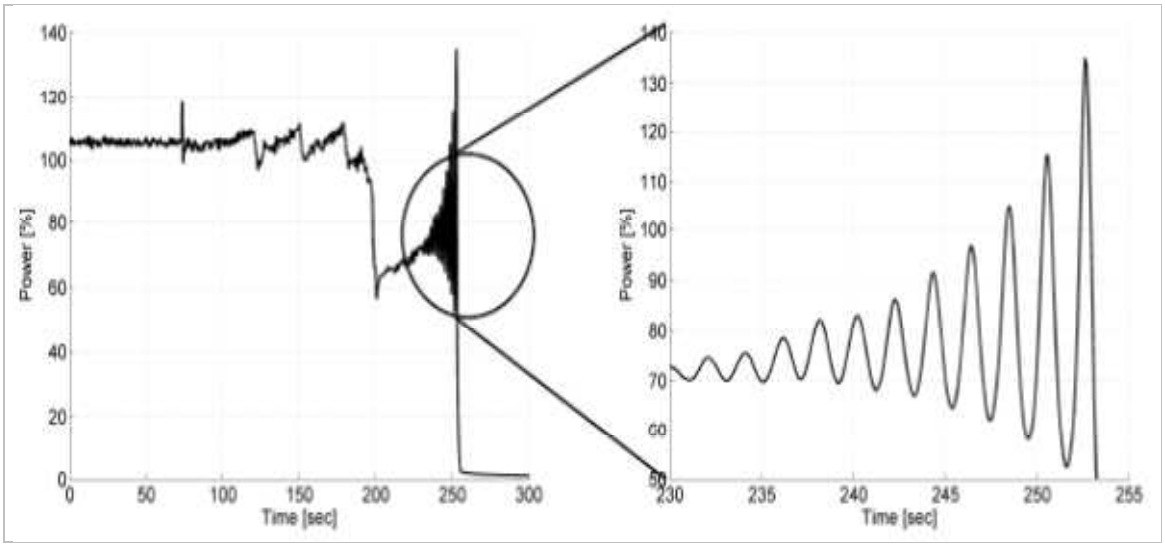

Figure 3-1. Oskarshamn-2, February 25th 1999 Feedwater Transient [1]

On February 25th 1999 the reactor operated at full power and a recirculation flow of 5500 kg/s. Maintenance work was under way; the batteries were in the switchyard. After finishing this task the normal electric supply was restored, during which the power supply to a bus bar was unexpectedly interrupted for 150 ms.

A complex situation occurred in Oskarshamn-2. In principle, there were only two condition indicators that were affected by the voltage drop. One was the indicator "station not connected to the grid", and the other was "station disconnected from the grid". Although these indicators in common language are synonyms, the short voltage drop caused the first indicator to be "true" and the second to be "false". In principle, the "true" indicator controlled the turbine and feedwater operation and the "false" indicator controlled the reactor.

The general situation was as follows: the turbine control system interpreted the situation so that the external grid was lost, two of the five feedwater pre-heaters were bypassed and preparations for supplying "in-house electricity consumption only" were initiated through

control of the turbine valves and the dump valves. In fact the station was still connected to the grid.

The reactor control system did not detect the loss of external grid situation and the reactor continued operating. The output power level of the generator decreased from 625 MWe to 585 MWe and steam line bypass valves opened to allow the excess steam into the main condenser while maintaining full reactor power. Scheduled actions to reduce power, such as main recirculation pump trip and partial scram, were not taken.

The first turbine valve operation caused a peak in the reactor power of short duration after 75 seconds. The reactor control terminated the peak at 117% power and the reactor returned to the allowed operating range. Bypass of the feedwater pre-heaters caused the feedwater temperature to decrease by 75°C. The automatic level control maintained a high feedwater flow to maintain the downcomer level, a fact that probably aggravated the temperature decrease at the core inlet.

Due to the positive reactivity feedback, the reactor responded to the decreasing temperature by increasing the reactor power. A pump controller in charge of the rotation of the recirculation pumps reduced the main recirculation flow when the reactor power increased more than 2% above the nominal power, thereby reducing the power. The controller was activated 45 s after the turbine trip when the power reached 108%, reducing the pump speed at a rate of 640 rpm until the power level decreased below 106%. However, the cold water continued entering into the vessel causing the same behavior described. The reactor reached the E25 limitation at 108% power three times (see Figure 3-2).

In the power-flow map shown in Figure 3-2, the fluctuating line represents the movement of the operational state during the transient. The full lines mark the allowed area. Dotted straight lines indicate operational limits that execute forced reduction in flow and partial scram. Lines marked with “E” indicate forced reduction in flow, while lines marked with “SS” indicate scram or partial scram and forced reduction in flow. The operational state hit the slope of the E4 line with automatic reduction in flow. The reduction in power was, however, not sufficient to move the operational state back within the allowed area.

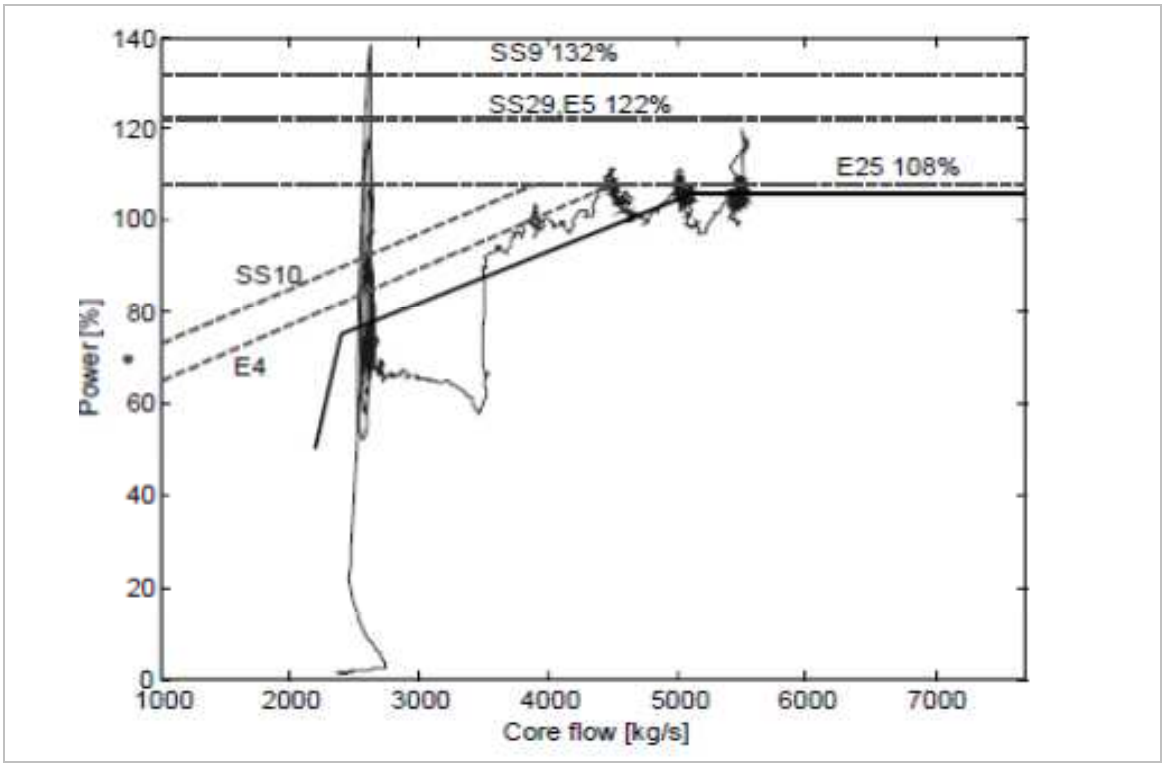

Figure 3-2. Power Flow Map for O2 with operational states during the transient [24]

Approximately 198 s after the event started, the operators initiated manual partial scram and forced reduction of the coolant flow. The operational state was close to the minimum flow of 2500 kg/s and reactor power 65%. The introduction of colder feedwater with a high flow rate continued caused by filtering in the controller. Core instability started with growing amplitude. Automatic scram was initiated at APRM = 132% and coolant flow was at 50%. The instability continued over a period of 20 seconds. The scram lines at lower power were adjusted to act with filtering for the APRM signals and therefore they were not reacting by the fast oscillation. The scram line at 132% was not filtered and finally reacted with scram of the reactor after about 254 s.

As it is shown in Figure 3-2, power oscillations started at APRM = 65% and coolant flow at 2800 kg/s. Many reactor protection lines were passed during the oscillations but they did not react on the fast power oscillations, as they were filtered.

In Figure 3-3 APRM and coolant flow are presented as a function of time. The disturbance recorder saved 300 s with data. The spike in reactor power at 75 s indicates the time at which turbine was informed about loss of grid. Immediately afterwards, power increases and hits the overpower line at 108% (straight line in the figure). Instability begins about 30 s after manual partial scram; the amplitude of oscillation increases rapidly, and scram is initiated when APRM = 132%. This unfiltered scram line is indicated with the upper straight line in the same figure.

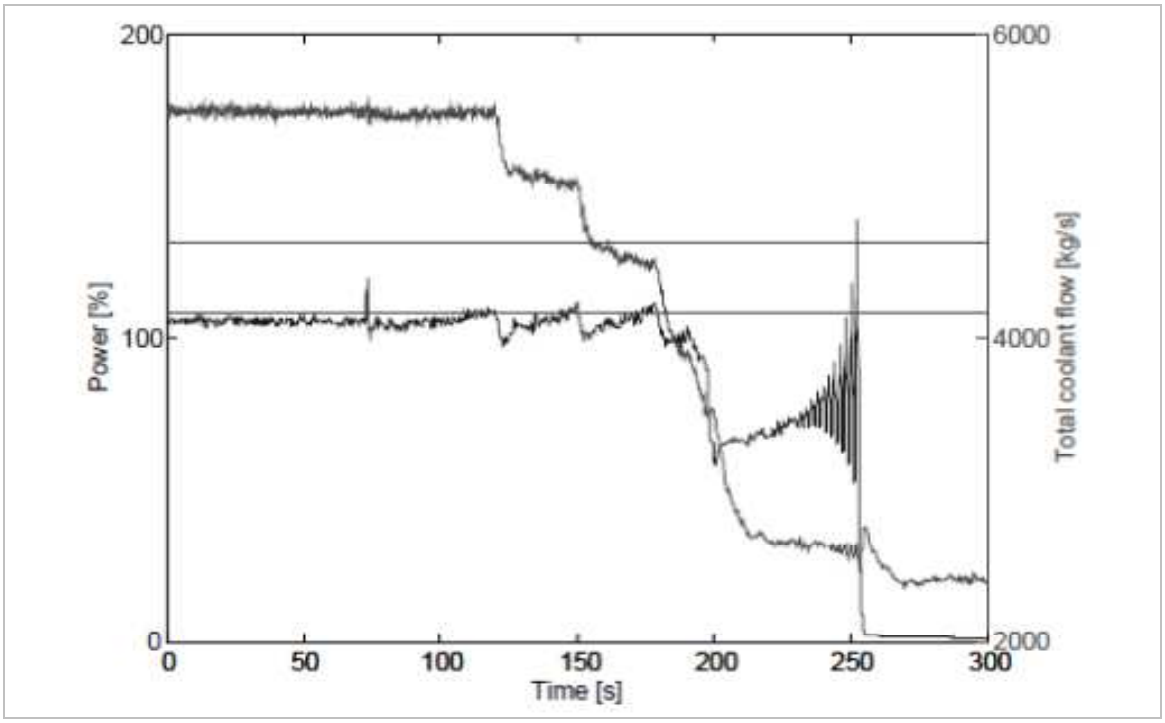

Figure 3-3. Reactor Power and Coolant Flow as function of time during the event [24]

3.2.2 Steady-State Phase

The TRACE input model used in this study was provided by the KIT, more details about it are presented in section 5.6. A standalone execution of the input file was performed in order to get the predicted values obtained by TRACE. There is a specific card in the main data of the input file that specifies that the core heat source is calculated by TRACE which uses a point kinetics model.

The standalone execution is performed only with TRACE. After this step, the steady-state phase is performed using the PARCS and TRACE programs coupled. It was expected to obtain the parameter values under nominal conditions of operation of the plant, before to continue with the simulation of the transient event. This is done in order to assure that the thermal-hydraulic values of the parameters are well simulated just a moment before the transient phase starts. Table 3-1 shows these parameters.

Table 3-1. Main parameters in nominal conditions of operation [27]

Data	Value	Units
Nominal electric output	627	MW
Nominal thermal power	1802	MW
Coolant temperature at inlet to the reactor	274	°C
Coolant temperature at outlet from the reactor	286	°C
Coolant pressure	7	MPa

In 1982, there was a power upgrade in Oskarshamn-2. At the present, the nominal thermal power is 1802 MW, corresponding to about 106% of the initial power of 1700 MW [25].

The core loading pattern in cycle 24 before the transient event is shown in Figure 3-4. The fuel assembly type nomenclature is defined in the benchmark [1] as shown in Table 3-2. The main characteristics for each one of these fuel assemblies are described in section 4.2.

Table 3-2. Fuel assembly types defined in the benchmark document

Label	Type
SO, SP, SQ, SR, SS	1
QA, QC	2
QB, QD	3
QE, LT	4

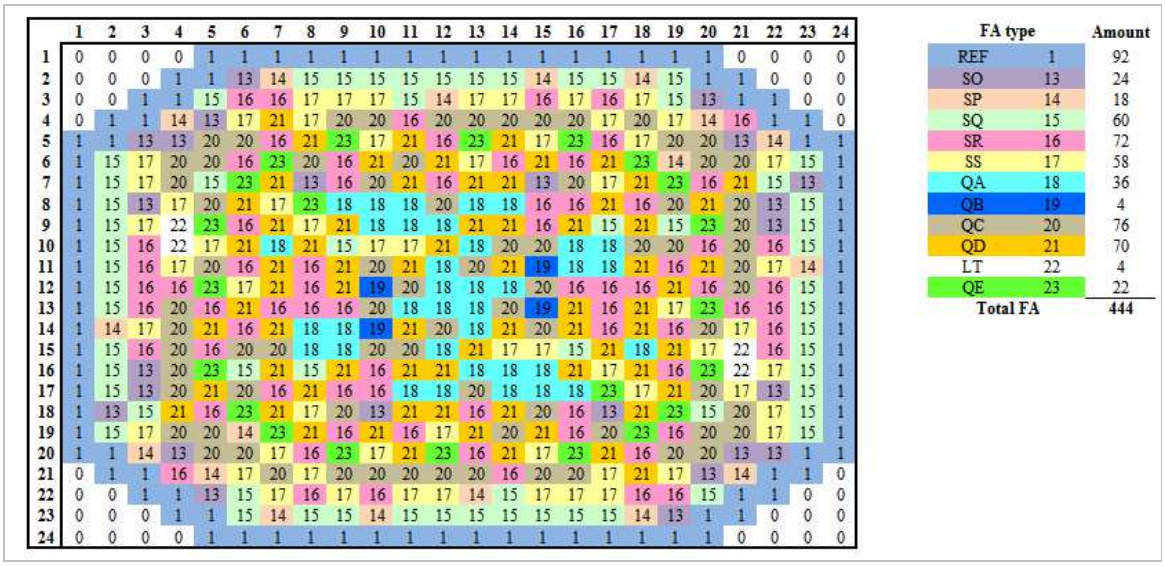

Figure 3-4. Core loading pattern of Oskarshamn-2 before the transient (cycle 24)

3.2.3 Transient Phase

The real plant data provided to define the boundary conditions in the input file for the simulation of the transient event are described and shown in this section.

According to a previous work reported in [17] and [26], the recommendations were applied in the current work regarding the adjustment in the feedwater temperature boundary condition. The reason found was that it exists a delay time in the resistance temperature detector (RTD) response at the moment of measuring the feedwater temperature, due to the time required for convection and conduction between the feedwater and the RTD, which is located in a well inside the feedwater pipe. Since the characteristics of the RTD were not available, the proposed solution was to assume that temperature would drop twice faster.

In this way, the boundary conditions defined in the TRACE input file for transient calculation were set in arrays for each parameter in the corresponding control blocks which are defined in section 5.2. The parameters that define the boundary conditions were obtained from real data measured in the plant, and are shown in Figure 3-5. The behavior of these signals corresponds to the previous explanation in the description of the event. The automatic reduction in the pump speed by the control system due to the increasing in the power; the steam dome pressure is a parameter that we want to evaluate and for this reason was not limited; the oscillation in the feedwater flow and the reduction in the feedwater temperature.

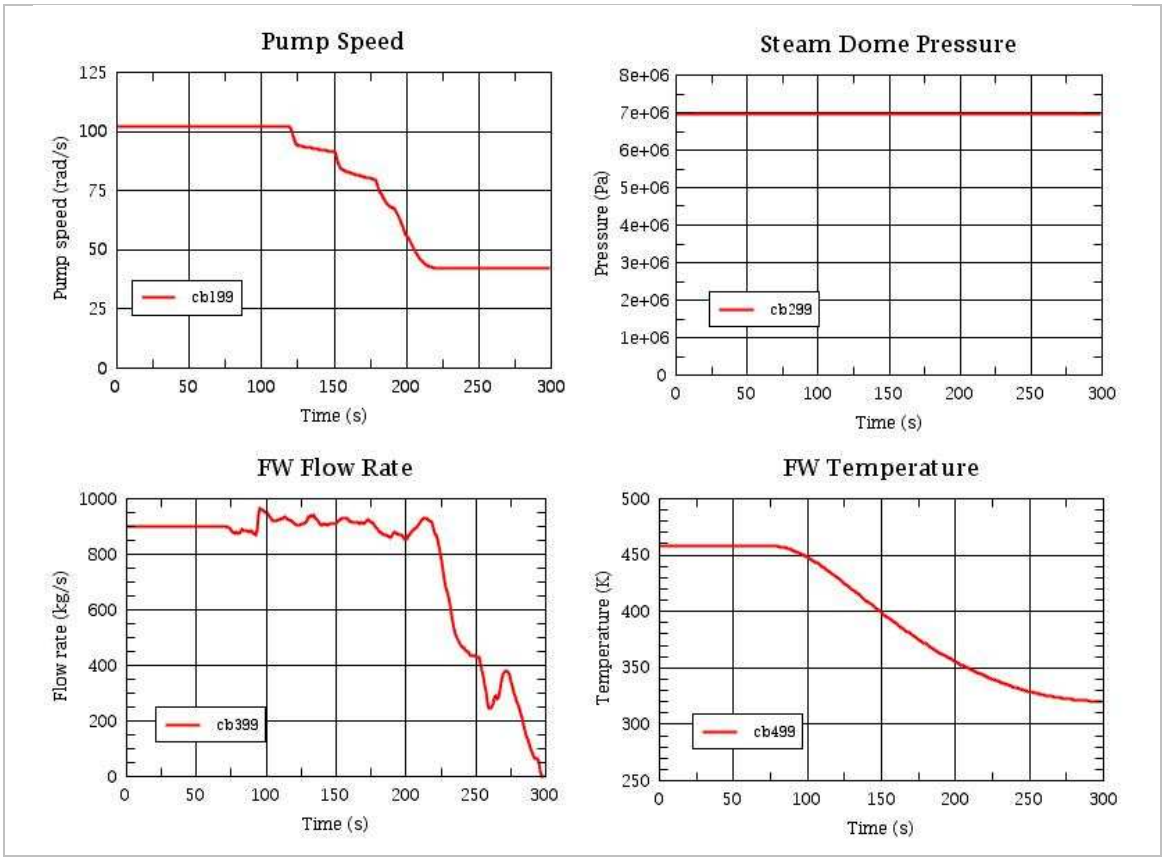

Figure 3-5. Boundary conditions set for the transient simulation

4 Description of the Oskarshamn-2 Power Plant

4.1 Plant Description

The information presented in this chapter corresponds to the data contained in the benchmark.

Oskarshamn-2 Nuclear Power Plant is a Boling Water Reactor of second generation (BWR/2) designed by ABB-Atom, with 4 external primary recirculation pumps and containment similar to GE Mark II.

The nominal circulation flow at full reactor power (106%) ranges from 5300 to 7700 kg/s. For lower flow rates, the allowable reactor power is reduced. The minimum allowed flow is 2500 kg/s; the maximum allowed recirculation flow is further limited at low reactor power due to the risk of pump cavitation.

The reactor pressure vessel is represented in Figure 4-1. The material of the vessel is alloy-treated steel/stainless steel lined. The diameter is 5.2 m, the height 20 m and the wall thickness is 0.134 m.

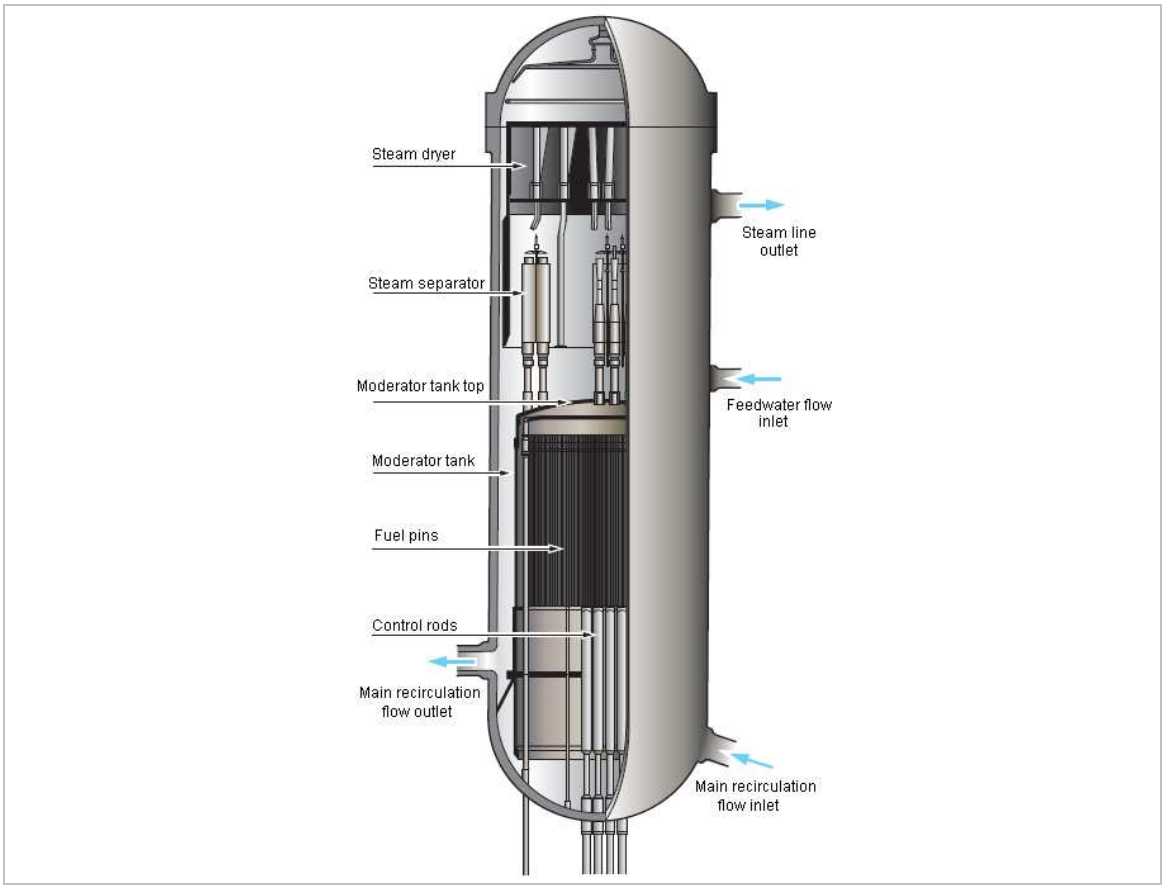

Figure 4-1. Oskarshamn-2 Reactor Pressure Vessel [1]

The standard data of the plant, including the safety systems and containment, are shown in Table 4-1 and 4-2.

Table 4-1. Technical standard data of the NPP O2 [27]

Data	Units	Value
Nominal electrical output	MW	627
Nominal thermal power	MW	1802
Dome pressure	MPa	7
Control rod type		B4C, cruciform blades
Secondary shutdown systems		Electric control rod insertion. Boron acid injection
Number of primary circuit loops and pumps		4
Nominal flow rate of the pumps	kg/s	7700
Nominal speed of the pumps	rpm	1400
Primary coolant flow rate	kg/s	7700 (maximum)
Steam pressure at turbine inlet	MPa	6.75
Steam temperature at turbine inlet	°C	283
Steam flow rate at turbine inlet	kg/s	900

Table 4-2. Safety systems [27]

Data	Units	Value
Type of safety related feedwater systems		Ordinary feedwater system, motor driven Auxiliary feedwater system, motor driven
Number of safety related feedwater systems		2
Capacity of safety related feedwater systems		2x100%
Number of low pressure core spray (LPCS)		1
Mass flow rate of the LPCS	kg/s	2x170
Operating pressure of LPCS	MPa	1.9 (start of injection with 0.1 MPa in wetwell)
Number and type of back-up generators on site		2 diesel generators
Number and capacity of primary system relief valves	kg/s	13 x 74.7 at 8.7 MPa 8 x 68.7 + 2 x 28.4 at 8.0 MPa

4.2 Description of the Core

The core is composed by 444 bundles and 109 cruciform control rod blades. The active length of the core is 3.712 m and the equivalent diameter is 3.672 m. The thermal power is 1802 MW and the electrical power 627 MW. Figure 4-2 shows the radial distribution of the four different types of fuel assemblies in the core. The surrounding zone in blue colour corresponds to the reflector.

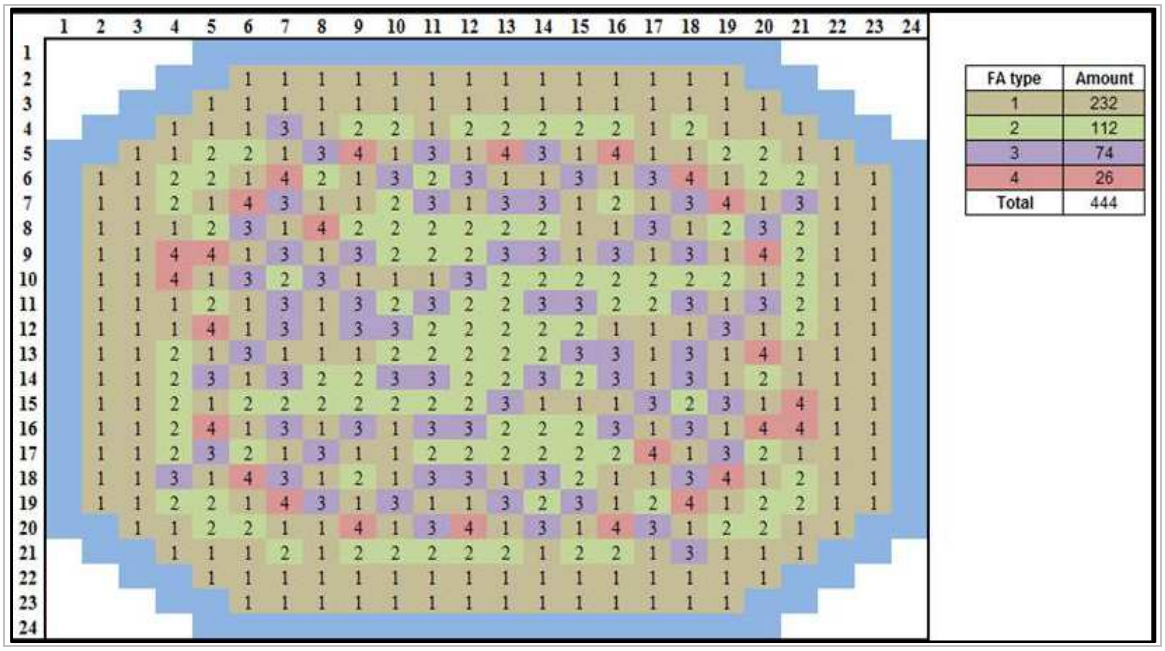

Figure 4-2. Radial distribution of the four fuel assembly types in the core

The coolant and moderator is light water, the fuel material composition is UO_2, the volume of coolant is 219 m^3, and the volume of water of the primary system is 374 m^3. The mass flow rate at nominal power is 5500 kg/s and the temperatures at the inlet and outlet of the core are 547 K and 559 K, respectively. Fuel type 4 contains 8 partial rods in the assembly of length 2.0945 m. Table 4-3 summarizes the fuel assembly types in the core. The data for the pins in each fuel assembly type are shown in Table 4-4.

Table 4-3. Fuel assembly geometry of the four types in the core [1]

	Type 1	Type 2 and 3	Type 4
Number of assemblies	232	186	22+4
Total length, m	4.3326	4.3326	4.3326
Lower inactive length, m	0.2391	0.2391	0.2391
Active length, m	3.712	3.712	3.712
Upper inactive length, m	0.3815	0.3815	0.3815
Number of spacer grids	6	6	6
Pins arrangement	8x8	9x9	10x10
Total fuel rods	64	72	91
Water rods	No	1	1

Table 4-4. PIN data of the four fuel assembly types [1]

	Type 1	Type 2 and 3	Type 4
Pellet diameter, m	0.010440	0.009500	0.008670
Pellet radius, m	0.005220	0.004750	0.004335
Gap width, m	0.000105	0.000170	0.000170
Cladding inner diameter, m	0.010650	0.009670	0.008840
Cladding outer diameter, m	0.012250	0.011000	0.010050
Zr-2 thickness, m	0.0008	0.000665	0.000605

For fuel type 2 and 3, the water rods are the same; the inner diameter and thickness are, 0.03840 m and 7.048E-04 m respectively. For fuel type 4 the corresponding values are 0.03489 m and 7.030E-04 m.

A radial visualization of the different fuel assembly types is shown in Figure 4-3 including the space for the water rod. Fuel assembly type number 1 does not have water rod.

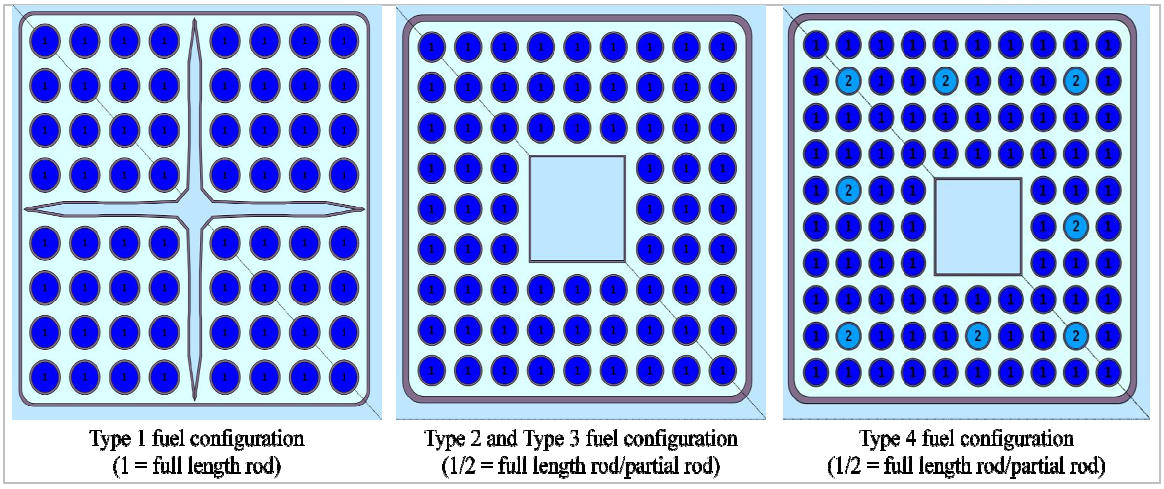

Figure 4-3. Radial PIN configuration of the different fuel assembly types [1]

5 Description of the Initial Plant Model

First of all an initial model of the O2 plant consisting of a TRACE and PARCS input was analyzed to get familiar with the modelling approach of TRACE/PARCS. The running of the TRACE input in standalone mode was performed in order to evaluate the initial model and to obtain the predicted parameters to compare them with the reference values in the benchmark. Hereafter this model will be described.

5.1 The Initial TRACE Model of the Oskarshamn-2 Power Plant

5.1.1 Components Description

The model consists of the following TRACE components to describe the O2 plant.

- Reactor pressure vessel. Represented by a VESSEL component. This is the only component which can be represented in three dimensions, defining different annular sections inside called rings, azimuthal positions in every plane of the chosen nodalization, and axial positions along the total height.

- Reactor core. Represented by 222 CHAN components, every component contains two fuel assemblies (FA) in the reference model.

- Separators. Represented by a SEPD component. In the model only one component appears physically but it represents the total 90 separators.

- External recirculation loop. Modelled by the following components:

  - Piping system. Represented by PIPE component. The corresponding pipe for the suction is nodalized in 4 cells and represents 4 pipes of length of 8.425 m. The flow area remains the same for every cell. The pipe at the outlet of the pump is also nodalized in 4 cells maintaining the flow area for each one, although the volumes and lengths for each cell are different. This pipe represents 4 pipes of 8.2825 m of length.

  - Recirculation pump. Represented by a PUMP component. The total nominal mass flow rate is defined constant in only one pump in the model to represent the four external pumps in the plant.

- Feedwater system. Modelled by the following components:

  - FILL component. Used to apply the desired coolant flow boundary conditions to perform steady-state and transient calculations.

- PIPE component. The feedwater pipe is represented by 4 pipes in total of 3 meters each. It is nodalized in 3 uniform cells.

- Steam line system. Modelled by the following components:

  - VALVE component. Used to represent the valves in the steam line.

  - PIPE component. This pipe represents the 4 pipes and is only one cell of 12.2 m.

  - BREAK component. This component is used to define the pressure boundary condition.

Figure 5-1, taken from SNAP, shows all the components involved in the model for the simulation. The boundary conditions values were set according to the recommendations given in the benchmark. In the transient input file, the feedwater flow and temperature are used as the inlet boundary condition and the steam line pressure as the outlet boundary condition as it can be seen in the figure.

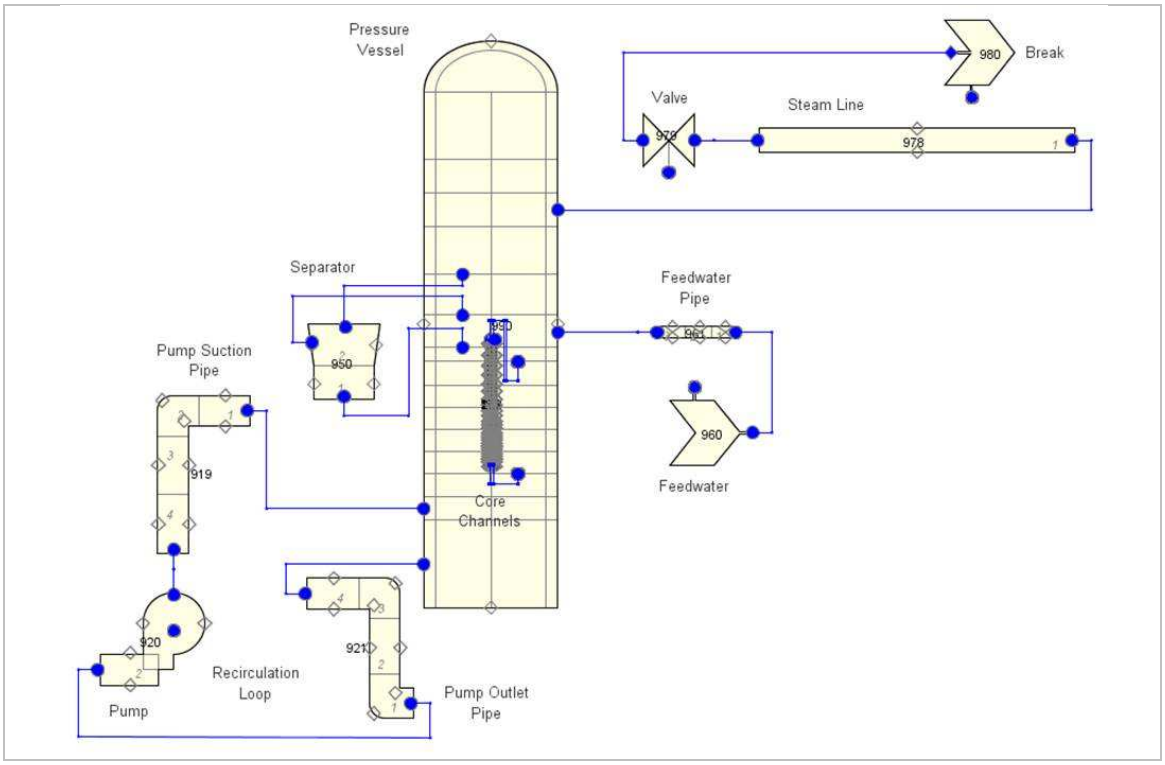

Figure 5-1. General view of the model components in TRACE

Since only one pump is included in the components view, the flow rate represents the total flow of the 4 external pumps and is defined in a control block as a constant. In the case of the separator, only one appears in the view but a total of 90 is actually modeled.

5.1.2 Power Component

A power component is included and described in the input file. It is available as a mean for delivering energy to the fluid via the heat structures or hydraulic component walls. HTSTR (heat structure) components modeling fuel elements or heated walls in the reactor system are available to compute two-dimensional conduction and surface-convection heat transfer in Cartesian or cylindrical geometries.

5.2 Control Systems

Control blocks are included in the model; they represent predefined mathematical functions and logic switches defined by the user that operate with zero or more input parameters, which are defined by means of signal variables and outputs from other control blocks. The user can string them together to model plant systems, such as control systems, or to calculate quantities not normally available from the code (and which in turn may be used to control component behavior), such as pressure drops across multiple components, liquid mass in one or more cells, etc.

Signal variables are predefined parameters, such as time, pressure, coolant levels, etc., that the code calculates and that the user can select as independent variables for tables, trips, and control blocks. With the signal variables and the control blocks, the user can define the necessary independent variables for the tables. The rate-factor table is a means to vary the rate of change of the independent variable of a component-action table, i.e., the rate-factor table provides a multiplier to the independent variable of a table that alters its magnitude before the code performs the table lookup.

There is a long list of control blocks in the corresponding section in the input file. For practical reasons, Table 5-1 contains only the function operations and the inputs for each one of the main control blocks. The boundary conditions data were set in control blocks in the input file for the transient simulation.

Observing the Figure 5-2, the Pump Controller consists of seven control blocks. The control block with identifier 199, sets the current pump speed. It also includes a signal variable named “Pump flow rate”. In Table 5-1, the first row describes briefly Figure 5-2. The block receives four input signals and performs a sum of these. The hydro input comes directly from the component number 920, which is the recirculation pump modeled.

The other rows in Table 5-1 describe the elements included in the Control View of the TRACE input model.

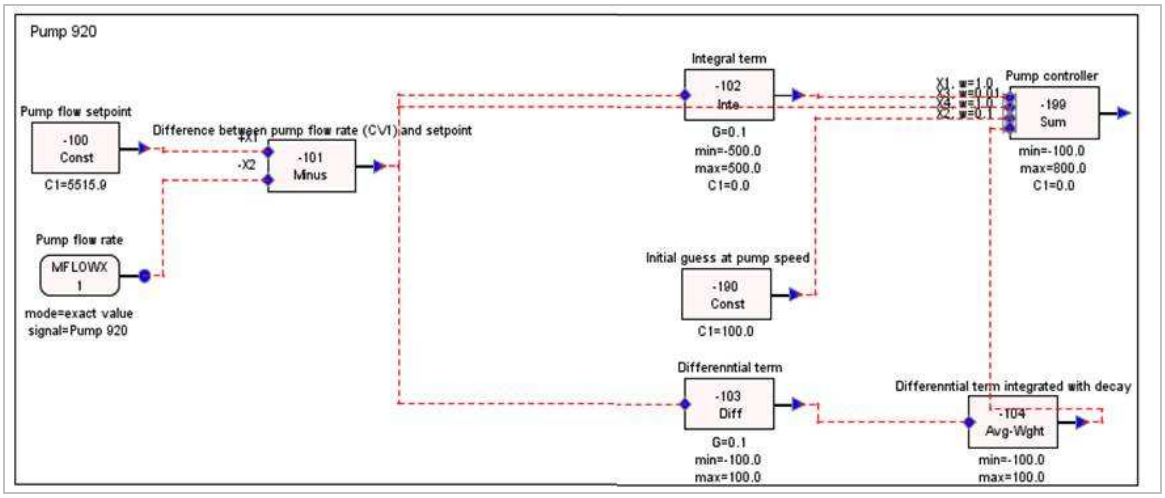

Figure 5-2. Pump speed controller defined in TRACE input model

Table 5-1. Input signals to the control blocks

Block	Input type	Value
Pump Controller	Input 1	Integrate -102 (Integral term)
Type: SUM	Input 2	Avg. Exponential Weight -104 (Differential term integrated with decay)
Control Block ID: 199	Input 3	Subtract -101 (Difference between pump flow rate and setpoint)
	Input 4	Constant -190 (Initial guess at pump speed)
	Hydro Input	Pump 920 (Recirculation Pump)
Pressure Controller	Input 1	Sum -201 (Difference between steam dome pressure and setpoint)
Type: SUM	Input 2	Integrate -202 (Integral term)
Control Block ID: 299	Input 3	Avg. Exponential Weight -204 (Differential term integrated with decay)
	Input 4	Constant -290 (Initial guess at turbine inlet pressure)
	Hydro Input	Break 980 (Turbine Break)
Water level / feedwater controller	Input 1	Integrate -302 (Integral term)
Type: SUM	Input 2	Avg. Exponential Weight -304 (Differential term integrated with decay)
Control Block ID: 399	Input 3	Sum -301 (Difference between water level and setpoint)
	Input 4	Avg. Exponential Weight -309 (Initial guess for feedwater flow rate)
	Hydro Input	Fill 960 (Feedwater Supply)
Subcooling controller	Input 1	Sum -401 (Difference between core inlet temperature and setpoint)
Type: SUM	Input 2	Integrate -402 (Integral term)
Control Block ID: 499	Input 3	Avg. Exponential Weight -404 (Differential term integrated with decay)
	Input 4	Constant -490 (Initial guess at feedwater temperature)
	Input 5	Sum -399 (Water level / feedwater controller)
	Hydro Input	Fill 960 (Feedwater Supply)

5.3 Core Model

The available input model of TRACE groups 2 FA per thermal-hydraulic channel, in this manner the total number of channels defined in the model is 222, which are listed by ID number in Table A-1 in Annex A. This model was named *Case A.*

There are in general 4 different types of fuel assemblies defined in TRACE model, SVEA 64 (8x8), KWU (9x9), ATRIUM (10x10) and GE 12 (10x10). It must be noticed that for type SVEA 64 there are three different sub-types in the model, SVEA 64 Peripheral, SVEA 64 Semi-Peripheral and SVEA 64 Central, which share most of the physical characteristics, the difference is in the inlet orifice loss factor, which for SVEA 64 Peripheral is 81.229, for SVEA 64 Semi-Peripheral is 55.096, and for SVEA 64 Central is 34.812.

Similar situation is with KWU type, which has two sub-types KWU 9x9-9A and KWU 9x9-9B, both with same FA dimensions but a difference can be seen in the position of the spacers and their respective loss coefficients.

The definition of one channel in the TRACE input file, for example ATRIUM, implies that this channel represents two fuel assemblies with the characteristics defined for the ATRIUM fuel assembly. Table 5-2 shows the total number of channels per FA type.

Table 5-2. Total number of channels defined in TRACE input file

Type	Amount
SVEA 64 Peripheral	34
SVEA 64 Semi-Peripheral	32
SVEA 64 Central	50
KWU 9x9-9A	56
KWU 9x9-9B	37
ATRIUM	11
GE 12	2
Total	222

Table 5-3 contains the geometric data of each fuel assembly type. Table 5-4 includes data of the water rods in the fuel assemblies.

The material composition of the fuel rods in all the different FA types is UO_2. The lengths of the zones in the channel are consistent for the different FA types in the model; total length of 4.36 m, active length of 3.712 m (equal in benchmark), lower and upper inactive length of 0.231 and 0.417, respectively.

Table 5-3. Geometry data of the fuel assemblies in TRACE model

	ABB	SIEMENS	AREVA	GE
	SVEA 64	KWU 9x9-9A/B	ATRIUM 10	GE 12
Number of assemblies	232	186	22	4
Outer Face-to Face distance, m	0.13960	0.13860	0.13860	0.13736
Inner Face-to-Face-distance, m	0.13740	0.13400	0.13400	0.13406
Inside perimeter of canister wall, m	0.5496	0.536	0.536	0.53624
Canister thickness, m	0.00110	0.00230	0.00230	0.00165
Pins arrangement	8x8	9x9	10x10	10x10
Number of pins	64	81	100	100
Total fuel rods	64	72	91	92
Number of partial rods	NA	NA	8	14

Table 5-4. Water rods data of the fuel assemblies in TRACE model

	Water rods			
	ABB	SIEMENS	AREVA	GE
	SVEA 64	KWU 9x9-9A/B	ATRIUM 10	GE 12
Water rods	no	1 (square)	1	2
Diameter, m		0.037046	0.034422	0.024900
Thickness, m		7.20E-04	7.20E-04	7.50E-04
Inlet Forward Loss		277.00	310.40	125.10
Outlet Forward Loss		153.00	80.40	2.65
Inlet Reverse Loss		277.00	310.40	125.10
Outlet Reverse Loss		153.00	80.40	2.65

The information about the respective spacer loss coefficients was taken directly from the TRACE model and is shown in Table 5-5. This data is important for evaluating the drop pressure in the channels and the effect in the flow rate, combination that could be the cause of power oscillations in the reactor.

The radial configuration of the PINs in each FA type in TRACE is shown in Figure 5-3. The FA containing partial rods and/or water rods are identified in a different color which corresponds to a number group having specific characteristics and data for the rod.

Table 5-5. Loss coefficients for fuel assemblies in TRACE model

SVEA 64		
Spacer #	Position, m	Loss Coeff
1	0.7486	0.598
2	1.3180	0.598
3	2.0221	0.598
4	2.5227	0.598
5	3.1566	0.598
6	3.5306	0.598

ATRIUM 10		
Spacer #	Position, m	Loss Coeff
1	0.8158	0.834
2	1.3180	0.834
3	2.0221	0.834
4	2.5227	0.834
5	3.1566	0.681
6	3.5306	0.681

KWU 9x9-9A		
Spacer #	Position, m	Loss Coeff
1	0.8158	0.877
2	1.3180	0.877
3	2.0221	0.877
4	2.5227	0.877
5	3.1566	0.877
6	3.5306	0.877

GE 12		
Spacer #	Position, m	Loss Coeff
1	0.6222	1.1
2	0.9778	1.1
3	1.3180	1.1
4	1.8131	1.1
5	2.2575	1.1
6	2.5227	1.1
7	3.1566	0.607
8	3.5306	0.607

KWU 9x9-9B		
Spacer #	Position, m	Loss Coeff
1	0.8158	0.812
2	1.3180	0.812
3	2.0221	0.812
4	2.5227	0.812
5	3.1566	0.812
6	3.5306	0.812

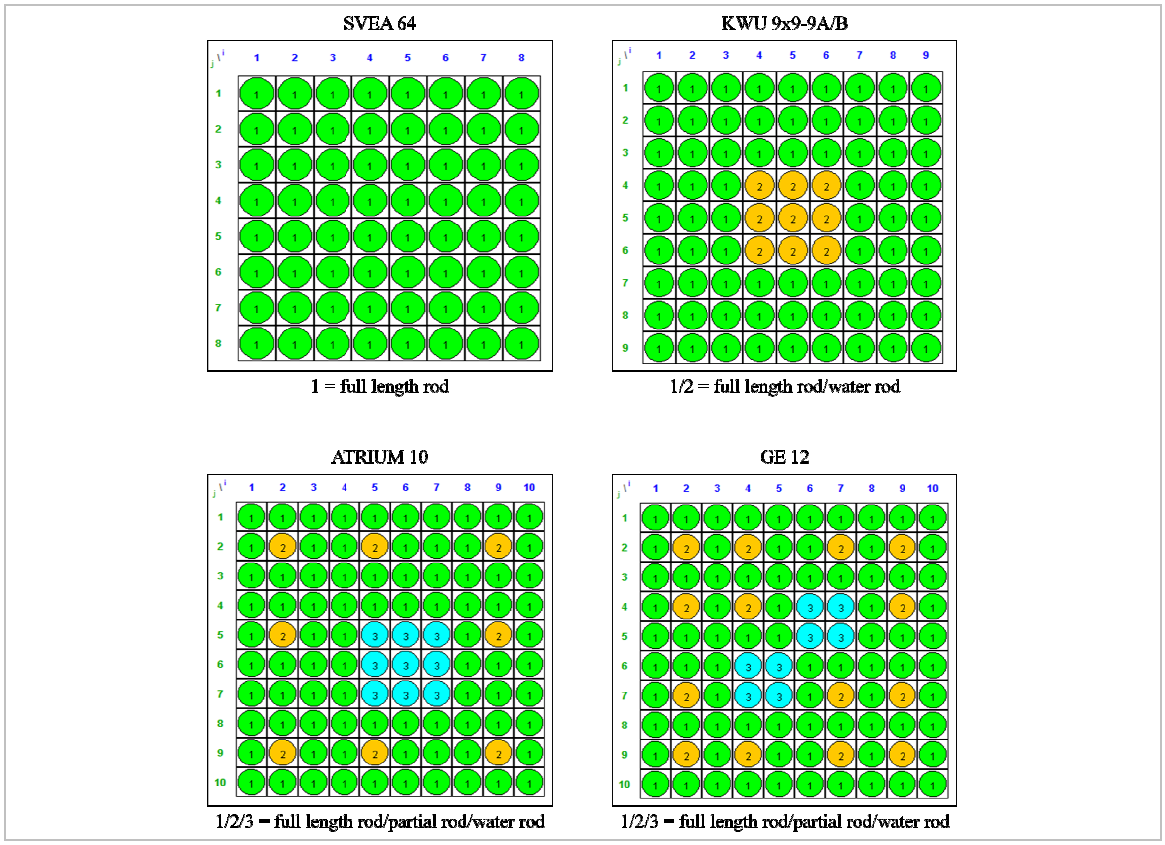

Figure 5-3. Radial configuration of the different fuel assembly types in TRACE model

5.4 Fuel PIN Nodalization

There are 3 radial regions defined in the fuel rods; the pellet, the gap and the material of the cladding. The Figure 5-4 shows these regions identifying fuel region with number 1 (composed by 5 equidistant nodes), two nodes for cladding with number 2, and one node for the gap with number 3. The corresponding data for each fuel rod in each fuel assembly type in the TRACE model is shown in Table 5-6.

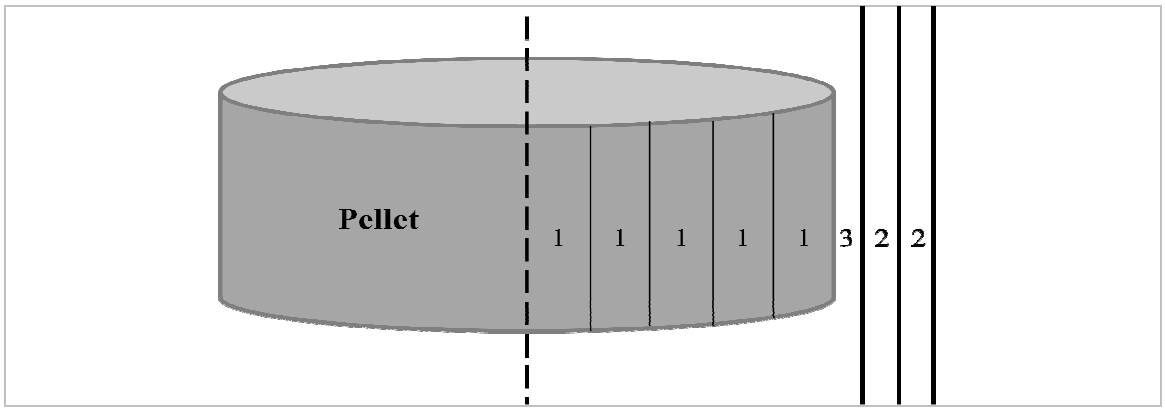

Figure 5-4. Radial nodes in fuel rods in TRACE model

Table 5-6. PIN data of the fuel assemblies in TRACE model

	PIN data			
	ABB	SIEMENS	AREVA	GE
	SVEA 64	KWU 9x9-9A/B	ATRIUM 10	GE 12
Pellet diameter, m	0.010440	0.009500	0.008670	0.008814
Pellet radius, m	0.005220	0.004750	0.004335	0.004407
Gap width, m	0.000105	0.000085	0.000085	0.000089
Cladding inner diameter, m	0.010545	0.009585	0.008755	0.008903
Cladding outer diameter, m	0.012145	0.010915	0.009965	0.010173
Zr-2 thickness, m	0.000800	0.000665	0.000605	0.000635
Pitch to diameter ratio	1.289800	1.218180	1.288560	1.261940

5.5 Nodalization of the Reactor Pressure Vessel

The vessel dimensions and nodalization are shown in Figure 5-5. The RPV is divided in 2 radial rings, 15 axial levels and 1 azimuthal sector. The core height is 4.36 m from axial level 4 to 8. The downcomer (DC) is located in ring 2 and its height is 6.668 m from axial level 2 to level 9. The core height is 3.712 m and the total volume is 38.455 m^3.

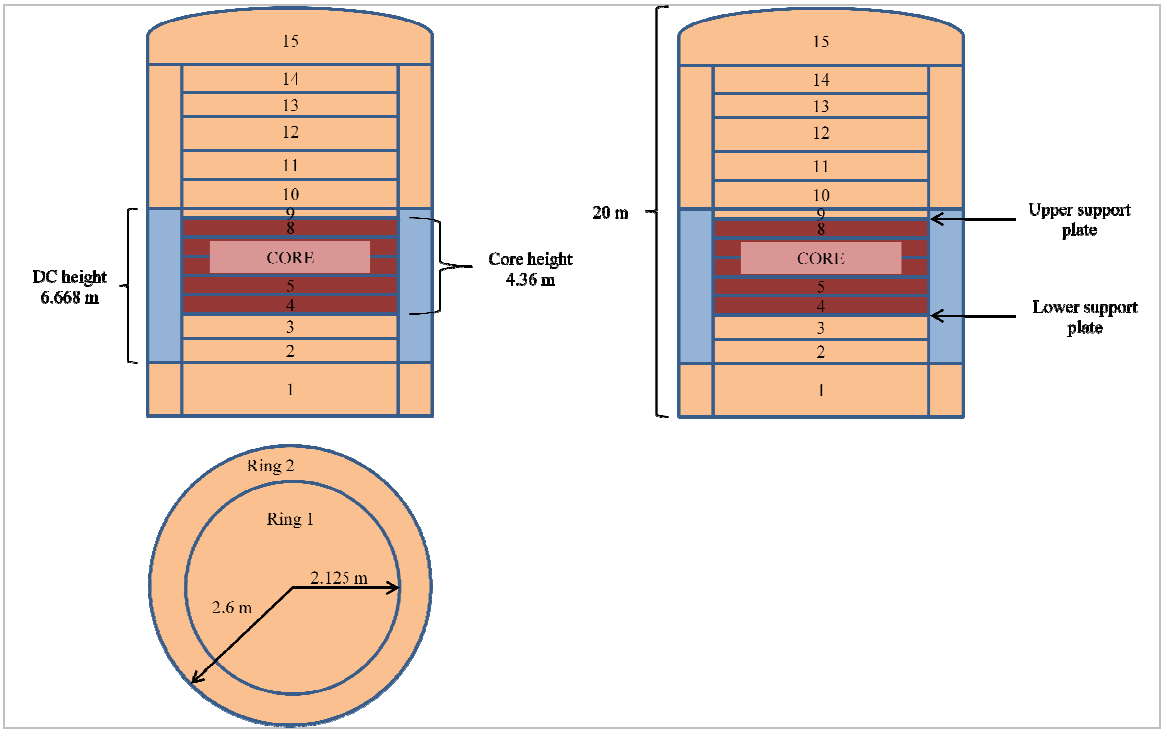

Figure 5-5. Reactor Pressure Vessel dimensions in TRACE model

5.6 Steady-State Simulation with TRACE

To do a coupled steady-state simulation with TRACE/PARCS, first of all a standalone TRACE simulation needs to be performed to verify the convergence of the parameters set in TRACE and validate the correct reproduction of these parameters for normal conditions.

A standalone simulation was performed with the TRACE version 5.0p2 using the initial TRACE model. Then, after convergence of the parameters, a steady-state simulation was performed with the same version. In Table 5-7 a comparison of the Oskarshamn-2 Benchmark data with the TRACE predictions is given.

Table 5-7. Comparison of the operating conditions at steady-state

	Benchmark data [1]	TRACE model SS	Relative deviation %
Reactor Power (MW)	1802	1802	0
Enthalpy Balance (MW)	1799.7	1798.99	0.03946659
Steam Dome Pressure (MPa)	7	7	0
Core Inlet Pressure (MPa)	7.1162	7.119	-0.039331367
Core Outlet Pressure (MPa)	7.0141	7.0132	0.012832944
Core Pressure Drop (kPa)	102	105.8077	-3.598698393
Core Average Void	0.42	0.40117	4.693770721
Feedwater Temperature (K)	456.62	456.62	0
Core Inlet Temperature (K)	543.57	543.85	-0.051484784
Inlet Subcooling (K)	16.59	16.304	1.754170756
Steam Temperature (K)	558.48	558.59	-0.01969244
Pump Speed (rad/s)	94.38	94.377	0.003178741
Total Core Flow Rate (kg/s)	5515.9	5515.9245	-0.000444169
Active Core Flow Rate (kg/s)	4800.4	4883.22	-1.696012058
Steam Flow Rate (kg/s)	903.1	900.77	0.258667584
Downcomer Water Level (m)	8.4	8.397	0.035727045

Observing the values in Table 5-7, in general terms, the deviation in the parameters of the TRACE model is not major, this represents a confidence in the parameter values set in the TRACE input file and a good agreement with the data defined in the reference.

Since the final specifications document of the benchmark is not yet issued, it is important to point out that some of the information included in the benchmark [1] served as reference. This data was only used to compare the parameters in the available input model of TRACE,

which was configured with some differences, such as the inlet orifice loss coefficients as showed in Table 5-8 or the nomenclature to identify the fuel assembly types in the core, as shown later in Figure 6-6.

Table 5-8. Inlet orifice loss coefficients comparison

Benchmark	Inlet orifice loss coefficient
Type 1	36.9
Type 1	58.4
Type 1	86.1
Type 2	45.94
Type 3	45.94
Type 4	45.94

TRACE model	Inlet orifice loss coefficient
SVEA 64 Central	34.812
SVEA 64 Semi-peripheral	55.096
SVEA 64 Peripheral	81.229
KWU 9x9-9A and KWU 9x9-9B	41.907
ATRIUM	40.858
GE	35.563

6 Extension of the Initial TRACE Model

6.1 TRACE Model with 444 Channels

In the previous study [19], a core model consisting of 222 CHAN components representing the core was developed. This previous model was extended in the frame of the current work. The O2 stability event will be simulated with both the coarser (*Case A*: 222 CHANs) and the finer (*Case B*: 444 CHANs) TRACE models and the results will be compared to each other to see the influence of the number of thermal-hydraulic channels on global and local parameters, and in the impact on the simulation of the transient.

To develop the finer model, the TRACE coarse model was extended; therefore, additional 222 CHANs, starting from the numbering 223 to 444, were added in the original TRACE model. In addition the other model parameters had to be changed respectively such as junctions, number of components, respective connections of the new CHANs with the VESSEL component. Table 6-1 shows the key thermal-hydraulic parameters for each CHAN component which were derived from the geometrical data of each fuel assembly type; these data were set in the input deck of TRACE.

Table 6-1. Derived thermal-hydraulic parameters

	ABB	SIEMENS	AREVA	GE
	SVEA 64	KWU 9x9-9A/B	ATRIUM 10	GE 12
PIN Heat transfer area, m²	0.141630	0.127286	0.116208	0.11863
FA Heat transfer area, m²	9.064322	9.164612	10.574906	10.91427
Core Heat transfer area, m²	2102.92274	1704.61780	232.64794	43.65708
FA coolant flow area, m²	0.009713	0.009551	0.009431	0.00989
Core flow area, m²	2.253416	1.776486	0.207473	0.03959
FA ideal flow area, m²	0.018879	0.017956	0.017956	0.01797
Area of all pins in FA, m²	0.007414	0.007579	0.007799	0.00812
Wetted perimeter, m	2.991497	3.313529	3.666597	3.73218
Heated perimeter, m	2.441897	2.468915	2.848843	2.94026
Hydraulic diameter, m	0.011140	0.012110	0.010700	0.14776
Lower tie plate loss coefficient*	6	2.51	2.87	4.79
Upper tie plate loss coefficient*	1.18	0.35	0.15	0.74
Heated diameter, m	0.015911	0.015474	0.013241	0.013465

* Reference area 100 cm²

Since the number of CHANs is very large, a Python Script was used to generate the input deck of the 222 additional CHANs. The script requires a file *.dat* which contains the

parameters to be read including the headers to identify each one of these parameters. Data of each fuel assembly type is provided to generate an output file containing the list of the additional 222 channels but defining the consecutive ID number for each one, i.e., from ID channel 223 to 444, as well as the respective identification numbers for the junctions to the vessel and to the water rods (only in case that the fuel assembly contains water rod).

For example, to create the full description of the new channel ATRIUM with the ID 348, the parameters to change are set in one file; these parameters are ID number *num*, the lower junction number to the first cell of the channel *jun1*, the junction number in the upper cell of the channel *jun2*, the water rod inlet junction *junlk*, the water rod outlet junction *junlk*, and the number of channels represented by the CHAN component *nchans*. In this way, the values will be set as follows:

- num = 348,
- jun1 = 1348,
- jun2 = 2348,
- junlk = 3348,
- junlk = 4348, and
- nchans = 1.

The remaining data like the geometry of the channel, number of cells, height, volume, flow area, etc. remain constant since the script will copy all the data that is not defined in the parameter file and is not necessary to change.

6.2 PARCS Model of the Core

In PARCS the core is represented in a Cartesian geometry, where each fuel assembly is a computational node. In total 444 fuel assembly nodes are contained in the model and 92 reflector nodes.

The input file in PARCS requires different data. In the control block the total number of control rod banks and their respective initial positions are defined, as well as the name of the external file *MAPTAB* to be read.

The core contains 109 boron carbide absorber elements (B_4C in a steel cladding) distributed within the core, see Figure 6-1. In the PARCS model, the 109 cruciform control elements are grouped in 19 groups (banks). The positions of the control elements just before the transient event are shown in Figure 6-2, where bank 18 and bank 19 are 23% and 98% withdrawn, respectively. All the other banks are totally out (100%). Bank number 5 is marked in color gray.

In PARCS input file, the partial scram is performed inserting bank 5 and 18 at simulation time 197.6 seconds (s) in position 1.72% withdrawn. The insertion is finished at simulation time 201 s. The partial scram is defined to be initiated at core power 120%, there is no delay time in the signal and the rod insertion time is 1.3 s.

	1	2	3	4	5	6	7	8	9	10	11	12	13	14	15	16	17	18	19	20	21	22	23	24
1					0	0	0	0	0	0	0	0	0	0	0	0	0	0	0	0				
2				0	0	13	13	14	14	17	17	10	10	11	11	14	14	15	15	0	0			
3			0	0	0	13	13	14	14	17	17	10	10	11	11	14	14	15	15	0	0	0		
4		0	0	1	1	2	2	7	7	8	8	5	5	6	6	3	3	4	4	9	9	0	0	
5	0	0	0	1	1	2	2	7	7	8	8	5	5	6	6	3	3	4	4	9	9	0	0	0
6	0	11	11	12	12	15	15	16	16	9	9	12	12	13	13	16	16	17	17	12	12	11	11	0
7	0	11	11	12	12	15	15	16	16	9	9	12	12	13	13	16	16	17	17	12	12	11	11	0
8	0	8	8	5	5	6	6	3	3	4	4	1	1	2	2	7	7	8	8	5	5	6	6	0
9	0	8	8	5	5	6	6	3	3	4	4	1	1	2	2	7	7	8	8	5	5	6	6	0
10	0	9	9	14	14	13	13	10	10	17	17	14	14	11	11	19	19	15	15	14	14	13	13	0
11	0	9	9	14	14	13	13	10	10	17	17	14	14	11	11	19	19	15	15	14	14	13	13	0
12	0	4	4	1	1	2	2	7	7	8	8	18	18	6	6	3	3	4	4	1	1	2	2	0
13	0	4	4	1	1	2	2	7	7	8	8	18	18	6	6	3	3	4	4	1	1	2	2	0
14	0	15	15	16	16	11	11	19	19	15	15	16	16	9	9	12	12	17	17	16	16	11	11	0
15	0	15	15	16	16	11	11	19	19	15	15	16	16	9	9	12	12	17	17	16	16	11	11	0
16	0	8	8	5	5	6	6	3	3	4	4	1	1	2	2	7	7	8	8	5	5	6	6	0
17	0	8	8	5	5	6	6	3	3	4	4	1	1	2	2	7	7	8	8	5	5	6	6	0
18	0	9	9	10	10	17	17	14	14	13	13	10	10	11	11	14	14	13	13	10	10	9	9	0
19	0	9	9	10	10	17	17	14	14	13	13	10	10	11	11	14	14	13	13	10	10	9	9	0
20	0	0	0	1	1	2	2	7	7	8	8	5	5	6	6	3	3	4	4	1	1	0	0	0
21		0	0	1	1	2	2	7	7	8	8	5	5	6	6	3	3	4	4	1	1	0	0	
22			0	0	0	15	15	16	16	9	9	12	12	17	17	16	16	15	15	0	0	0		
23				0	0	15	15	16	16	9	9	12	12	17	17	16	16	15	15	0	0			
24					0	0	0	0	0	0	0	0	0	0	0	0	0	0	0	0				

Figure 6-1. Control Rod Banks in the Core

	1	2	3	4	5	6	7	8	9	10	11	12	13	14	15	16	17	18	19	20	21	22	23	24
1					Re	Re	Re	Re	Re	Re	Re	Re	Re	Re	Re	Re	Re	Re	Re	Re				
2				Re	Re	---	---	---	---	---	---	---	---	---	---	---	---	---	---	Re	Re			
3			Re	Re	---	---	---	---	---	---	---	---	---	---	---	---	---	---	---	---	Re	Re		
4		Re	Re	---	---	---	---	---	---	---	---	---	---	---	---	---	---	---	---	---	---	Re	Re	
5	Re	Re	---	---	---	---	---	---	---	---	---	---	---	---	---	---	---	---	---	---	---	---	Re	Re
6	Re	---	---	---	---	---	---	---	---	---	---	---	---	---	---	---	---	---	---	---	---	---	---	Re
7	Re	---	---	---	---	---	---	---	---	---	---	---	---	---	---	---	---	---	---	---	---	---	---	Re
8	Re	---	---	---	---	---	---	---	---	---	---	---	---	---	---	---	---	---	---	---	---	---	---	Re
9	Re	---	---	---	---	---	---	---	---	---	---	---	---	---	---	---	---	---	---	---	---	---	---	Re
10	Re	---	---	---	---	---	---	---	---	---	---	---	---	---	---	98	98	---	---	---	---	---	---	Re
11	Re	---	---	---	---	---	---	---	---	---	---	---	---	---	---	98	98	---	---	---	---	---	---	Re
12	Re	---	---	---	---	---	---	---	---	---	---	23	23	---	---	---	---	---	---	---	---	---	---	Re
13	Re	---	---	---	---	---	---	---	---	---	---	23	23	---	---	---	---	---	---	---	---	---	---	Re
14	Re	---	---	---	---	---	---	98	98	---	---	---	---	---	---	---	---	---	---	---	---	---	---	Re
15	Re	---	---	---	---	---	---	98	98	---	---	---	---	---	---	---	---	---	---	---	---	---	---	Re
16	Re	---	---	---	---	---	---	---	---	---	---	---	---	---	---	---	---	---	---	---	---	---	---	Re
17	Re	---	---	---	---	---	---	---	---	---	---	---	---	---	---	---	---	---	---	---	---	---	---	Re
18	Re	---	---	---	---	---	---	---	---	---	---	---	---	---	---	---	---	---	---	---	---	---	---	Re
19	Re	---	---	---	---	---	---	---	---	---	---	---	---	---	---	---	---	---	---	---	---	---	---	Re
20	Re	Re	---	---	---	---	---	---	---	---	---	---	---	---	---	---	---	---	---	---	---	---	Re	Re
21		Re	Re	---	---	---	---	---	---	---	---	---	---	---	---	---	---	---	---	---	---	Re	Re	
22			Re	Re	---	---	---	---	---	---	---	---	---	---	---	---	---	---	---	---	Re	Re		
23				Re	Re	---	---	---	---	---	---	---	---	---	---	---	---	---	---	Re	Re			
24					Re	Re	Re	Re	Re	Re	Re	Re	Re	Re	Re	Re	Re	Re	Re	Re				

Figure 6-2. Control Rod Banks in % withdrawn before the transient event

In the *MAPTAB*, which is read by PARCS, the radial configuration for *Case A* is defined as shown in Figure 6-3. It can be seen the symmetrical radial distribution. The numbers in each position correspond to the ID of each channel in TRACE input. Each number from 1 to 222 appears two times due to the fact that each channel in TRACE groups two fuel assemblies as described before.

The changes made in the corresponding radial configuration for *Case B* are shown in Figure 6-4, where each position is occupied by one of the 444 fuel assemblies in TRACE keeping the ½ diagonal symmetry in the core.

0	1	2	3	4	5	6	7	8	9	10	11	12	13	14	15	16	17	18	19	20	21	22	23	24
1	*	*	*	*	0	0	0	0	0	0	0	0	0	0	0	0	0	0	0	0	*	*	*	*
2	*	*	*	0	0	1	2	3	4	5	6	7	8	9	10	11	12	13	14	0	0	*	*	*
3	*	*	0	0	15	16	17	18	19	20	21	22	23	24	25	26	27	28	29	30	0	0	*	*
4	*	0	0	31	32	33	34	35	36	37	38	39	40	41	42	43	44	45	46	47	48	0	0	*
5	0	0	49	50	51	52	53	54	55	56	57	58	59	60	61	62	63	64	65	66	67	68	0	0
6	0	69	70	71	72	73	74	75	76	77	78	79	80	81	82	83	84	85	86	87	88	89	90	0
7	0	91	92	93	94	95	96	97	98	99	100	101	102	103	104	105	106	107	108	109	110	111	112	0
8	0	113	114	115	116	117	118	119	120	121	122	123	124	125	126	127	128	129	130	131	132	133	134	0
9	0	135	136	137	138	139	140	141	142	143	144	145	146	147	148	149	150	151	152	153	154	155	156	0
10	0	157	158	159	160	161	162	163	164	165	166	167	168	169	170	171	172	173	174	175	176	177	178	0
11	0	179	180	181	182	183	184	185	186	187	188	189	190	191	192	193	194	195	196	197	198	199	200	0
12	0	201	202	203	204	205	206	207	208	209	210	211	212	213	214	215	216	217	218	219	220	221	222	0
13	0	222	221	220	219	218	217	216	215	214	213	212	211	210	209	208	207	206	205	204	203	202	201	0
14	0	200	199	198	197	196	195	194	193	192	191	190	189	188	187	186	185	184	183	182	181	180	179	0
15	0	178	177	176	175	174	173	172	171	170	169	168	167	166	165	164	163	162	161	160	159	158	157	0
16	0	156	155	154	153	152	151	150	149	148	147	146	145	144	143	142	141	140	139	138	137	136	135	0
17	0	134	133	132	131	130	129	128	127	126	125	124	123	122	121	120	119	118	117	116	115	114	113	0
18	0	112	111	110	109	108	107	106	105	104	103	102	101	100	99	98	97	96	95	94	93	92	91	0
19	0	90	89	88	87	86	85	84	83	82	81	80	79	78	77	76	75	74	73	72	71	70	69	0
20	0	0	68	67	66	65	64	63	62	61	60	59	58	57	56	55	54	53	52	51	50	49	0	0
21	*	0	0	48	47	46	45	44	43	42	41	40	39	38	37	36	35	34	33	32	31	0	0	*
22	*	*	0	0	30	29	28	27	26	25	24	23	22	21	20	19	18	17	16	15	0	0	*	*
23	*	*	*	0	0	14	13	12	11	10	9	8	7	6	5	4	3	2	1	0	0	*	*	*
24	*	*	*	*	0	0	0	0	0	0	0	0	0	0	0	0	0	0	0	0	*	*	*	*

Figure 6-3. Radial configuration in *MAPTAB* file for Case A

0	1	2	3	4	5	6	7	8	9	10	11	12	13	14	15	16	17	18	19	20	21	22	23	24
1	*	*	*	*	0	0	0	0	0	0	0	0	0	0	0	0	0	0	0	0	*	*	*	*
2	*	*	*	0	0	1	2	3	4	5	6	7	8	9	10	11	12	13	14	0	0	*	*	*
3	*	*	0	0	15	16	17	18	19	20	21	22	23	24	25	26	27	28	29	30	0	0	*	*
4	*	0	0	31	32	33	34	35	36	37	38	39	40	41	42	43	44	45	46	47	48	0	0	*
5	0	0	49	50	51	52	53	54	55	56	57	58	59	60	61	62	63	64	65	66	67	68	0	0
6	0	69	70	71	72	73	74	75	76	77	78	79	80	81	82	83	84	85	86	87	88	89	90	0
7	0	91	92	93	94	95	96	97	98	99	100	101	102	103	104	105	106	107	108	109	110	111	112	0
8	0	113	114	115	116	117	118	119	120	121	122	123	124	125	126	127	128	129	130	131	132	133	134	0
9	0	135	136	137	138	139	140	141	142	143	144	145	146	147	148	149	150	151	152	153	154	155	156	0
10	0	157	158	159	160	161	162	163	164	165	166	167	168	169	170	171	172	173	174	175	176	177	178	0
11	0	179	180	181	182	183	184	185	186	187	188	189	190	191	192	193	194	195	196	197	198	199	200	0
12	0	201	202	203	204	205	206	207	208	209	210	211	212	213	214	215	216	217	218	219	220	221	222	0
13	0	444	443	442	441	440	439	438	437	436	435	434	433	432	431	430	429	428	427	426	425	424	423	0
14	0	422	421	420	419	418	417	416	415	414	413	412	411	410	409	408	407	406	405	404	403	402	401	0
15	0	400	399	398	397	396	395	394	393	392	391	390	389	388	387	386	385	384	383	382	381	380	379	0
16	0	378	377	376	375	374	373	372	371	370	369	368	367	366	365	364	363	362	361	360	359	358	357	0
17	0	356	355	354	353	352	351	350	349	348	347	346	345	344	343	342	341	340	339	338	337	336	335	0
18	0	334	333	332	331	330	329	328	327	326	325	324	323	322	321	320	319	318	317	316	315	314	313	0
19	0	312	311	310	309	308	307	306	305	304	303	302	301	300	299	298	297	296	295	294	293	292	291	0
20	0	0	290	289	288	287	286	285	284	283	282	281	280	279	278	277	276	275	274	273	272	271	0	0
21	*	0	0	270	269	268	267	266	265	264	263	262	261	260	259	258	257	256	255	254	253	0	0	*
22	*	*	0	0	252	251	250	249	248	247	246	245	244	243	242	241	240	239	238	237	0	0	*	*
23	*	*	*	0	0	236	235	234	233	232	231	230	229	228	227	226	225	224	223	0	0	*	*	*
24	*	*	*	*	0	0	0	0	0	0	0	0	0	0	0	0	0	0	0	0	*	*	*	*

Figure 6-4. Radial configuration in *MAPTAB* file for Case B

In the geometry block within PARCS input, it is defined the *geometry* file to be read. This file contains information about the geometry measures for the fuel assembly to perform the mapping to the channels in TRACE. This geometry was used in both *Case A* and *B*. These data are shown with the graphical representation of the axial levels in Figure 6-5. The bottom and upper reflector, in blue colour, have the same measures for the nodalization.

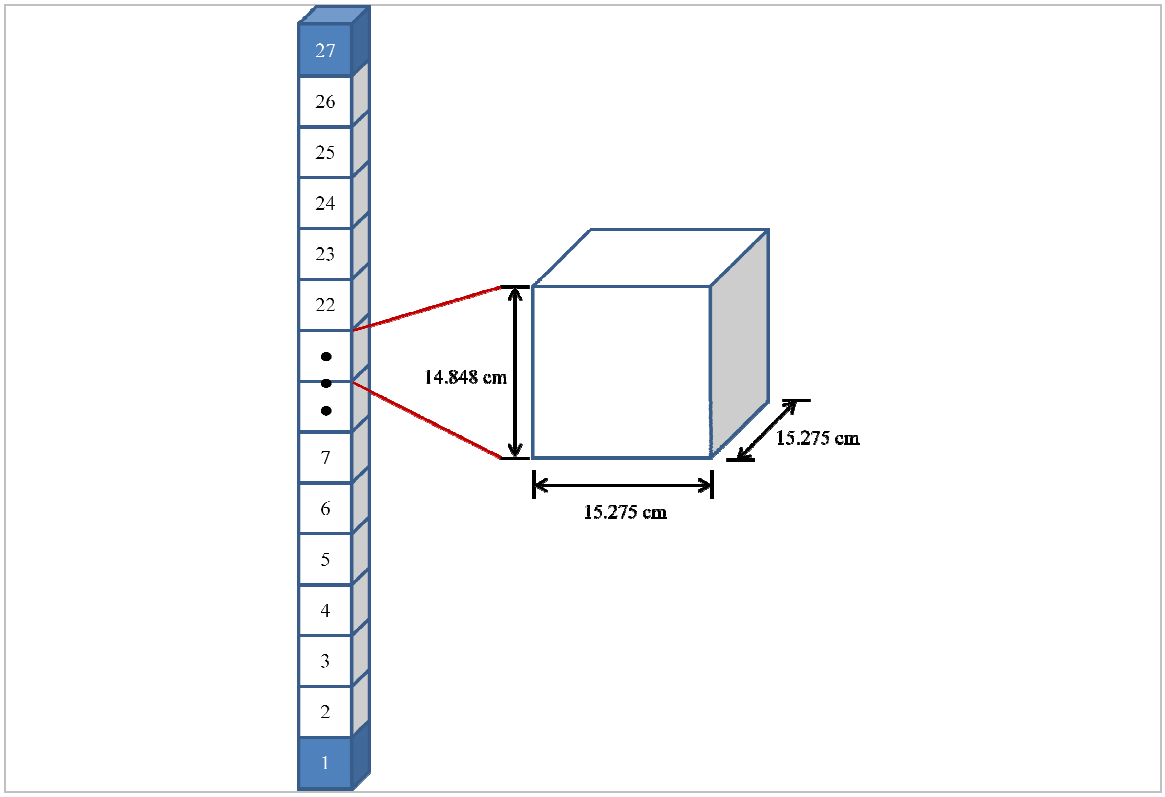

Figure 6-5. Axial nodalization of the fuel assemblies in *geometry* file for both cases

The fuel assemblies in the TRACE model were compared with the data contained in the draft of the benchmark. In this document there are four different types subdivided according the axial composition.

For *Case A*, Figure 6-6 shows the radial configuration of the fuel assemblies in the core identifying the TRACE FA with their respective ID number and, in different colors, the corresponding fuel assemblies defined in the benchmark. It is shown also the total amount of each fuel assembly type in the table on the right side.

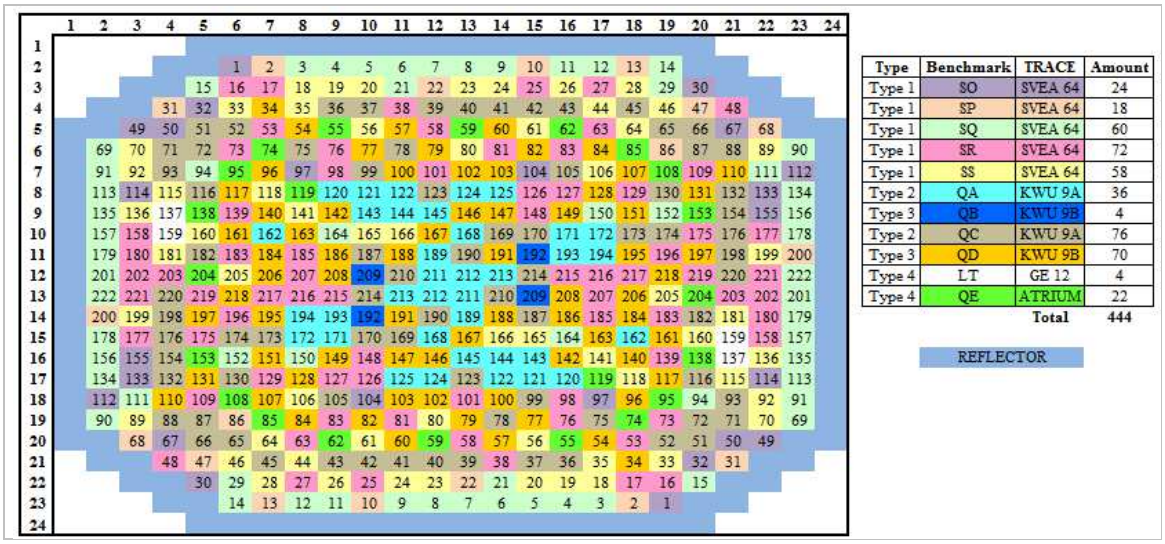

Figure 6-6. Matching between TRACE model and Benchmark code data for each FA

In the geometry file read by PARCS, besides the definition of the total number of axial nodes, top and bottom reflector, and the geometry dimensions of each axial level or planar region, the axial composition in each planar region for each radial position is also defined. One number in each region corresponds to a PMAXS file. In Table 6-2 the relation of each ID number to each PMAXS file is shown. In Table 6-3 the axial regions of the fuel assemblies are presented, where each cell or planar region contains the corresponding number of PMAXS file, which is listed in Table 6-2.

Table 6-2. List of PMAXS files

PMAXS files							
1	REFLB	51	e15_red	68	e17_p10	76	e22d_dn_nat
2	REFLR	52	e16_red	69	e18_p10	77	e22d_dn_p10
3	REFLT	53	e17_red	70	e19_p10	78	e22d_up_p10
38	e16_p10	54	e18_red	71	e20_dn_p10	79	e22d_up_nat
39	e16_p08	55	e20_nat	72	e20_up_p10	80	e23_dn_p10
48	e15_p10	56	e23_dn_nat	73	e21_p10	81	e23_up_p10
49	e15_p08	57	e23_up_nat	74	e22_p10	100	e23_mi_p10

Table 6-3. Axial definition of fuel assemblies related to PMAXS files

			FA type										
Planar region	Mesh (cm)	Plane Type	13 SO	14 SP	15 SQ	16 SR	17 SS	18 QA	19 QB	20 QC	21 QD	22 LT	23 QE
1	14.848	Bottom ref	1	1	1	1	1	1	1	1	1	1	1
2	14.848	Fuel	51	52	53	54	54	55	55	55	55	76	56
3	14.848	Fuel	48	38	68	69	70	71	71	73	74	77	80
4	14.848	Fuel	48	38	68	69	70	71	71	73	74	77	80
5	14.848	Fuel	48	38	68	69	70	71	71	73	74	77	80
6	14.848	Fuel	48	38	68	69	70	71	71	73	74	77	80
7	14.848	Fuel	48	38	68	69	70	71	71	73	74	77	80
8	14.848	Fuel	48	38	68	69	70	71	71	73	74	77	80
9	14.848	Fuel	48	38	68	69	70	71	71	73	74	77	80
10	14.848	Fuel	48	38	68	69	70	71	71	73	74	77	80
11	14.848	Fuel	48	38	68	69	70	71	71	73	74	77	80
12	14.848	Fuel	48	38	68	69	70	71	71	73	74	77	80
13	14.848	Fuel	48	38	68	69	70	71	71	73	74	77	80
14	14.848	Fuel	48	38	68	69	70	71	71	73	74	77	80
15	14.848	Fuel	48	38	68	69	70	71	71	73	74	77	80
16	14.848	Fuel	48	38	68	69	70	72	72	73	74	77	100
17	14.848	Fuel	48	38	68	69	70	72	72	73	74	77	100
18	14.848	Fuel	48	38	68	69	70	72	72	73	74	78	81
19	14.848	Fuel	48	38	68	69	70	72	72	73	74	78	81
20	14.848	Fuel	48	38	68	69	70	72	72	73	74	78	81
21	14.848	Fuel	48	38	68	69	70	72	72	73	74	78	81
22	14.848	Fuel	48	38	68	69	70	72	72	73	74	78	81
23	14.848	Fuel	48	38	68	69	70	72	72	73	74	78	81
24	14.848	Fuel	49	39	68	69	70	72	72	73	74	78	81
25	14.848	Fuel	49	39	68	69	70	72	72	73	74	78	81
26	14.848	Fuel	51	52	53	54	54	55	55	55	55	79	57
27	14.848	Top ref	3	3	3	3	3	3	3	3	3	3	3

A depletion file is also necessary for PARCS, this contains history and thermal-hydraulic data. The file used is configured to perform the calculations of Control Rod History (HCR), Moderator Density History (HMD) and Fuel Temperature History (HTF).

6.3 Mapping between TRACE and PARCS

Thermal-hydraulic conditions for PARCS are provided by an external system code, in this case TRACE. The temperature/fluid condition required at each neutronics node for the feedback calculation consists of the coolant density/temperature and the effective fuel temperature. The nodal power information determined by PARCS is then transferred back to the systems code. During the course of data transfer, the differences in the neutronic and thermal-hydraulic nodalization are reconciled by the mapping scheme described below.

In general, coarser node sizes are used in the core for TRACE TH calculation than in the PARCS neutronics calculation. Therefore, a TH node usually consists of several neutronics nodes. However, it is possible that a neutronics node can belong to multiple TH nodes. Because of this possibility, the PARCS TH variable is obtained as the weighted average of the TH variables of several TH nodes as:

$$T_i^P = \sum_{k=1}^{N_i^P} \alpha_{i,j(i,k)}^P T_{j(i,k)}^T$$

where the superscript *P* and *T* stands for PARCS and TRACE codes, and *j(i,k)* is the *k-th* TH node number out of the N_i^P TH nodes belonging to the *i-th* PARCS node. $\alpha_{i,j}^P$ is the volume fraction of the *j-th* TH node in the *i-th* PARCS node which must sum the unity.

In the model used in the present work, the automatic mapping option was selected.

On the other hand, the nodal power of the *j-th* TH node is obtained as follows:

$$P_j^T = \sum_{k=1}^{N_j^T} \alpha_{j,i(j,k)}^T P_{i(j,k)}^P$$

where *i(j,k)* is the *k-th* PARCS node number out of the N_j^T PARCS nodes belonging to the *j-th* TH node. $\alpha_{j,i}^T$ is the volume fraction of the *i-th* PARCS node in the *j-th* TH node, and it satisfies the following conditions:

$$\sum_{j=1}^{N^T} \alpha_{j,i}^T = 1 \quad ; \quad \sum_{k=1}^{N_j^T} \alpha_{j,i(j,k)}^T > 1$$

where N^T is the total number of TH nodes. The second relation above implies that the TH node is larger than the PARCS nodes.

In general, the neutronic node structure is different from the TH node structure. The difference is to be mitigated by a proper mapping scheme. This mapping used to be explicit

in that the fractions of different TH nodes belonging to a neutronic node had to be specified in a file called *MAPTAB.*

The General Interface (GI) code, which is the central interface unit between TRACE and PARCS, is included in PARCS as a separate module. In this configuration, the Parallel Virtual Machine (PVM) communication between PARCS and the GI has been replaced with direct data copy logic, and the GI continues to manage all PVM communication with TRACE. Thus, two processes (TRACE and PARCS) need to be executed.

An automatic mapping kernel for the GI manages the mapping configuration used, where PARCS must process the 1D kinetics data from its own input deck and a *MAPTAB* file is required.

The radial mapping for volumes and heat structures is performed based on the mapping configurations; the axial mapping is performed automatically, a linear interpolation scheme is used for both the hydraulic cells and the heat structures. This scheme provides a fluid/fuel temperature distribution in the channel which is more accurate than without interpolation. For the mapping of axial hydraulic cells, it is assumed that the fluid conditions exist at the exit of the cell.

6.4 Feedback Model (XS)

The coupling between PARCS and TRACE is achieved by the interprocess communication protocol, Parallel Virtual Machine (PVM). The two processes are loaded in parallel and the PARCS process transfers the nodal power data to the TH process, this sends back the temperature of fuel and coolant, and density data to the PARCS process. The two processes are to be run in parallel.

In a LWR, there are two primary TH feedback mechanisms that affect the neutronics solutions during a transient: the Doppler Effect resulting from changes in the fuel temperature and the moderator/coolant effect resulting from changes in the water density. The Doppler Effect is a prompt reactivity feedback, whereas the moderator/coolant feedback is delayed because there is a time delay on the order of seconds in the heat transfer from the fuel to the coolant.

The Doppler fuel temperature feedback is calculated by PARCS using data set in the additional file called *MAPTAB.* Either the volume average fuel temperature or a linear combination of the fuel centerline and surface temperatures can be used for calculating the effective temperature. In the current work, the volume-averaged fuel temperature option was chosen.

These feedbacks have an impact on the numerical solution since the Doppler Effect needs to be incorporated in the iteration process to resolve the nonlinearity in a problem involving TH feedback. Since the cross sections needed to formulate a Transient Fixed Source Problem (TFSP) should be obtained at the end of the time step, the transient heat conduction calculation should advance first to the end of the time step to determine the

change in the fuel temperature during the time step. This calculation requires an estimate of the power distribution at the end of the time step. Since the new power distribution is not known, the current power distribution is extrapolated based on the two most recent time step values. The fuel temperature distribution obtained from the first heat conduction solution can now be used to calculate the nodal cross sections.

Figure 6-7 shows the information to be exchanged each time step.

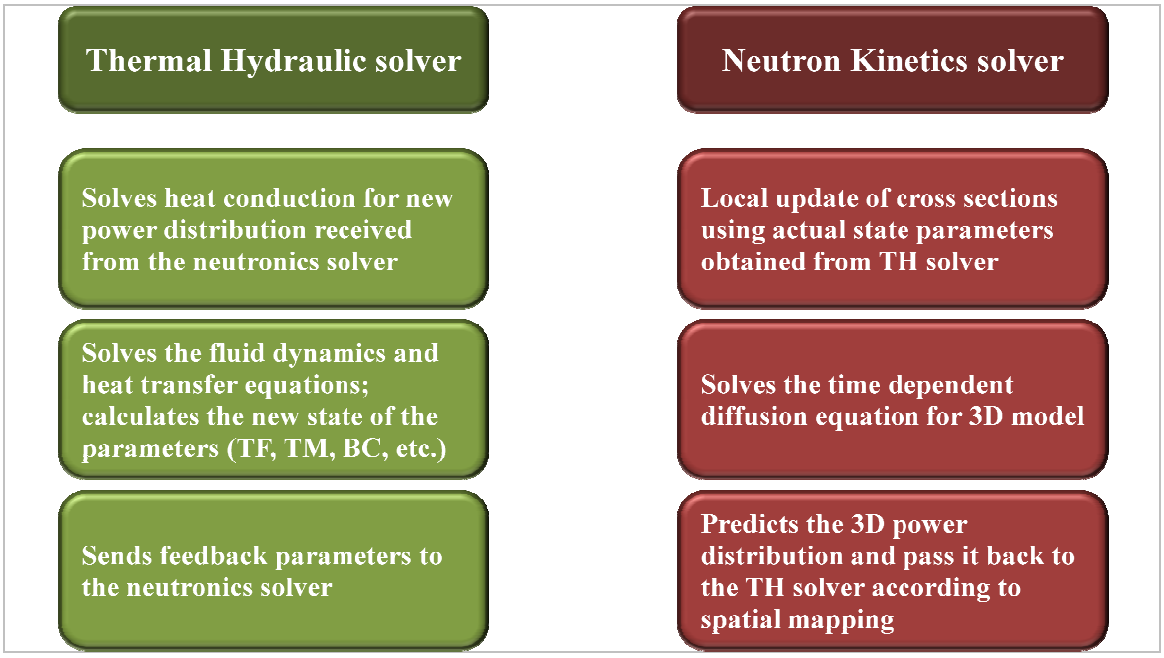

Figure 6-7. Information exchanged between TRACE and PARCS at each time step

For core simulation and depletion analysis, PMAXS (Purdue Macroscopic Cross Section, XS) files are needed to be used by PARCS. The code counts on a depletion module and a cross section module for retrieving node wise cross section for its burnup history and current TH state from PMAXS. The overview of PARCS package for core depletion analysis is shown in Figure 6-8.

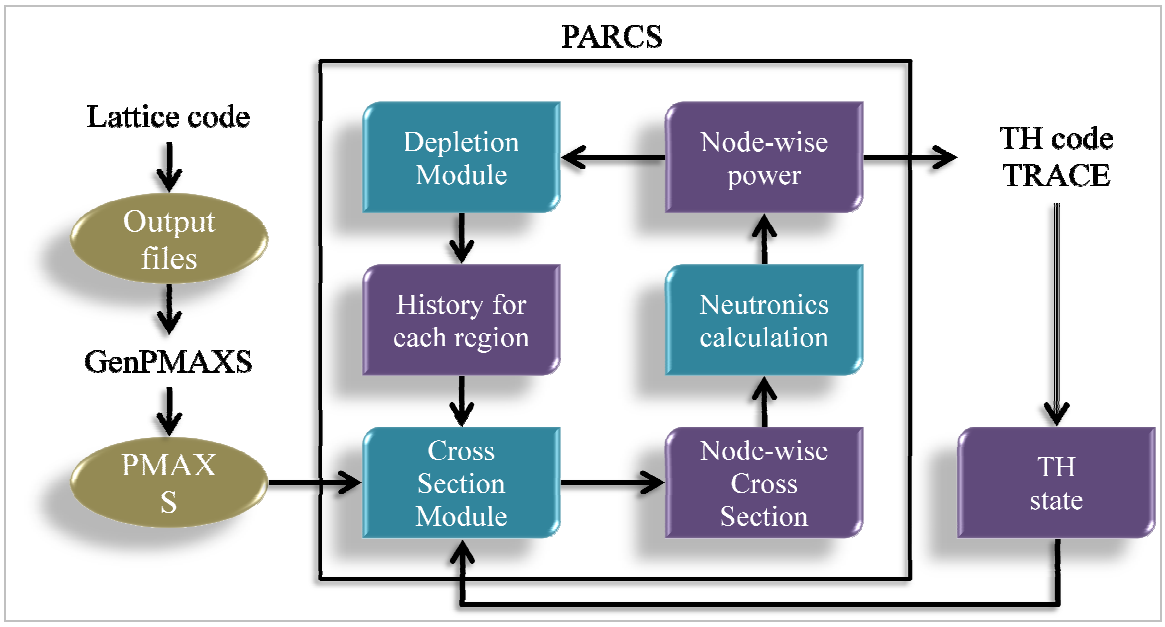

Figure 6-8. Overview of PARCS code system

The depletion module generates new burnup and other history state information corresponding to the PARCS neutron flux solution. The cross section module calculates XS based on burnup and history state information, as well as on the current TH state. Then, the PARCS neutronic module calculates the neutron flux with the XS generated previously by the cross section module.

The macroscopic XS, at the appropriate fuel conditions, are prepared using a lattice physics code such as HELIOS, CASMO, TRITON. Because the output format of each lattice code is unique, the program GenPMAXS [28] (Generation of the Purdue XS set), is used to process the output of the lattice codes and prepare the PMAXS formatted cross section. The PMAXS file is constructed using the output of the lattice code providing the XS data in the specific format that can be read by PARCS. Therefore, GenPMAXS code is the interface between the lattice code and the depletion code.

Figure 6-9 shows a general view of the tasks flow in GenPMAXS to generate the macroscopic cross section file PMAXS for PARCS.

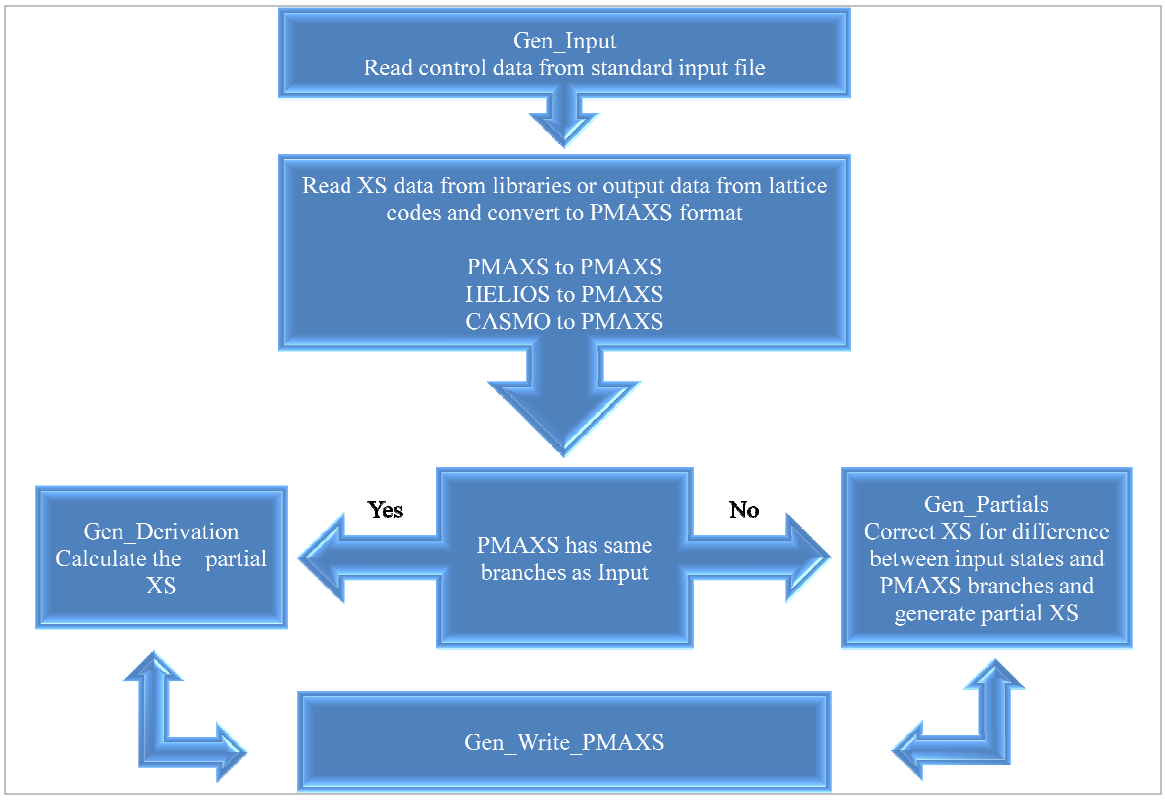

Figure 6-9. Overall flow chart in GenPMAXS

The PMAXS files provided have as source files the ones generated by CASMO. Each one of the PMAXS files is structured as function of one reference and specific state variables. The number of total burnup sets is different for each file.

7 Results of Testing the TRACE Model Case B

To test the detailed core model (*Case B*), the stationary plant conditions just before the transient were simulated with TRACE/PARCS and the obtained results were compared to the ones obtained for the *Case A*.

Selected parameters of the TRACE standalone simulation for the *Case B* were compared to the ones of the *Case A* to verify the agreement of both cases, which permitted the continuation of the tasks to achieve the correct values for the selected parameters just before the transient to start the simulation of the event. In Figure 7-1 it is possible to observe, for *Cases A* and *B*, the plotting of the pressure drop between the lower and the upper core level, and the temperature increase from the bottom to the top of the core. According to the data in this graphic, the pressure drop is 105.8 kPa and the change in the temperature is 15.3 K.

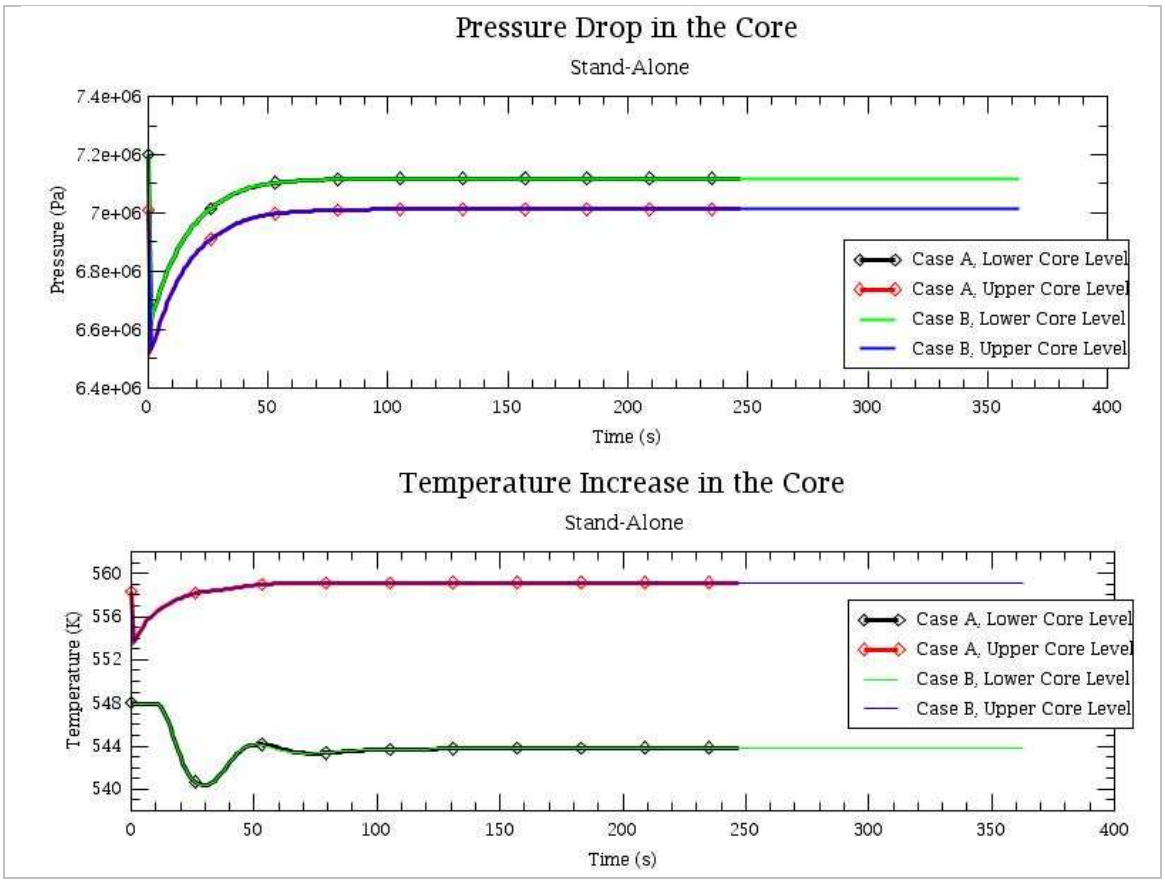

Figure 7-1. Standalone. Pressure drop and temperature increase in the core

Figure 7-2 shows the reactor power evolution during the time of the simulation. The oscillations observed before 100 s represent how precise were the data set in the model to achieve the steady-state condition; once that convergence is reached, the power remains constant after 100 s until the end of the calculation.

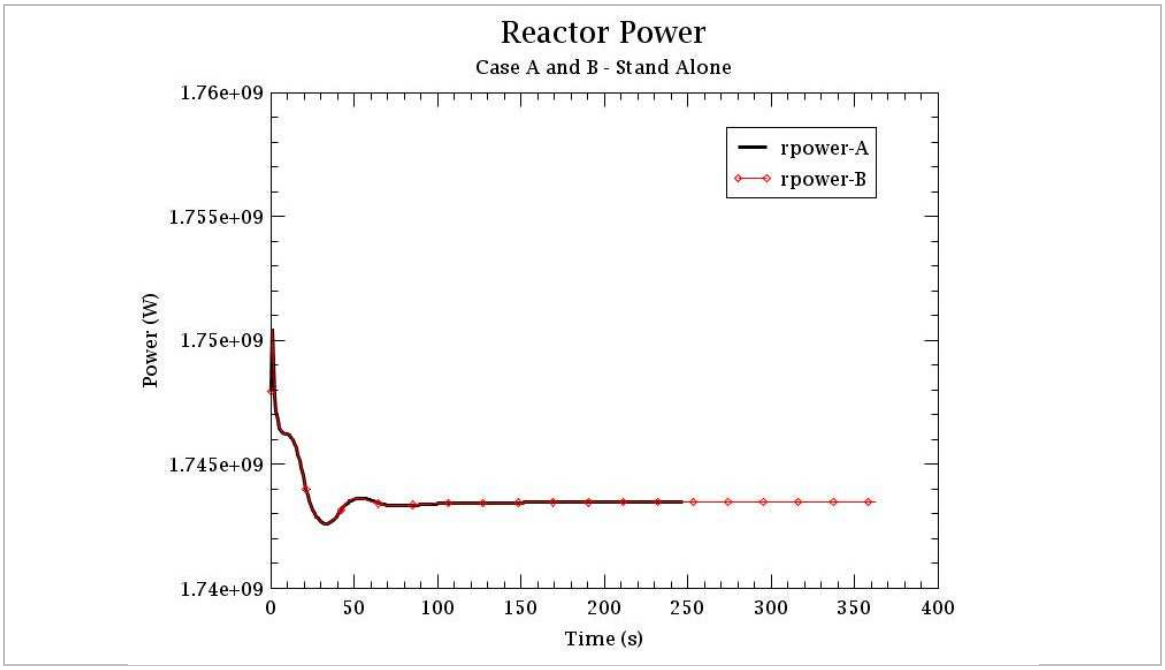

Figure 7-2. Standalone. Power in the reactor comparison for Case A and Case B

Figures 7-3 to 7-6 show the plotting for the mass flow rate, pressure, temperature and void fraction, respectively, in the 27 axial nodes in the core. For each one of these graphics, four different fuel assemblies in the TRACE model were chosen to make a comparison of the parameters obtained for *Case B* with the reference *Case A*. The curves presented in these four graphics are at the simulation time 247 s, when the convergence was achieved in the stand-alone simulation for *Case A.*

Figure 7-3 shows the mass flow rate. It should be taken into account that for *Case A*, one channel represents two fuel assemblies and the values in the graphic are approximately the double compared with the same channel for *Case B,* which represents only one fuel assembly.

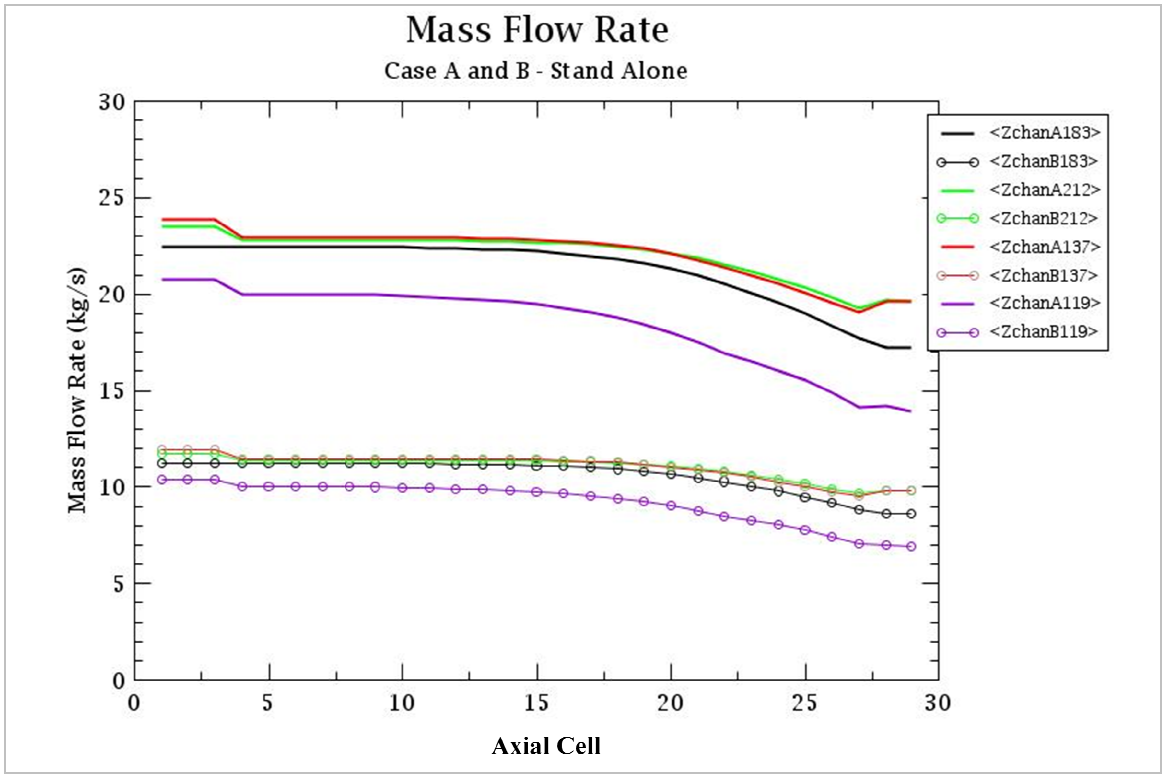

Figure 7-3. Standalone. Mass flow rate in channels for Case A and Case B

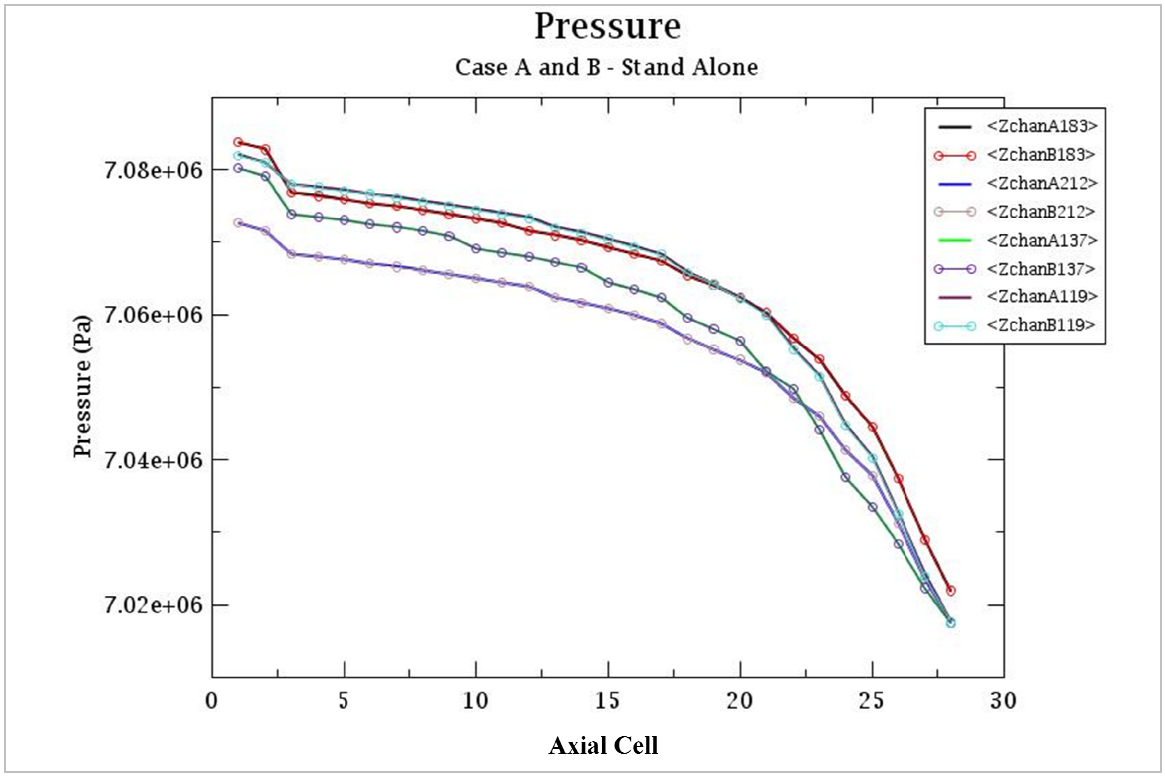

Figure 7-4. Standalone. Pressure drop in channels for Case A and Case B

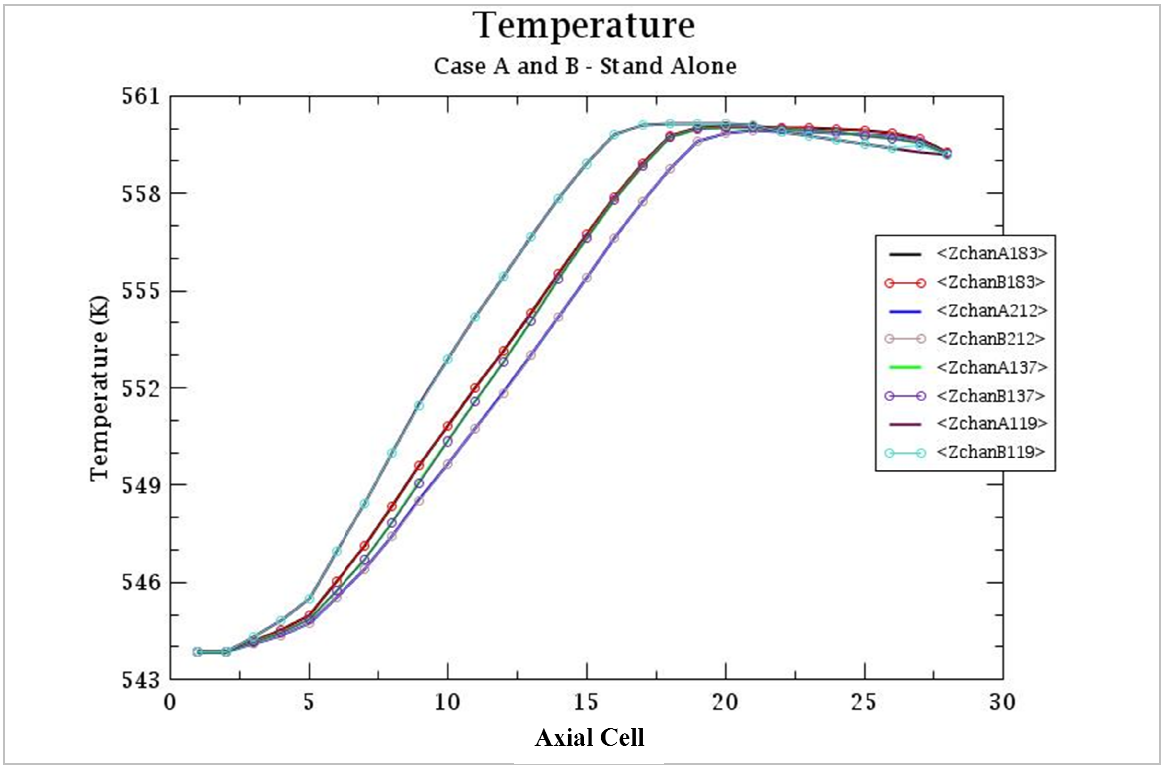

Figure 7-5. Standalone. Temperature increase in channels for Case A and Case B

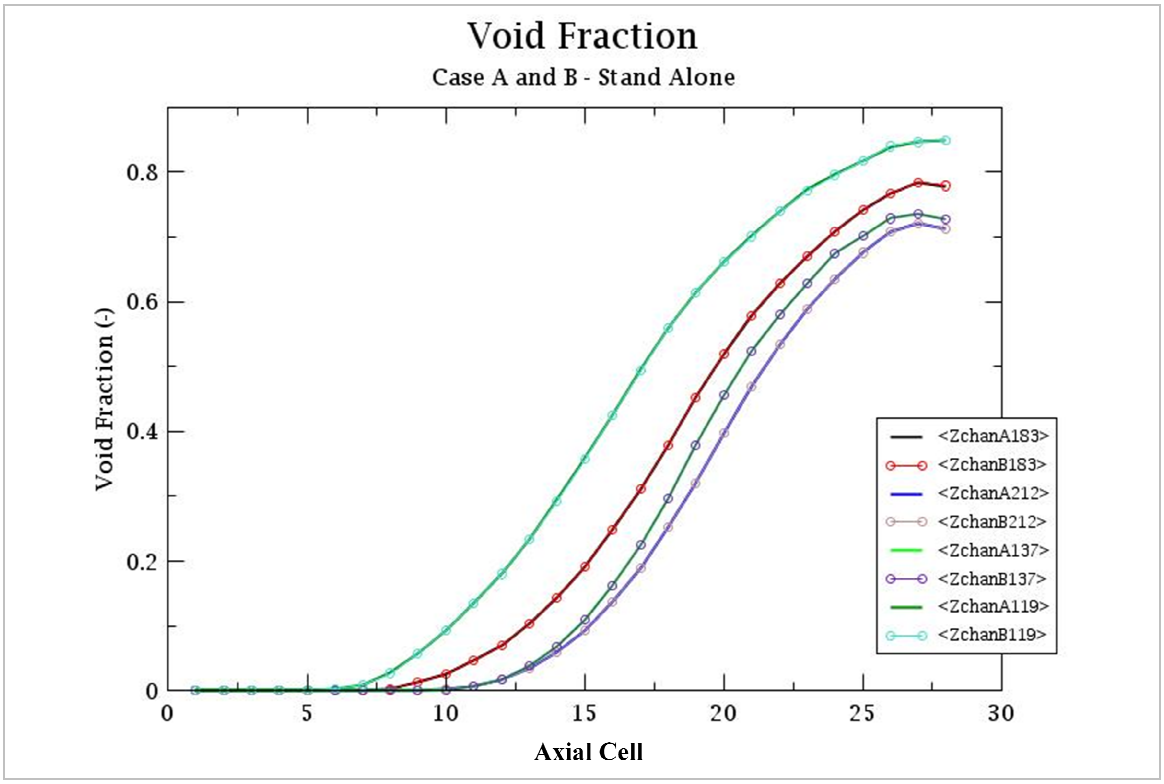

Figure 7-6. Standalone. Void fraction in channels for Case A and Case B

7.1 Coupled TRACE / PARCS Steady-State Simulation for Case B

After convergence of the standalone initialization, a steady-state calculation was performed with the PARCS/TRACE coupled system code to achieve a converged coupled neutronics / thermal-hydraulics solution in order to establish the initial conditions for the transient calculation. The SETS numerical method [29] is used in the TRACE steady-state calculation and an explicit coupling is used between the TRACE and PARCS solutions with an automatic mapping.

The eigenvalue problem [30] is solved during the steady-state initialization prior to a transient calculation, as well as during fuel depletion analysis. The parameters tested for convergence in TRACE are:

- Pressure
- Liquid velocity
- Gas velocity
- Void fraction
- Liquid temperature
- Gas temperature
- Non condensable gas pressure
- Heat structure temperature

The convergence criteria used in TRACE were:

Convergence criterion for the outer-iteration pressure calculation: 1.0E-4
Convergence criterion for the steady-state calculation: 1.0E-4

The convergence criteria set in PARCS were:

- Eigenvalue (k-eff) convergence: 1.0E-6
- Global fission source convergence: 1.0E-5
- Local fission source convergence: 5.0E-4
- Fuel temperature convergence: 1.0E-3

The input TRACE model was created based in the input file for the standalone calculation. Only the necessary data was copied to have a condensed input file for the steady-state calculation. This file contains the set of global parameters and flags to govern the behaviour of the code during the run, the list of all the components in the model containing only information of the type of component, name of the component, ID number and junctions.

Then appears the signal variables, control blocks and trips defined in the standalone input file, for this it was not necessary to have all the detailed information, it was set the value zero for each one of these three control systems to call all the data from the restart file obtained from the previous standalone calculation.

Finally, in the input file appears the time step data which specifies the minimum and maximum time step sizes, frequencies and the end of the problem for specified time intervals. There is also a parameter to control the time step size to conserve convection heat-transfer energy between heat structures and hydraulic components.

In the following figures the results of the steady-state calculation after convergence of some selected parameters from the coupled simulation are presented. In Figure 7-7 it can be observed the pressure drop in the core of 106.6 kPa and the gradient of temperature of 14.76 K.

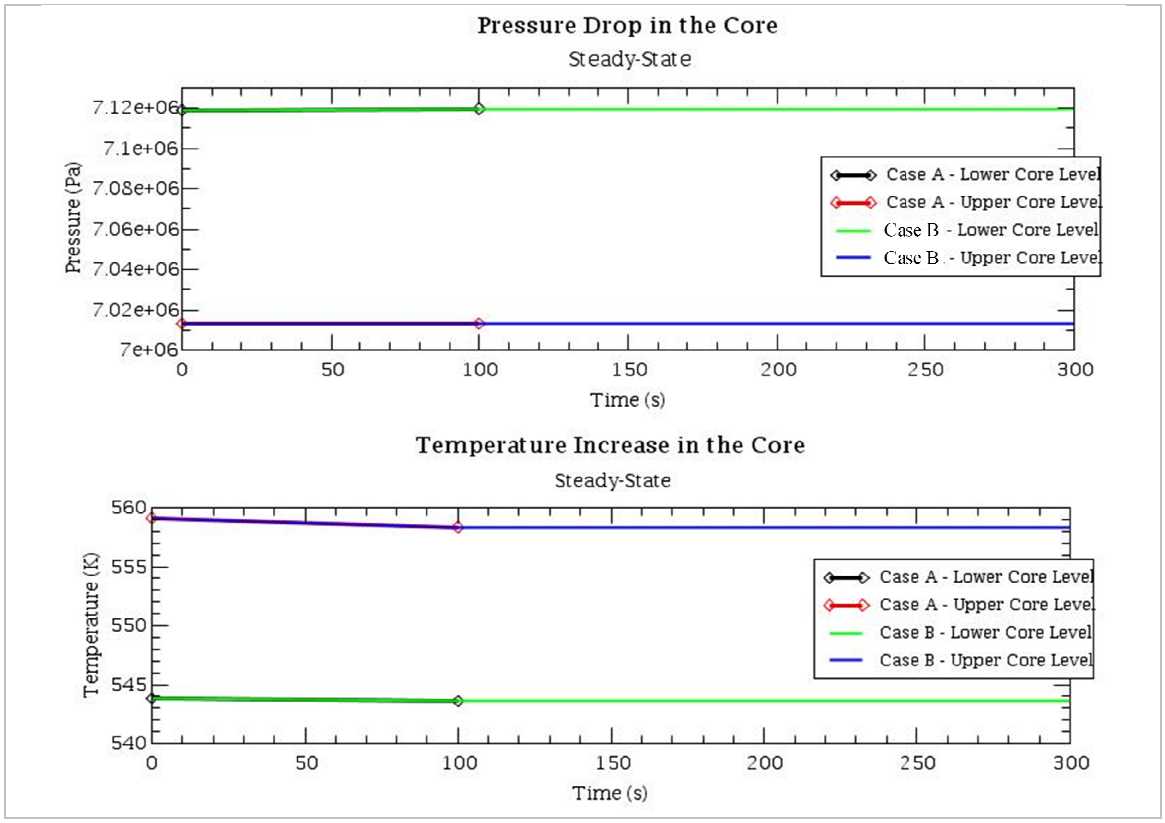

Figure 7-7. Steady-state. Pressure drop and temperature increase in the core

The reactor power is shown in Figure 7-8 which remains constant at 1802 MW_{th} (106%). The Core k-eff in PARCS for *Case A* was 1.030115; for *Case B* was 1.030201.

The averaged axial relative power distribution resulting in PARCS output is shown in Figure 7-9. For axial plane 1 and 27 it is not included any value because these positions correspond to the lower and upper reflector, respectively. This figure is at simulation time 300 s for both cases.

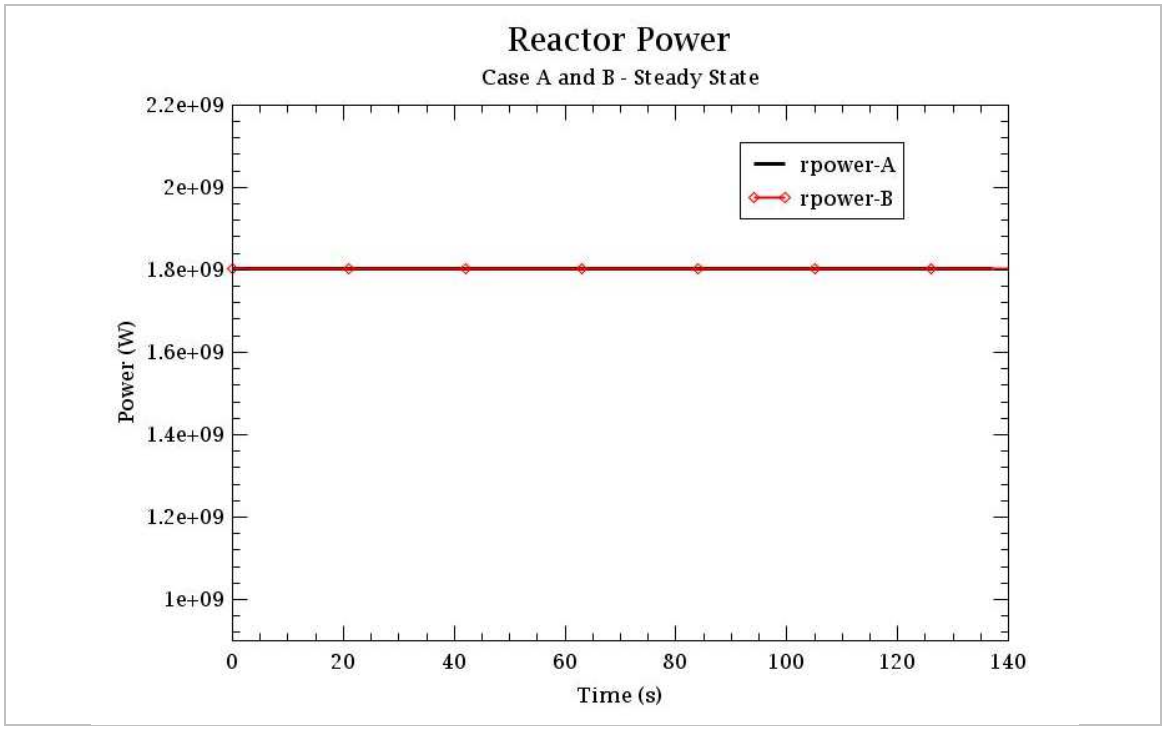

Figure 7-8. Steady-state. Power in the reactor for Case A and Case B

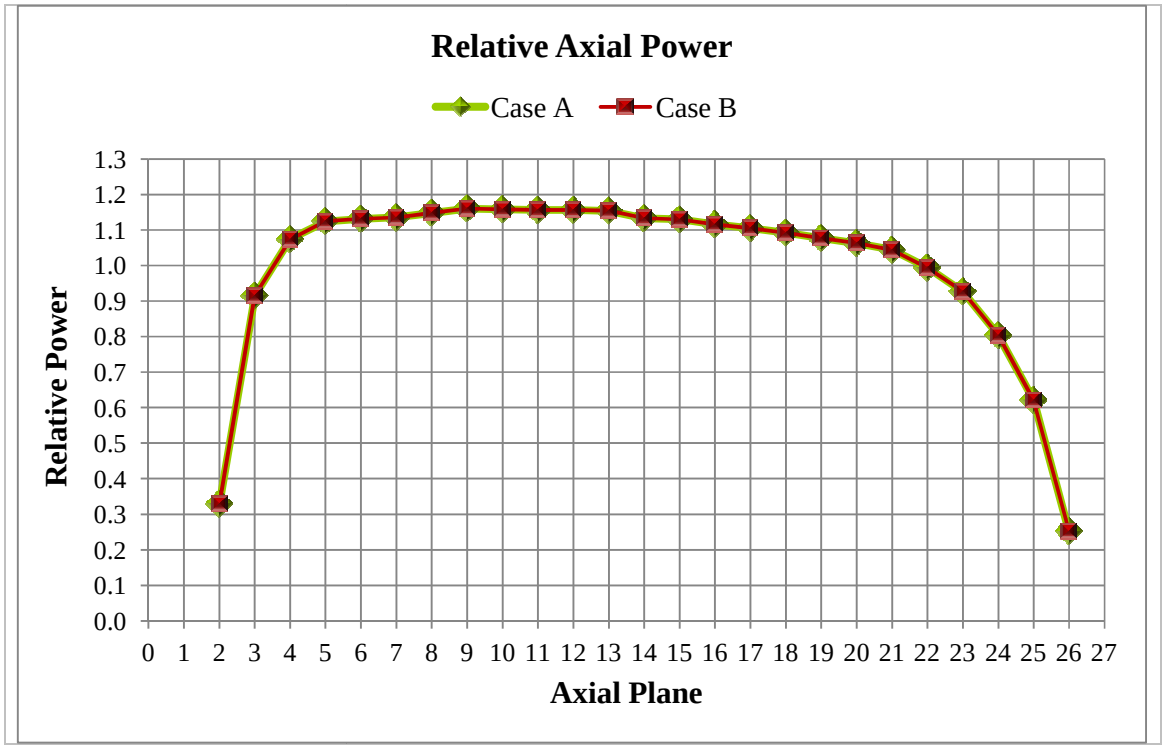

Figure 7-9. Steady-state. Averaged axial relative power in the core for Case A and B

For Figures 7-10, 7-11, 7-12 and 7-13, the same channels considered for standalone graphics were taken into account to remain consistent with the comparisons of the parameters mass flow rate, pressure, temperature and void fraction. These graphics were made considering data at simulation time 137 s in order to compare the chosen parameters at the point of interest, which is when the convergence is achieved in *Case A.*

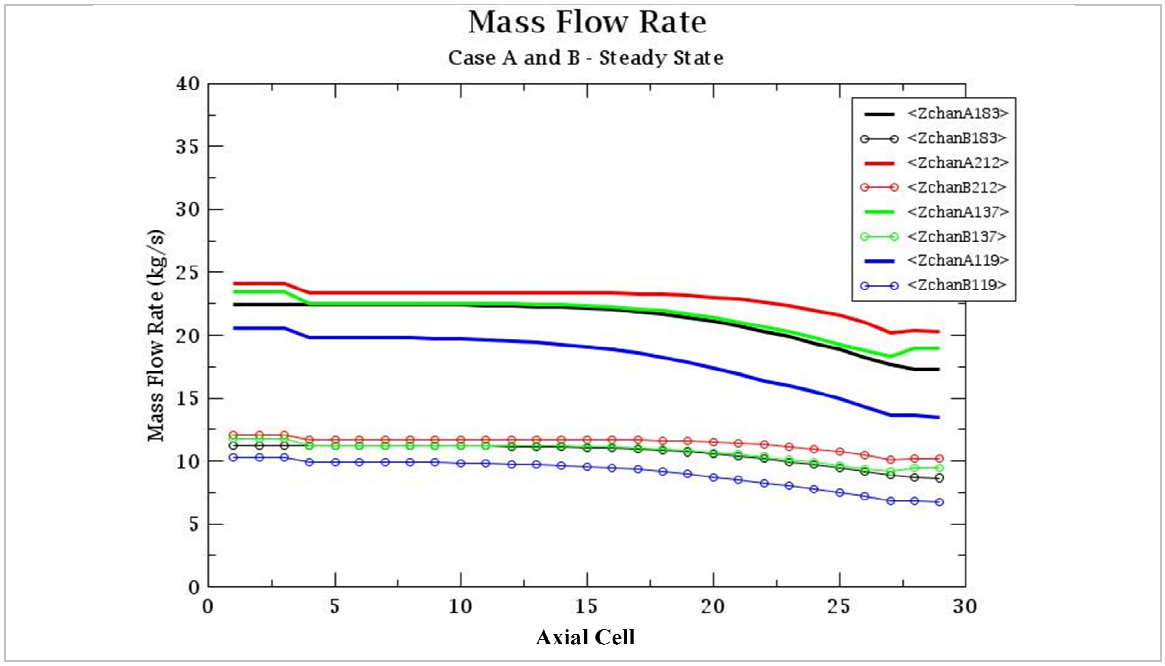

Figure 7-10. Steady-state. Mass flow rate in channels for Case A and Case B

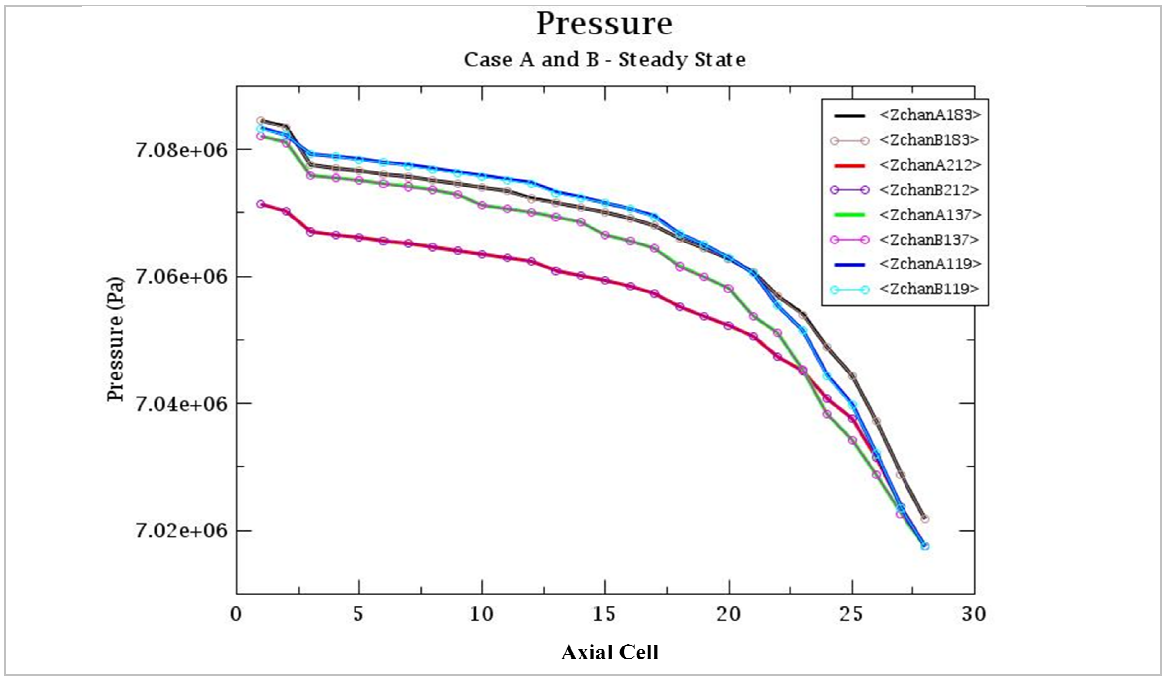

Figure 7-11. Steady-state. Pressure drop in channels for Case A and Case B

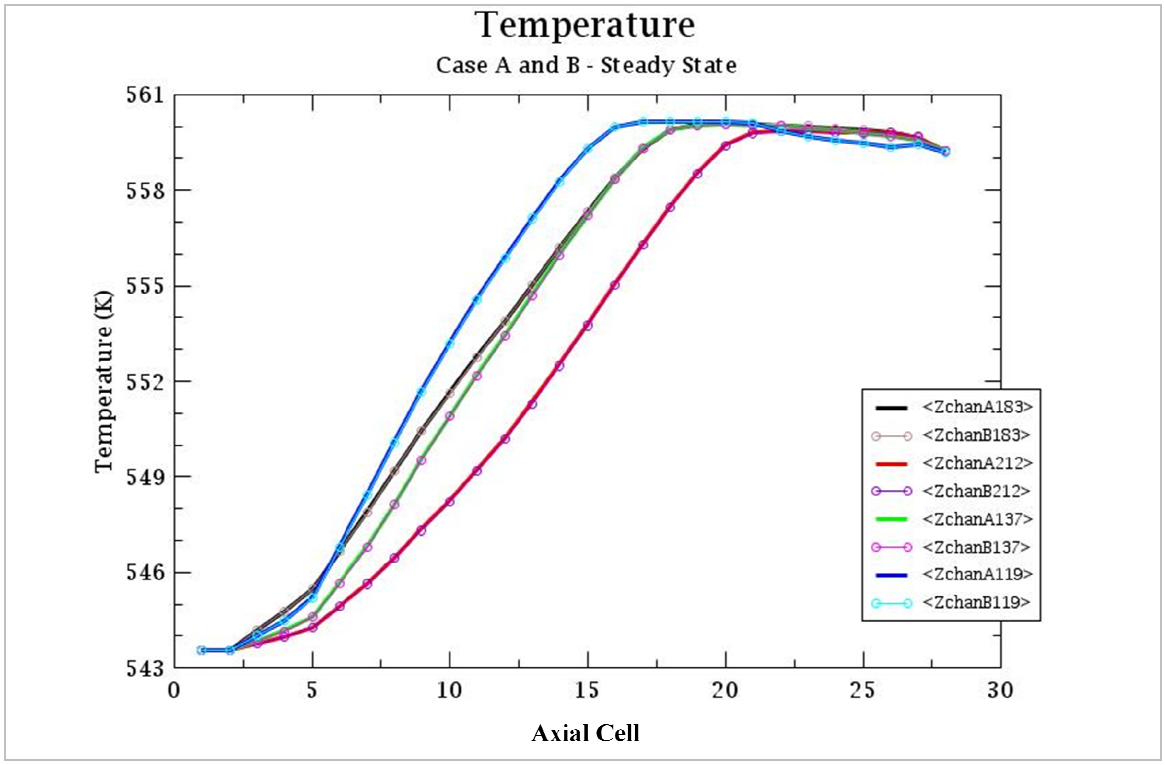

Figure 7-12. Steady-state. Temperature increase in channels for Case A and Case B

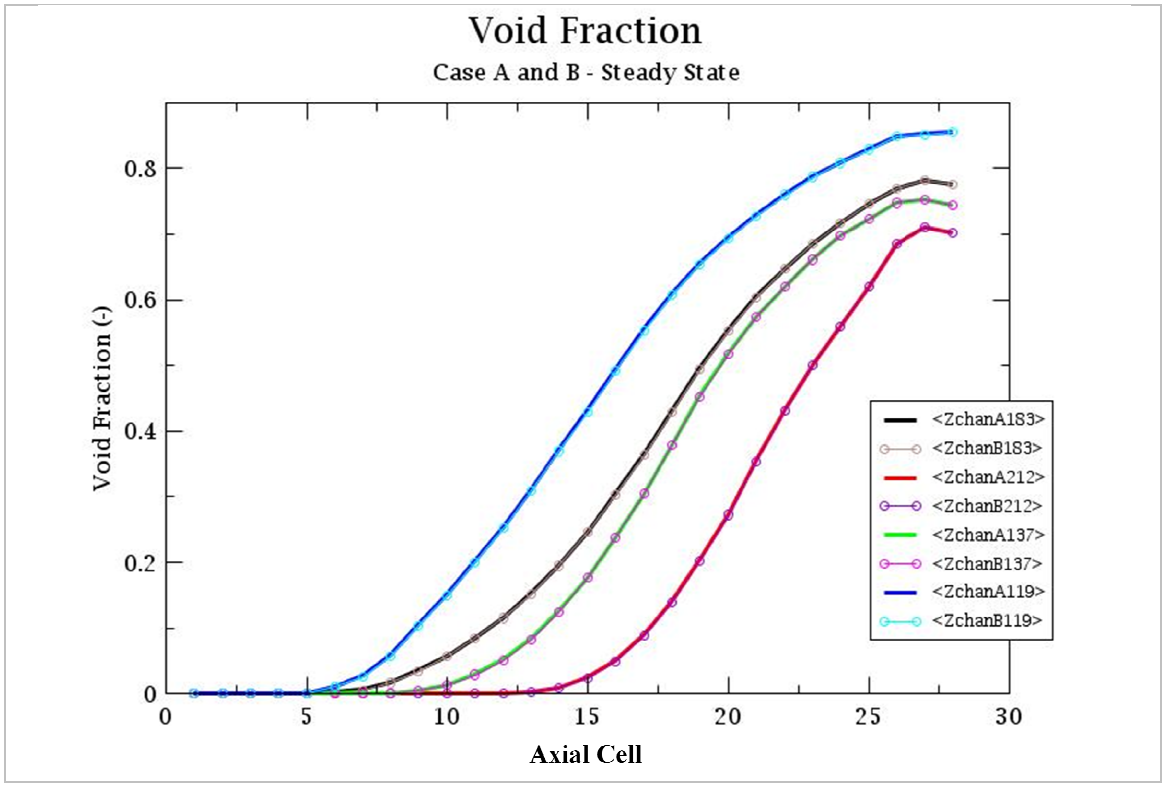

Figure 7-13. Steady-state. Void fraction in channels for Case A and Case B

7.2 Simulation of the Transient Event

After establishing the initial conditions for the transient simulation with the execution of the steady-state, the next step was to prepare an input file for TRACE containing the same information as the steady-state, the change was done in the parameter to perform a transient calculation and the boundary conditions were defined in the corresponding control blocks.

According to previous work in [17] and [27], the recommendations were followed in the current work regarding the adjustment in the feedwater temperature boundary condition (the temperature drops twice faster).

Figure 7-14 is shown to demonstrate that the new configuration of *Case B* did not alter the behavior of the pressure nor the temperature in the core compared with the configuration in *Case A.*

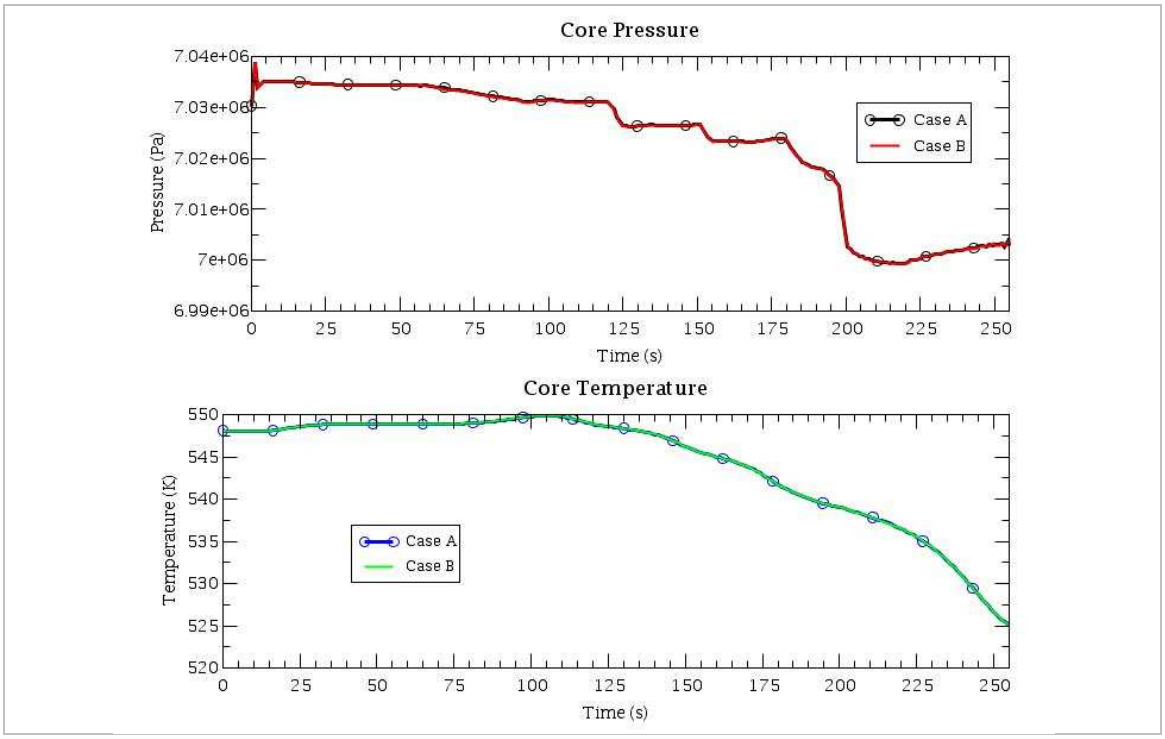

Figure 7-14. Transient. Pressure and temperature in the core

Figure 7-15 shows the power oscillations through the transient event. The blue line shows the measure from the APRM, which is the real behavior of the thermal power evolution through the time. The red line represents the model of the current work. In green color the result of the study performed in [19] is shown.

The red line presents a peak in the beginning of the transient simulation, besides an over prediction in the power evolution compared with the other two curves, which show a good agreement from the start. This may be due to the differences showed in Table 5-7.

From simulation time 110 s to 190 s, the oscillations are due to the low feedwater temperature increasing the power and the action of the pumps, controlling the situation by reducing the speed to stabilize the power level.

To simulate the partial scram, the rods insertion started at 197.606 s, and the rods were placed in the final position at simulation time 201.008 s. This event is showed in the figure as a sudden drop in the power, just after the run-down of the pumps.

After the partial scram, it is shown that the power oscillations started with increasing amplitude. From this point, the green curve under predicts the power, while the red curve shows a good agreement with the blue curve, but the amplitude did not increased as it was expected to continue reproducing the transient event. This could be caused by an auto control of the thermal-hydraulic parameters of the system.

To simulate the scram, it was configured to be performed on a trip set point at 120% of the nominal power with a duration time of 1.3 s. In the same figure it is possible to observe that around time 265 s, there is a high power peak, crossing the power limit set, but the scram was not performed. In fact, the oscillations observed after 254 s seem to be totally out of the attempt of reproducing the transient event.

Despite the oscillations after 255 s are not part of the correct reproduction, the scram should be performed when the red curve shows a high peak. After reading in detail the TRACE manual, it was found that in the input model it is also needed to define a *trip* in the TRIP section but it was not possible to make a test because of the short time for the investigations.

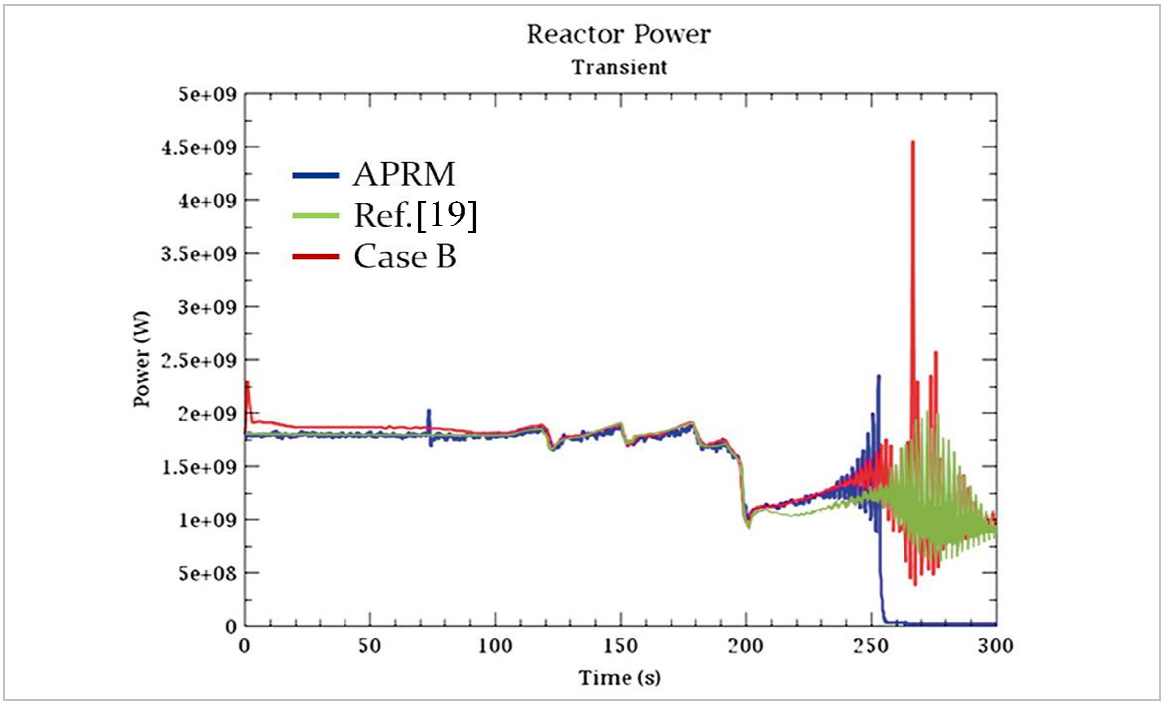

Figure 7-15. Transient. Power in the reactor, APRM vs Case B

The fuel assembly that showed the averaged higher relative power during the transient simulation was the one with ID 368, which is similar to the fuel assembly with ID 146. Both are KWU 9x9-9B type. That is the reason why the next figures, from 7-16 to 7-19, show the respective parameters referred to the fuel assembly 368. For representation purposes, only the lower, medium and upper cells of the selected fuel assembly are shown.

As expected, the lower part presents a higher mass flow rate, zero voids and major pressure than the other cells. In Figure 7-16, the mass flow rate is following the behavior of the run-down of the pumps due to the auto control to reduce the power level of the reactor.

In Figure 7-18 it is clear the decrease in the temperature of the water in the lower part of the fuel assembly due to the loss of the pre-heaters.

In Figure 7-19 the upper part of the fuel assembly presents a higher value of voids, reaching the value of 0.9 but it is important to point out that this is the profile of only one fuel assembly. The average of voids in the core should be around 0.7.

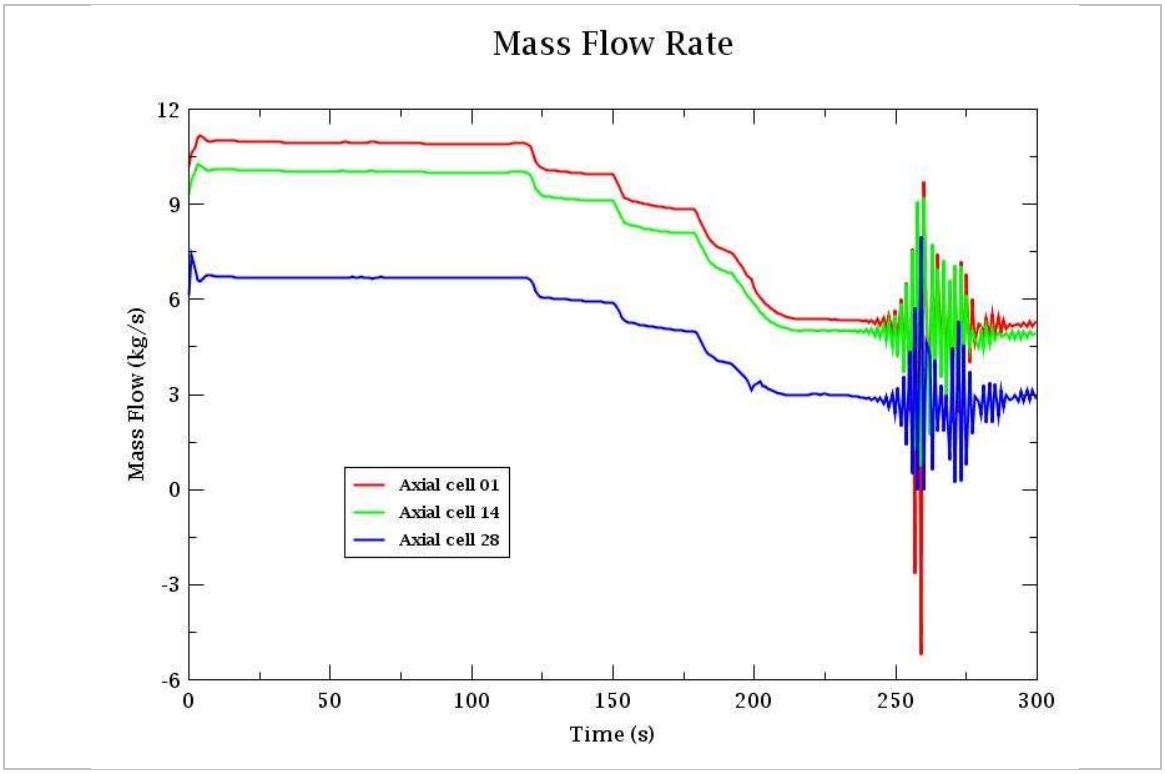

Figure 7-16. Transient. Mass flow rate in channel 368 for Case B

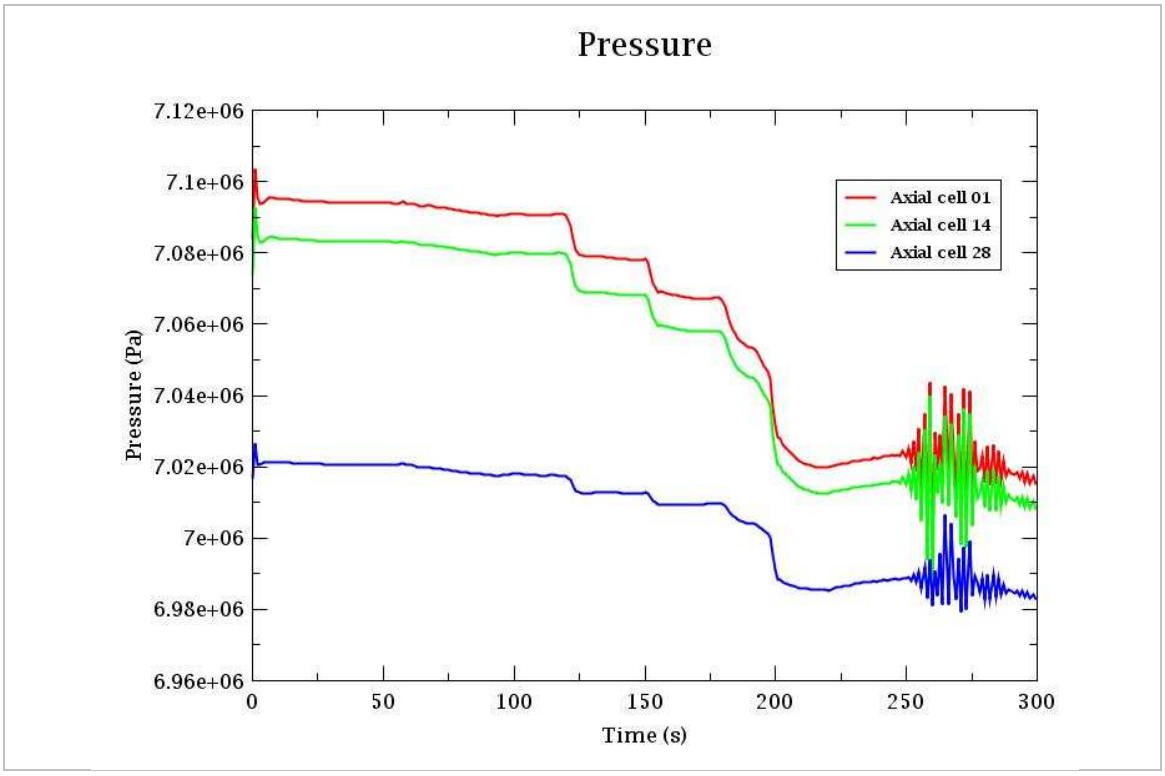

Figure 7-17. Transient. Pressure drop in channel 368 for Case B

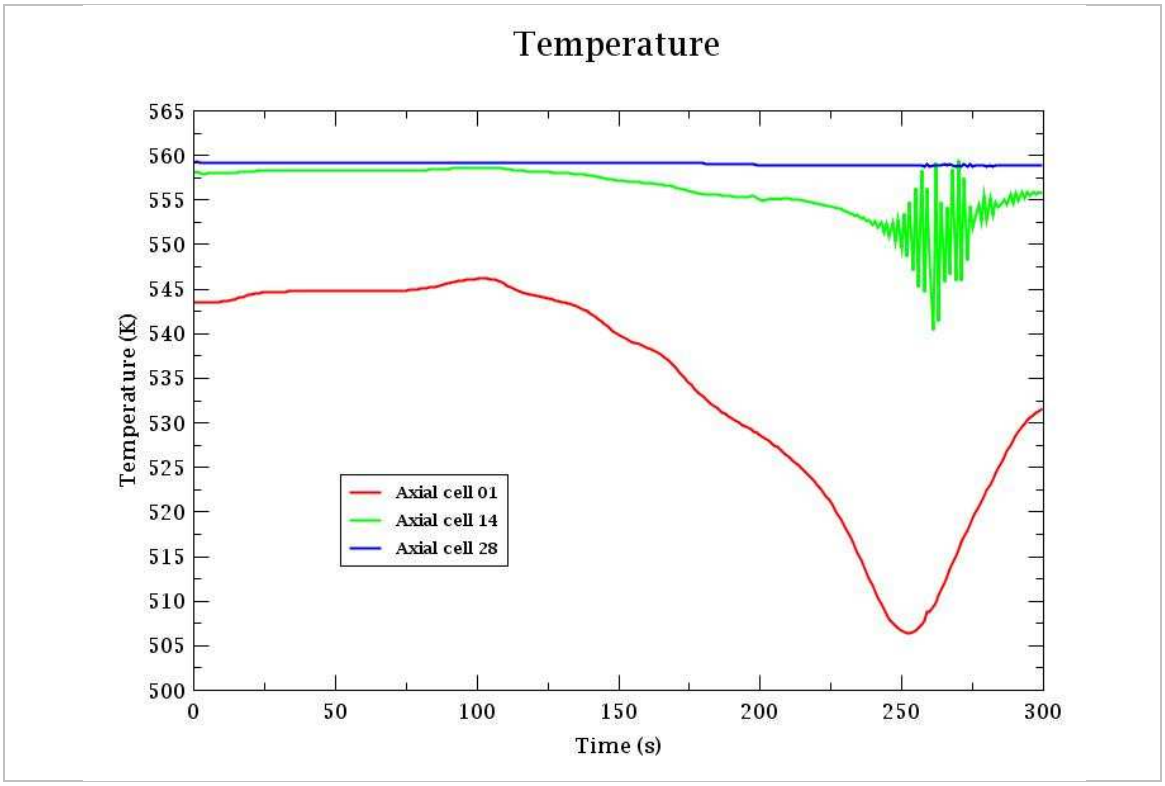

Figure 7-18. Transient. Temperature increase in channel 368 for Case B

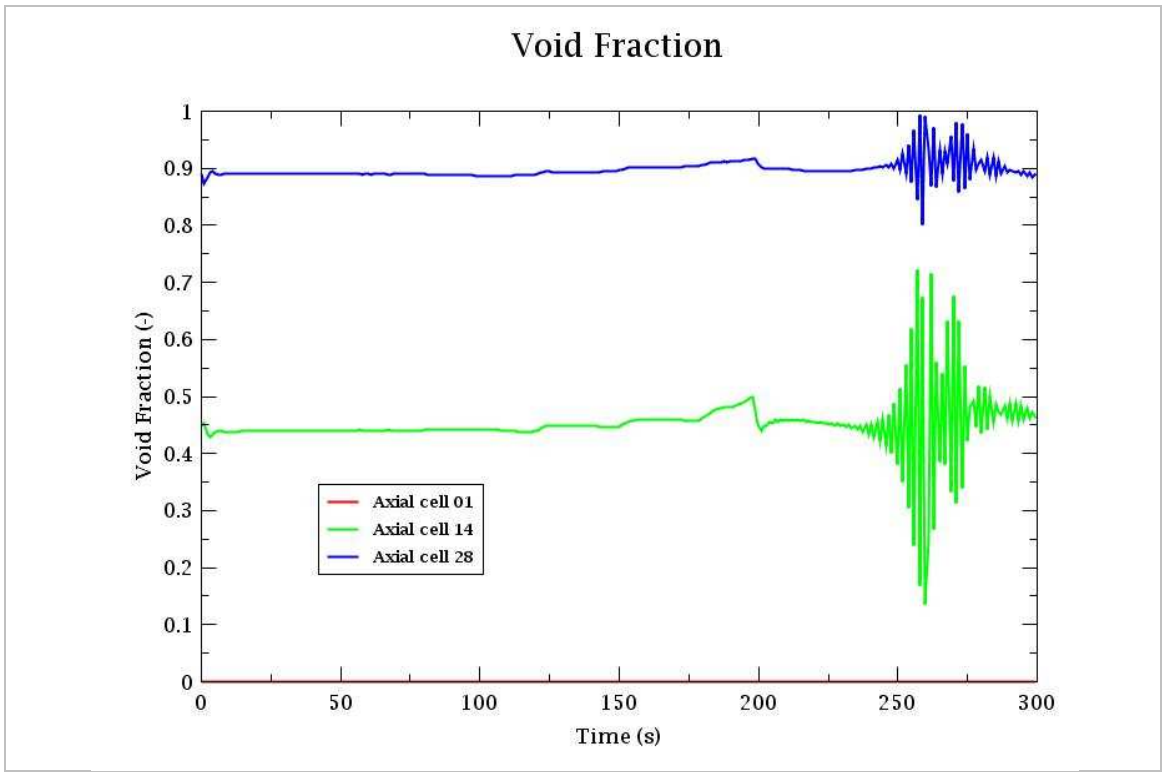

Figure 7-19. Transient. Void fraction in channel 368 for Case B

The relative radial power distribution at simulation time 200 s is shown in Figure 7-20. The fuel assembly with ID 368 is located in the red circle, in coordinates (12,16). This position presented the higher value in the core at that simulation time (right after the partial scram), which was 1.9784.

	1	2	3	4	5	6	7	8	9	10	11	12	13	14	15	16	17	18	19	20	21	22	23
2						0.1976	0.2400	0.2783	0.2860	0.2850	0.2421	0.2160	0.2177	0.2467	0.2722	0.2953	0.2847	0.2472	0.1974				
3					0.2822	0.4169	0.5124	0.5458	0.5735	0.5533	0.4552	0.3758	0.3823	0.4689	0.5545	0.6040	0.5675	0.5255	0.4105	0.2787			
4				0.3081	0.4892	0.8499	1.0334	0.9249	1.1577	1.0680	0.7569	0.5252	0.5103	0.8619	1.0935	1.1684	1.0607	1.0624	0.8385	0.4830	0.3159		
5			0.2459	0.4552	0.8608	1.1523	1.1017	1.3916	1.5399	1.0814	1.1645	0.6488	0.8090	1.1739	1.0494	1.5180	1.1490	1.1000	1.1624	0.8669	0.4552	0.2500	
6		0.1539	0.3336	0.7103	1.0438	1.0220	1.6045	1.5049	1.2661	1.4799	1.3383	1.3311	1.0823	1.2825	1.4615	1.2834	1.5041	1.6143	1.0489	1.0613	0.7174	0.3325	0.1518
7		0.1766	0.3528	0.7446	0.8177	1.4486	1.4852	1.2782	1.3252	1.4687	1.7457	1.3340	1.5694	1.7341	1.2885	1.5722	1.3391	1.5245	1.4799	0.8282	0.7345	0.3586	0.1701
8		0.1869	0.3396	0.4429	0.6470	1.2572	1.2082	1.7273	1.3912	1.4229	1.4783	1.7211	1.5191	1.4719	1.4156	1.4169	1.7538	1.3007	1.2740	0.6853	0.4450	0.3206	0.1805
9		0.2073	0.3852	0.5330	0.7731	1.0826	1.4868	1.3086	1.7921	1.4475	1.4885	1.5210	1.9744	1.7566	1.4428	1.8205	1.3718	1.4926	0.9880	0.7567	0.5064	0.3361	0.1935
10		0.2364	0.4616	0.9289	0.9409	1.3772	1.4153	1.6273	1.2579	1.5053	1.5722	1.7503	1.5569	1.6928	1.6203	1.4820	1.4790	1.4333	1.3644	0.9234	0.8010	0.4405	0.2287
11		0.2685	0.5193	0.9741	1.3288	1.2637	1.7424	1.4006	1.7118	1.6637	1.8953	1.4526	1.6816	1.9106	1.5137	1.4803	1.4292	1.7016	1.2202	1.2443	0.9655	0.5196	0.2560
12		0.2917	0.5896	1.0393	1.4966	1.1665	1.5791	1.4246	1.8917	1.5623	1.6778	0.9835	0.9516	1.4617	1.7461	1.4475	1.3957	1.3157	1.4520	1.1604	1.1152	0.5840	0.2895
13		0.2882	0.5830	1.1148	1.1593	1.4519	1.3153	1.3955	1.4447	1.7481	1.4665	0.9534	0.9835	1.6762	1.5425	1.8916	1.4253	1.5796	1.1671	1.4965	1.0394	0.5901	0.2932
14		0.2544	0.5184	0.9654	1.2445	1.2202	1.7017	1.4295	1.4801	1.5145	1.9133	1.6847	1.4570	1.8983	1.6650	1.7147	1.4028	1.7447	1.2658	1.3273	0.9727	0.5195	0.2697
15		0.2270	0.4377	0.8010	0.9234	1.3651	1.4344	1.4788	1.4778	1.6211	1.6950	1.9004	1.7552	1.5772	1.5298	1.2633	1.6322	1.4203	1.3790	0.9296	0.9270	0.4620	0.2374
16		0.1918	0.3347	0.5060	0.7566	0.9887	1.4931	1.3710	1.8196	1.4423	1.7588	1.9784	1.5284	1.4971	1.4549	1.8014	1.3151	1.4912	1.0842	0.7735	0.5327	0.3846	0.2084
17		0.1781	0.3184	0.4442	0.6850	1.2742	1.2978	1.7526	1.4160	1.4148	1.4733	1.9776	1.7261	1.4847	1.4313	1.4023	1.7337	1.2123	1.2608	0.6489	0.4443	0.3405	0.1879
18		0.1665	0.3503	0.7324	0.8274	1.4789	1.5232	1.3385	1.5722	1.2914	1.7330	1.5709	1.3406	1.7507	1.4727	1.3295	1.2810	1.4888	1.4524	0.8314	0.7484	0.3543	0.1775
19		0.1480	0.3296	0.7157	1.0611	1.0484	1.6134	1.5041	1.2824	1.4594	1.2670	1.0792	1.3331	1.3400	1.4828	1.2684	1.5076	1.6070	1.0231	1.0469	0.7124	0.3364	0.1546
20			0.2480	0.4517	0.8662	1.1626	1.0996	1.1484	1.5161	1.0451	1.1707	0.8075	0.6498	1.1660	1.0827	1.5415	1.3918	1.1024	1.1530	0.8609	0.4577	0.2502	
21				0.3135	0.4823	0.8386	1.0635	1.0612	1.1676	1.0916	0.8597	0.5088	0.5249	0.7579	1.0685	1.1584	0.9251	1.0328	0.8489	0.4911	0.3088		
22					0.2781	0.4162	0.5250	0.5667	0.6022	0.5526	0.4670	0.3807	0.3749	0.4547	0.5526	0.5732	0.5454	0.5124	0.4185	0.2875			
23						0.1990	0.2464	0.2832	0.2932	0.2700	0.2446	0.2158	0.2149	0.2404	0.2796	0.2846	0.2774	0.2390	0.1981				

Maximum Pos. Maximum Value
(12, 16) 1.9784

Figure 7-20. Transient. Relative radial power distribution in the core for Case B

In Figure 7-21, the averaged axial relative power in the core at simulation time 200 s (green curve), presents a different distribution due to the fact that in the lower region, at the inlet

of the core, the feedwater temperature is lower, therefore, there is higher water density and moderation of the neutrons, having as a consequence an increasing in the power. The axial node which presented the higher value was the number 8 with 1.3952. The red curve shows a similar behavior at simulation time 255 s; presenting the higher value again in node 8 with 1.5126.

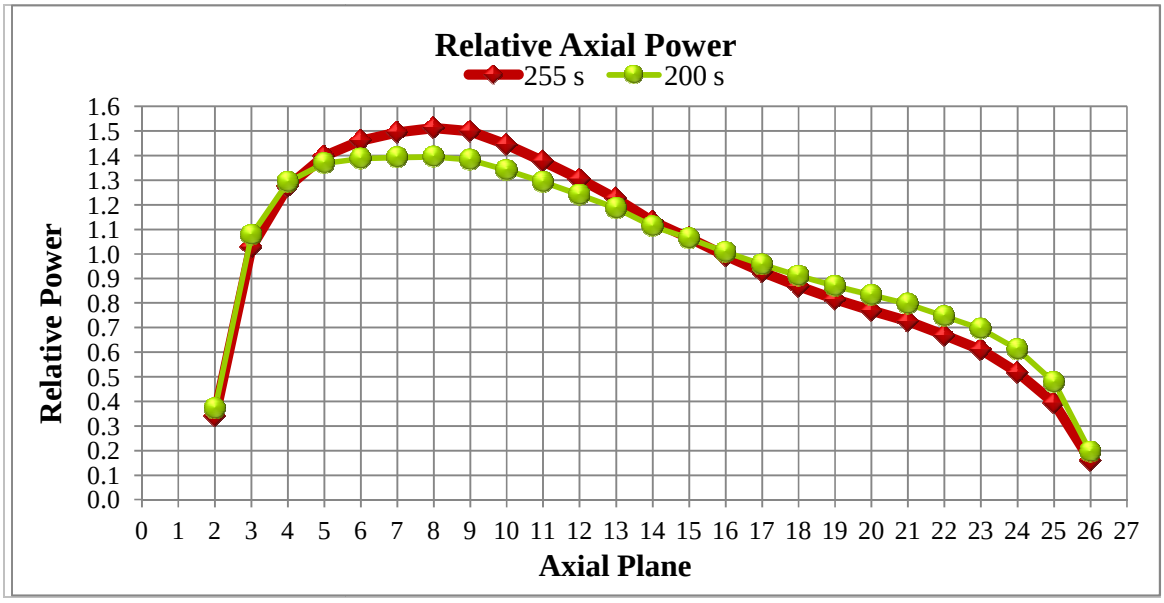

Figure 7-21. Transient. Averaged axial relative power in the core for Case B

The following figures, from 7-22 to 7-27, present the results obtained from the PARCS output at simulation time 200 s, right after the partial scram. The second point of interest considered is at 255 s, when the scram should be performed and where I can assure that the simulation of the transient was performed correctly, just before the strange behavior of the power oscillations observed in the curve of *Case B*. The figures are presented in both 2D and 3D ways for a better appreciation, each one with the respective color map on the right side

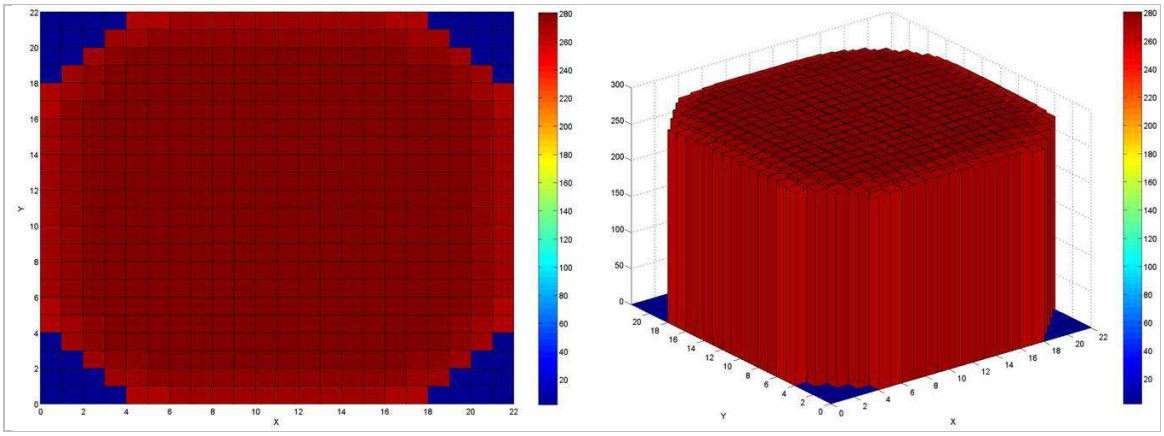

Figure 7-22. Assemblywise Moderator Temperature Distribution at 200 s

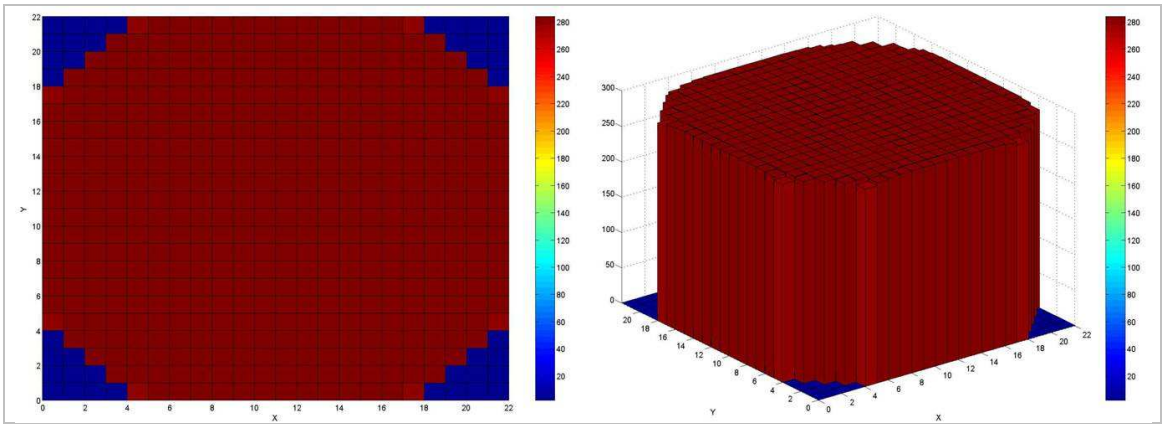

Figure 7-23. Assemblywise Moderator Outlet Temperature Distribution at 200 s

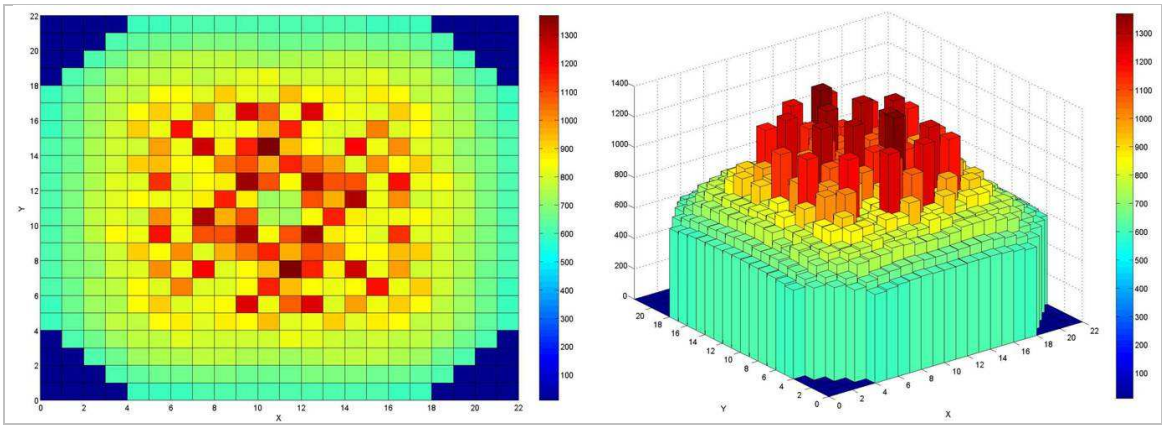

Figure 7-24. Assemblywise Fuel Temperature Distribution at 200 s

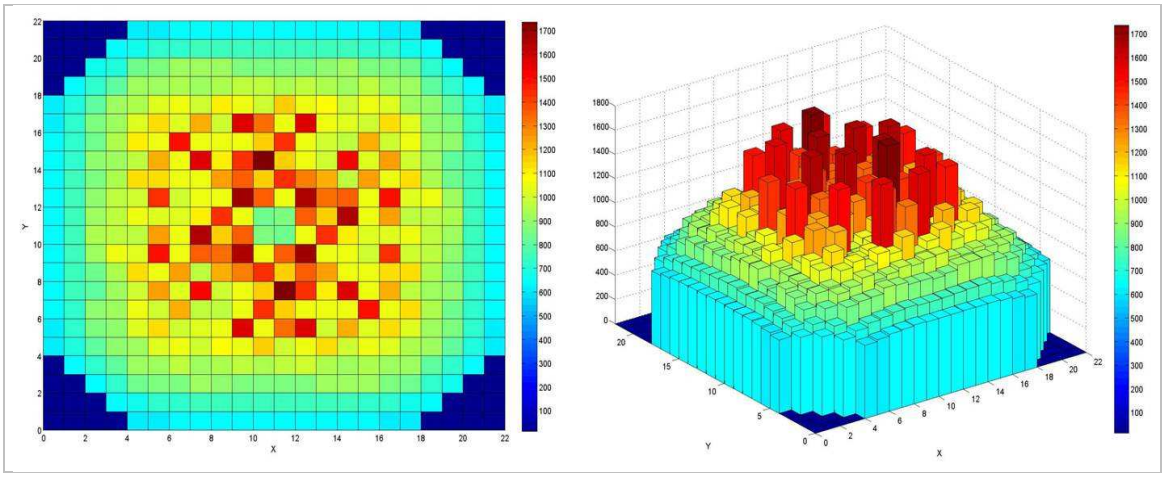

Figure 7-25. Assemblywise Averaged Fuel Centerline Temperature at 200 s

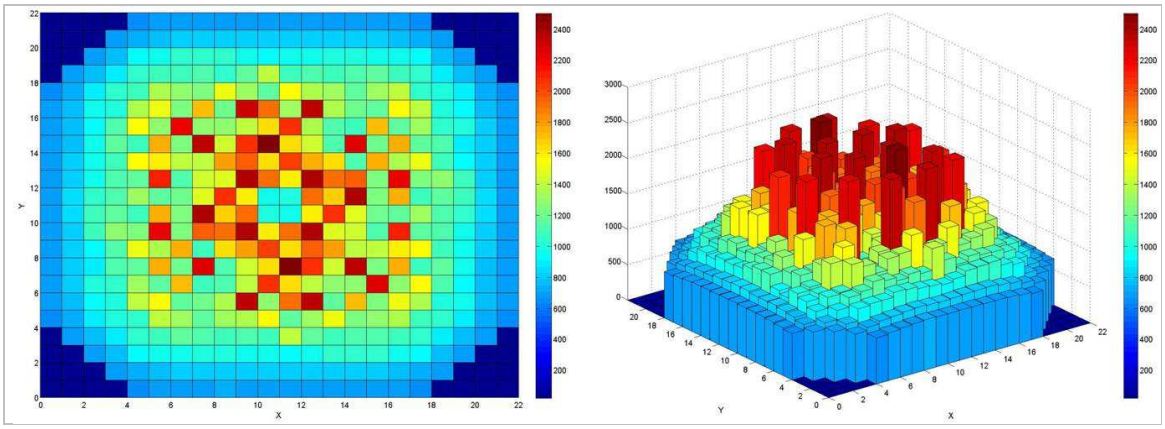

Figure 7-26. Assemblywise Maximum Fuel Centerline Temperature at 200 s

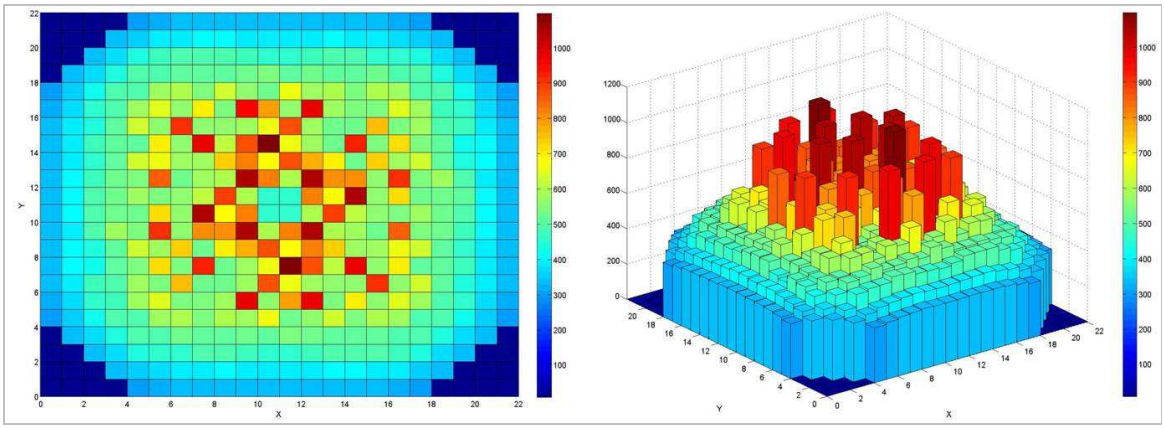

Figure 7-27. Assemblywise Doppler Temperature Distribution at 200 s

Now, the assemblywise temperatures at 255 s are presented from Figures 7-28 to 7-33.

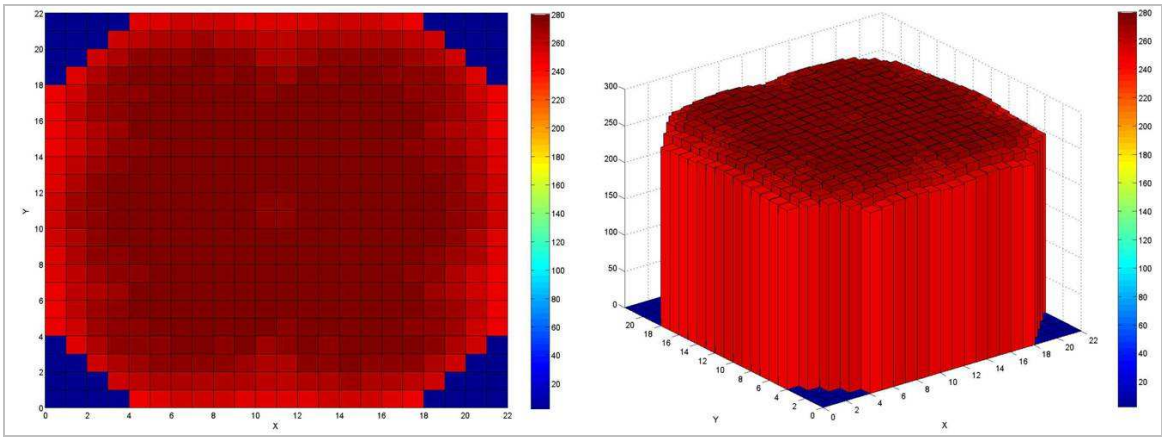

Figure 7-28. Assemblywise Moderator Temperature Distribution at 255 s

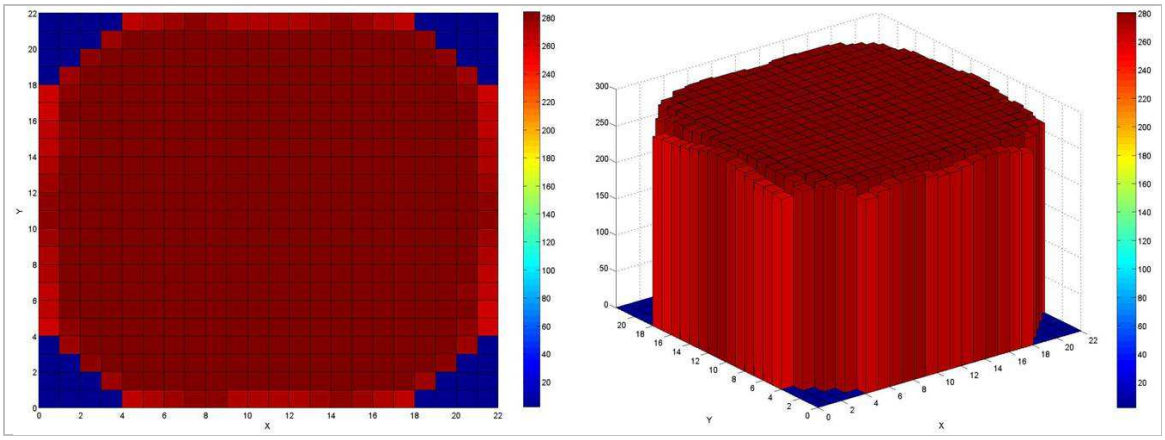

Figure 7-29. Assemblywise Moderator Outlet Temperature Distribution at 255 s

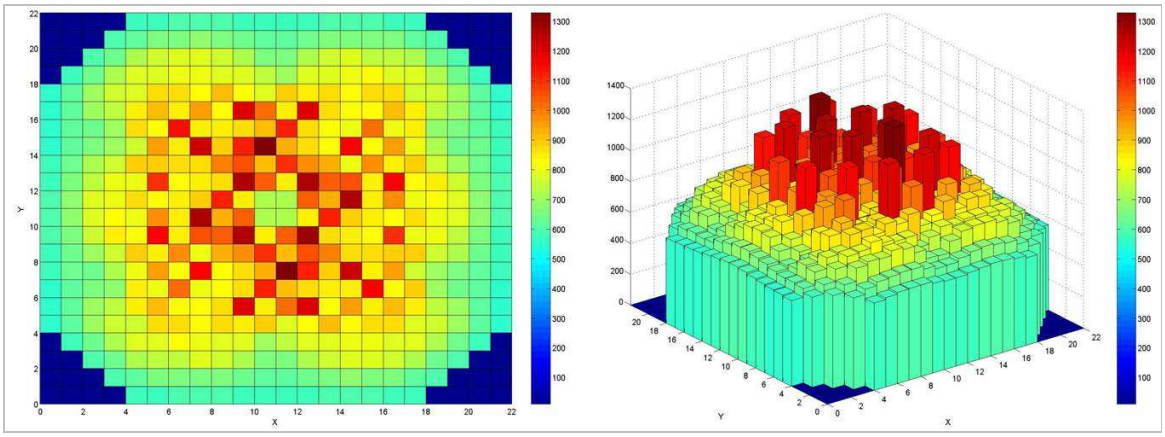

Figure 7-30. Assemblywise Fuel Temperature Distribution at 255 s

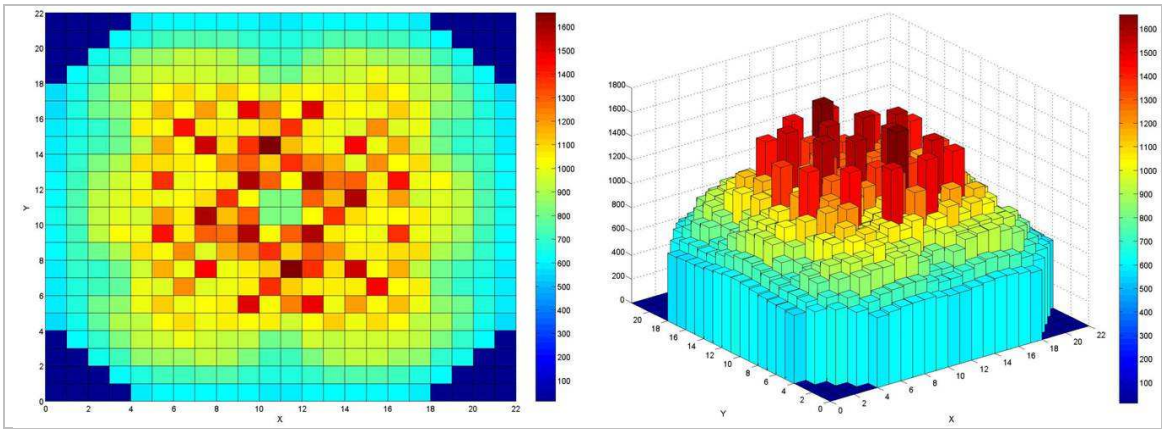

Figure 7-31. Assemblywise Averaged Fuel Centerline Temperature at 255 s

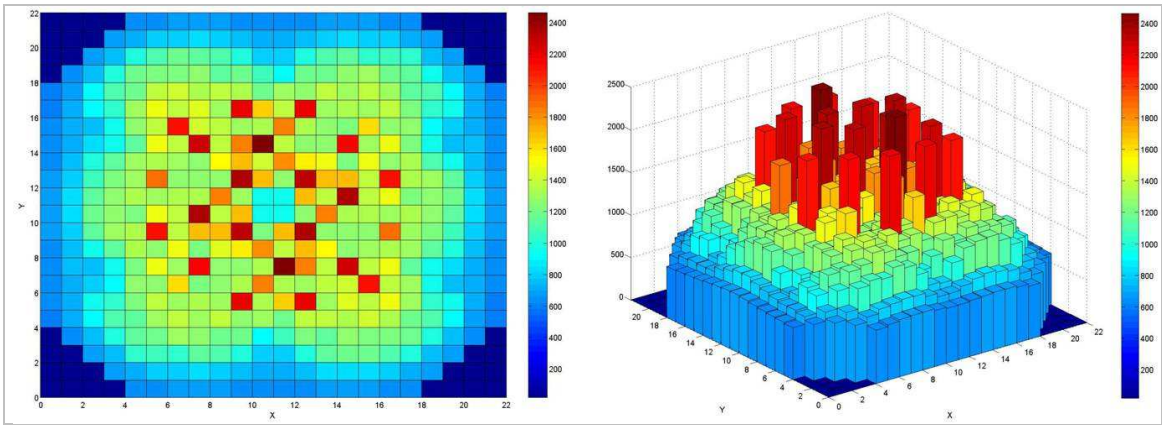

Figure 7-32. Assemblywise Maximum Fuel Centerline Temperature at 255 s

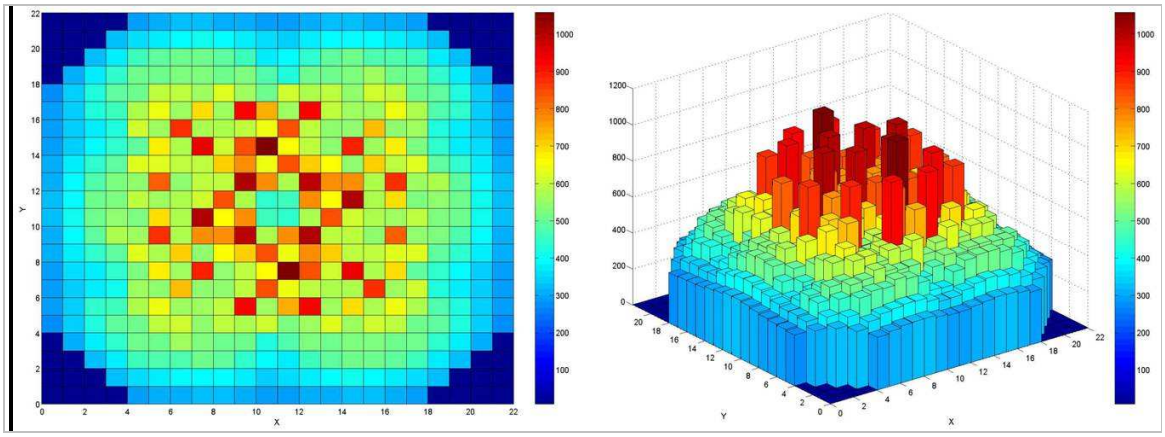

Figure 7-33. Assemblywise Doppler Temperature Distribution at 255 s

The summary of the last figures, from 7-22 to 7-33, is presented in Table 7-1 and 7-2.

Table 7-1. Temperatures in the core for Case B at 200 s

	At simulation time 200 s			
	Location	**FA ID**	**FA Type**	**Max. Value [°C]**
Assemblywise Moderator Temp. Dist.	12,16	368	KWU 9x9-9B	282.72
Assemblywise Moderator Outlet Temp. Dist.	17,13	429	SVEA 64 Central	286.12
Assemblywise Fuel Temperature Dist.	13,9	146	KWU 9x9-9B	1378.63
Assemblywise Averaged Fuel Centerline Temp.				1748.40
Assemblywise Maximum Fuel Centerline Temp.				2518.70
Assemblywise Doppler Temp. Dist.				1105.48

Table 7-2. Temperatures in the core for Case B at 255 s

	At simulation time 255 s			
	Location	**FA ID**	**FA Type**	**Max. Value [°C]**
Assemblywise Moderator Temp. Dist.	14,14	410	KWU 9x9-9B	279.13
Assemblywise Moderator Outlet Temp. Dist.	17,12	216	SVEA 64 Central	286.06
Assemblywise Fuel Temp. Dist.	13,9	146	KWU 9x9-9B	1338.20
Assemblywise Averaged Fuel Centerline Temp.				1671.40
Assemblywise Maximum Fuel Centerline Temp.				2479.80
Assemblywise Doppler Temp. Dist.				1065.05

Figure 7-34 shows the relative radial power distribution of *Case B.* These values were taken from PARCS output at simulation time 200 s.

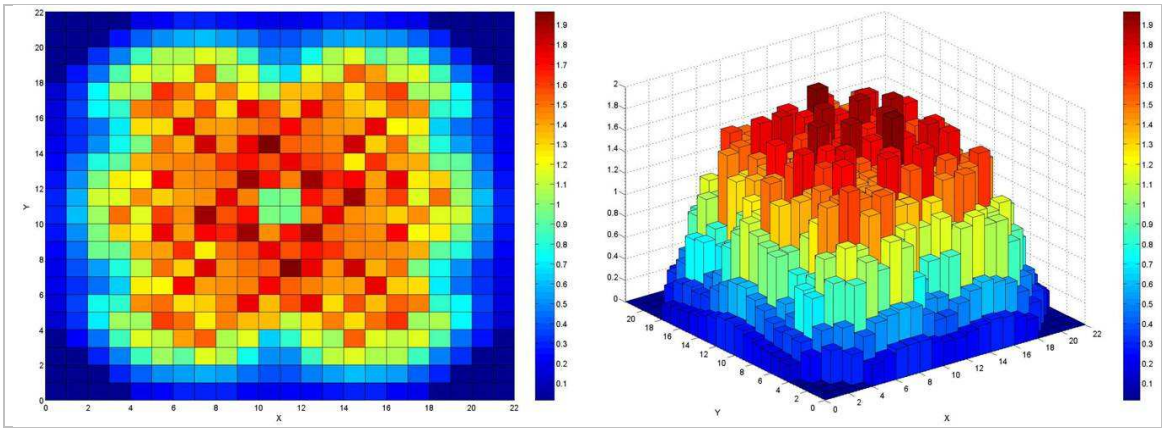

Figure 7-34. Transient. Relative Radial Power Distribution for Case B at 200 s

Figure 7-35 shows the relative difference in power between both C*ase A* and *Case B* in percentage at simulation time 200 s. It was obtained considering as reference the results of Case A.

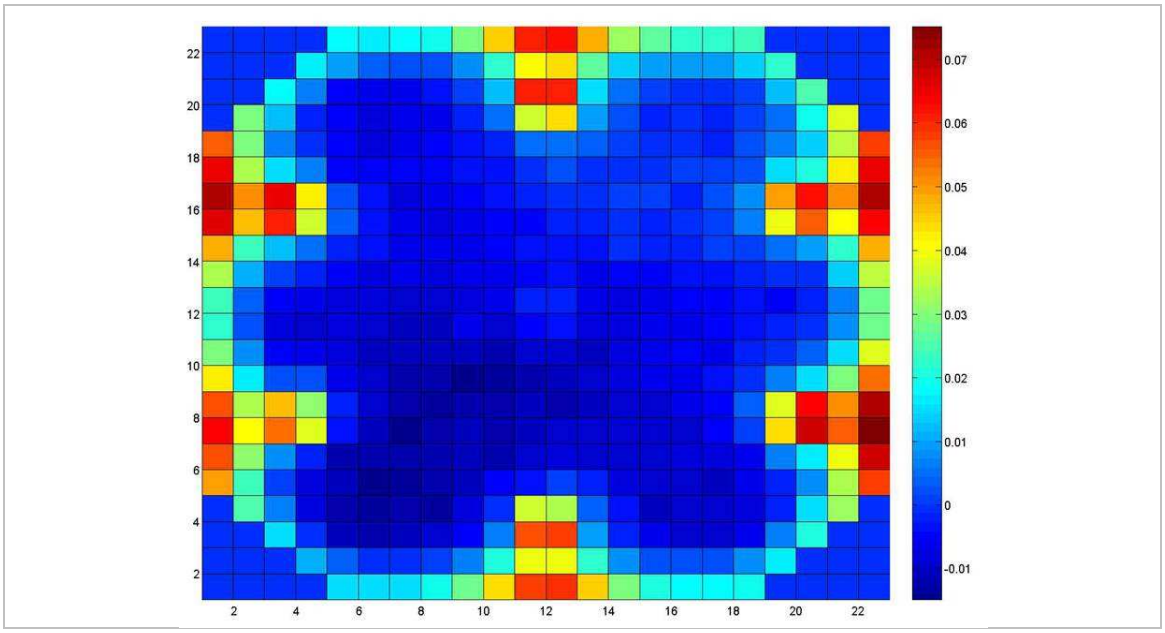

Figure 7-35. Difference in Radial Power Distribution between Case A and B at 200 s

Figure 7-36 shows the relative radial power distribution of *Case B.* These values were taken from PARCS output at simulation time 255 s.

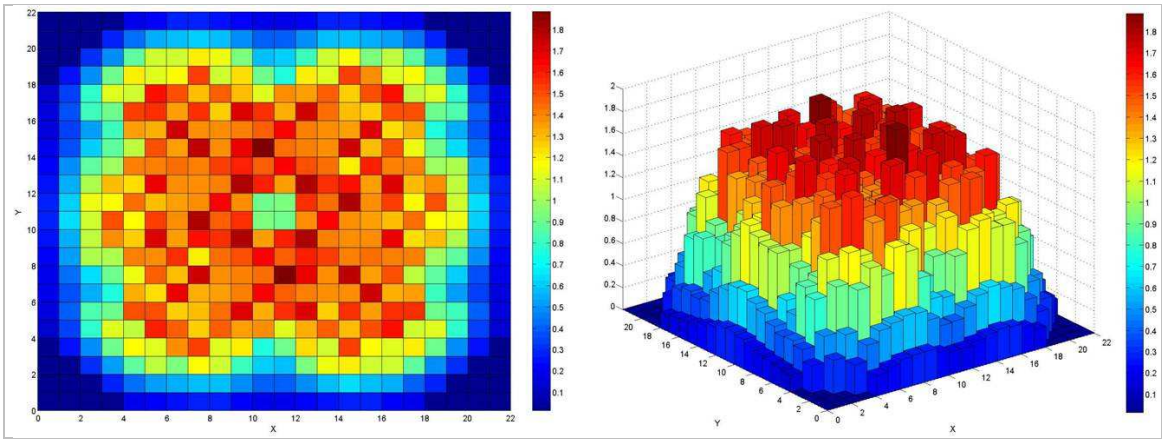

Figure 7-36. Transient. Relative Radial Power Distribution for Case B at 255 s

Figure 7-37 shows the relative difference in power between both C*ase A* and *Case B* in percentage at simulation time 255 s.

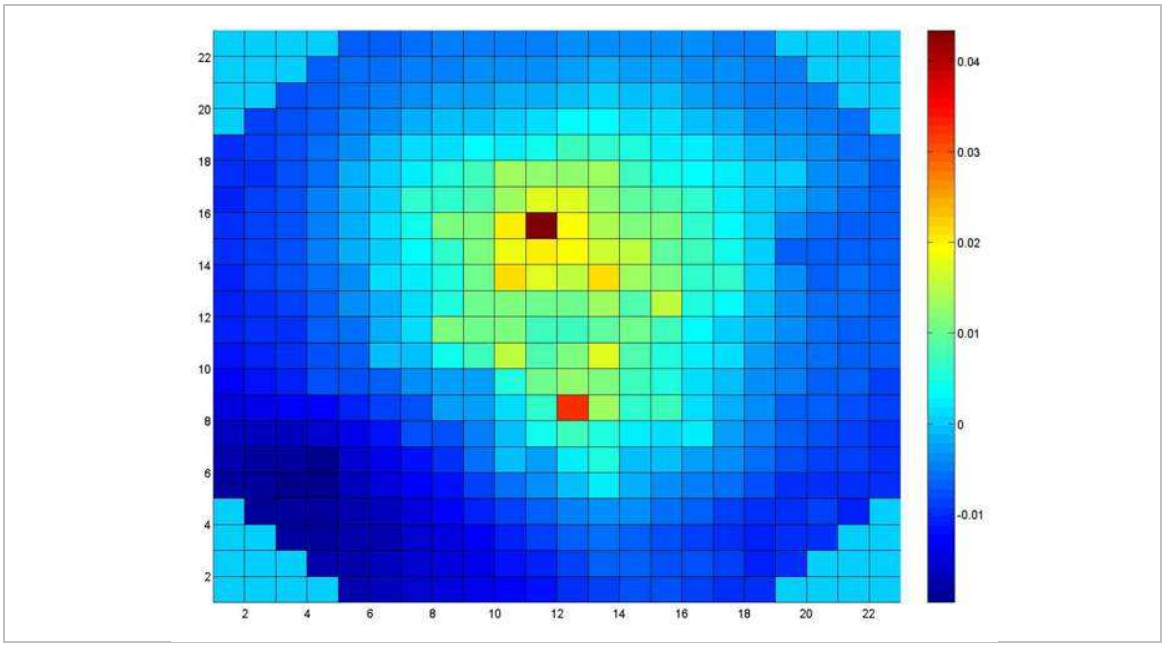

Figure 7-37. Difference in Radial Power Distribution between Case A and B at 255 s

7.3 Computational Time

The summary of the calculation time for the standalone, steady-state and transient simulations for the respective *Case A* and *B* are presented in Table 7-1. It is shown, as it was expected, that the execution time is increased in *Case B* due to the detailed model.

All the executions were performed having a "limited" output for TRACE. For PARCS the output options selected were planar power distribution, assemblywise power distribution, TH state variables, point kinetics data and radial power shape.

Table 7-3. Summary of calculation time for Case A and Case B

Case A				
input	**converged at problem time (s)**	**time steps**	**cpu time (minutes)**	**Method**
SA	247.376	15905	325.78	SETS
SS	137.34	1695	50.45	SETS
TR	NA	11289	488.38	Semi-Implicit

Case B				
input	**converged at problem time (s)**	**time steps**	**cpu time (minutes)**	**Method**
SA	358.278	17170	734.32	SETS
SS	300.0	3122	181.05	SETS
TR	NA	11330	944.18	Semi-Implicit

When performing the steady-state simulation for Case B, the convergence was not obtained explicitly in the TRACE output file, this because the oscillations of the evaluated parameters around the convergence criteria never were below the value set, but they were very close. In fact, a test was performed extending the simulation time in order to try to obtain the convergence but after 900 s it did not converged. For this reason, the comparison of some parameters was made, as shown in figures 7-8 to 7-14, to ensure that the parameters were simulated correctly. The likeness in the graphics only means that similar input parameters were used in the two cases.

8 Conclusions and Future Work

A TRACE model of the nuclear power plant Oskarshamn-2 was analysed and evaluated to perform a stability analysis by using the TRACE/PARCS coupled code system simulations.

After the standalone calculation, selected parameters were compared with the reference values defined in the benchmark to decide if the provided model agrees in good way with the reference. For the TRACE/PARCS coupled steady-state execution, the parameters were also evaluated to define the operating conditions of the plant before the transient.

An extension of the original model with 222 channels was done adding the missing 222 channels in *Case B* in order to have a one-to-one model.

According to the results showed in the graphics presented in the previous sections for standalone and steady-state simulation, the behaviour of the selected parameters for the both scenarios, *Case A* and *Case B,* agrees in a good manner. For the radial distribution of the power, the maximum relative error in the core is 0.6% in the outer positions; meanwhile for the axial power the two curves fit very well.

After the steady-state simulation for *Case B* the solution did not converged; it was observed that the evaluated parameters were oscillating around the convergence criteria. This is one of the reasons to compare the selected parameters showed in the figures presented in the previous sections 7.1 and 7.2, to observe if there are undesirable behaviours or significant changes in the selected parameters.

According to these figures, despite steady-state for *Case B* did not converged, the comparison shows good agreement with the reference *Case A,* but it could be the cause of the peak and the over prediction of the power showed in the beginning of the transient simulation.

During the simulation of the transient event, it was found in the PARCS output that the scram is not being performed. The value set to insert the control blades is at 120% but it was observed that after getting this point, the position of the banks is totally withdrawn. The power continues increasing and the control rods were not inserted during the whole simulation.

The power during the simulation of the transient agrees on time with the different events. After 257 s of the transient simulation, the power shows a different behavior compared to reference measured with the APRM. This should be corrected in further works.

For future simulations it is necessary to review the trip controller to simulate the scram and compare the parameters to observe the behaviour of the power, if it matches to the reference, and to clarify if the addition of the 222 channels (as it was performed in *Case B* in this work), really represents an improvement and a better precision in the results.

Since the coupling of TRACE and PARCS is currently being validated for BWR stability, the results obtained allow to define new objectives for future work including the coupling of TRACE/PARCS, putting special attention in the programming area, which will also help for the correct verification and validation of the codes used.

A source code analysis should be performed, in particular because during the preliminary simulations of the transient, an error was sent at simulation time 254 s, indicating that the value of void fraction was greater than 1, situation that would mean to have only steam in the core. Due to this message, the execution stopped without finishing the calculations until the end of the time simulation.

To continue with the simulation, the advice of the supervisor was to edit the source file of the TRACE code to permit the simulation to continue. For this, the instruction registering the thresholds of the allowed values of void fraction was modified. With this change, it was possible to continue with the simulation indeed but, after that point, the oscillations do not correspond to the correct reproduction of the transient event.

References

[1] Kozlowski, T., Sean, R., Lefvert, T., Netterbrant, C., Downar, T., Xu, Y., et. al. *BWR Stability Event Benchmark based on Oskarshamn-2 1999 Feedwater Transient.* Last Update: September 22, 2011.

[2] Downar, T., Xu, Y., Seker, V. *User Manual for the PARCS Neutronics Core Simulator*. School of Nuclear Engineering, Purdue University, W. Lafayette, Indiana. November 2006.

[3] *TRACE V5.435 User's Manual. Volume 1: Input Specification.* Division of Safety Analysis Office of Nuclear Regulatory Research, U. S. Nuclear Regulatory Commission. Washington, DC.

[4] Applied Programming Technology, Inc. *Symbolic Nuclear Analysis Package (SNAP), User's Manual.* February 2011.

[5] Applied Programming Technology, Inc. *AptPlot*.

[6] The RELAP5 Code Development Team. *RELAP5 Code Manual Volume I. Code Structure, System Models, and Solution Methods.* Idaho National Engineering and Environmental Laboratory. Idaho Falls, Idaho.

[7] Lerchl, G., Austregesilo, H. *The ATHLET Code Documentation Package*. Gesellschaft für Anlagen und Reaktorsicherheit (GRS-P-1) mbH Vol.1 User's Manual. Germany. October, 1995.

[8] Grundmann, U., Mittag, S., Rohde, U. *DYN3D – Three Dimensional Core Model for Steady-State and Transient Analysis of Thermal Reactors.* 1996.

[9] Farvaque, M. *User's Manual of CATHARE 2 – version V1.3E*. CEA, CENG, STR/LML/EM/91-61, November 1991.

[10] Lautard, J.J., Loubière, S., Fedon-Magnaud, C. CRONOS2 A Modular Computational System for Neutronic Core Calculations. Spec. IAEA Meeting. Cadarache, France. September, 1990.

[11] Francesca, M. *Contributions to Study Instability in BWR: Application to Peach Bottom-2 NPP*. University of Pisa, Italy. 2004.

[12] François, J.L. *Class Notes from Nuclear Reactors Analysis, section 4.3 - Fuel Temperature Coefficient (Doppler Coefficient)*. p.23-26. School Year 2011-2.

[13] Nam, D. *Nuclear Power Safety: Basic Principles and Modern Issues*. Guest Lecture for "Nuclear Reactor Physics" Course at Royal Institute of technology (KTH) – Stockholm.

[14] Lombardi, A., Petruzzi, A., D'Auria, F., Ambrosini, W. Hindawi. *Analyses of Instability Events in the Peach Bottom-2 BWR Using Thermal-Hydraulic and 3D Neutron Kinetic Coupled Codes Technique*. Publishing Corporation. Science and Technology of Nuclear Installations. Volume 2008, Article ID 423175.

[15] Magedanz, J. *Development of Model of Oskarshamn-2 Reactor for Assesment of TRACE/PARCS for Boiling Water Reactor Stability Analysis*. MSc Thesis in Nuclear Engineering. The Pennsylvania State University, The Graduate School, College of Engineering. May 2010.

[16] Xu, Y., Downar, T., Walls, R., Ivanov, K., Staudenmeier, J., March-Leuba, J. *Application of TRACE/PARCS to BWR stability analysis*, Annals of Nuclear Energy, Volume 36, Issue 3, *PHYSOR 2008*.

[17] Xu, Y., Downar, T., Ivanov, K., Vedovi, J., Petruzzi, A., Staudenmeier, J., 2005b. *Analysis of the OECD/NEA Ringhalls instability benchmark with TRACE/PARCS*. ANS Mathematics and Computation Meeting, Avignon, France.

[18] Lefvert, T. *Ringhals-1 Stability Benchmark*. Final Report. NEA/NSC/DOC (96)22. Paris, France, 1996.

[19] Wysocki, A. *Oskarshamn-II Stability Analysis with TRACE/PARCS*. University of Michigan, August 31, 2010.

[20] "RAMONA5-FA: A Computer Program for BWR Transient Analysis in the Time Domain" Volume 1, User's Manual" March 2006.

[21] Ivanov, K., Beam, T., Baratta, A. "Pressurised Water Reactor Main Steam Line Break (MSLB) Benchmark", Volume I: Final Specifications. Nuclear Engineering Program. The Pennsylvania State University. April 1999.

[22] Solis, J., Ivanov, K., Sarikaya, B. "Boiling Water Reactor Turbine Trip (TT) Benchmark - Volume I: Final Specifications". Nuclear Engineering Program. The Pennsylvania State University. February 2001.

[23] Ivanov, B., Ivanov, K. "VVER-1000 Coolant Transient Benchmark. PHASE 1 (V1000CT-1) Vol. I: Main Coolant Pump (MCP) switching On - Final Specifications". 2002.

[24] *Neutronics / Thermal-Hydraulics Coupling in LWR Technology*, Vol. 1. CRISSUE-S – WP1: Data Requirements and Databases Needed for Transient Simulations and Qualification. Nuclear Energy Agency. OECD 2004.

[25] http://www.okg.se/templates/Page____939.aspx

[26] Ivanov, K. *TRACE/PARCS Validation for BWR Stability Based on OECD/NEA Oskarshamn-2 Benchmark.* Seminar on Applications of the nonlinear dynamics in the nuclear reactor stability analysis. INR, KIT. October 6, 2011.

[27] European Comission. *Main Characteristics of Nuclear Power Plants in the European Union and Candidate Countries*. EUR 20056. October 2001.

[28] Xu, Y., Downar, T. *GenPMAXS. Code for Generating the PARCS Cross Section Interface File PMAXS.* School of Nuclear Engineering, Purdue University. November 2006.

[29] Borkowski, J., et al., 1996. SIMULATE-3K simulation of the Ringhals 1 BWR stability measurements. PHYSOR96, Mito, Japan.

[30] Downar, T., Xu, Y., Seker, V. *PARCS v3.0 U.S. NRC Core Neutronics Simulator Theory Manual.* Department of Nuclear Engineering and Radiological Sciences. University of Michigan.

Annex A

Table A-1. ID and channel type in TRACE Model

1 and 223	SVEA 64 Peripheral	42 and 264	KWU 9x9-9A	83 and 305	SVEA 64 Central
2 and 224	SVEA 64 Peripheral	43 and 265	KWU 9x9-9A	84 and 306	KWU 9x9-9B
3 and 225	SVEA 64 Peripheral	44 and 266	SVEA 64 Central	85 and 307	ATRIUM 10
4 and 226	SVEA 64 Peripheral	45 and 267	KWU 9x9-9A	86 and 308	SVEA 64 Central
5 and 227	SVEA 64 Peripheral	46 and 268	SVEA 64 Central	87 and 309	KWU 9x9-9A
6 and 228	SVEA 64 Peripheral	47 and 269	SVEA 64 Semi-Peripheral	88 and 310	KWU 9x9-9A
7 and 229	SVEA 64 Peripheral	48 and 270	SVEA 64 Peripheral	89 and 311	SVEA 64 Semi-Peripheral
8 and 230	SVEA 64 Peripheral	49 and 271	SVEA 64 Peripheral	90 and 312	SVEA 64 Peripheral
9 and 231	SVEA 64 Peripheral	50 and 272	SVEA 64 Semi-Peripheral	91 and 313	SVEA 64 Peripheral
10 and 232	SVEA 64 Peripheral	51 and 273	KWU 9x9-9A	92 and 314	SVEA 64 Semi-Peripheral
11 and 233	SVEA 64 Peripheral	52 and 274	KWU 9x9-9A	93 and 315	KWU 9x9-9A
12 and 234	SVEA 64 Peripheral	53 and 275	SVEA 64 Central	94 and 316	SVEA 64 Central
13 and 235	SVEA 64 Peripheral	54 and 276	KWU 9x9-9B	95 and 317	ATRIUM 10
14 and 236	SVEA 64 Peripheral	55 and 277	ATRIUM 10	96 and 318	KWU 9x9-9B
15 and 237	SVEA 64 Peripheral	56 and 278	SVEA 64 Central	97 and 319	SVEA 64 Central
16 and 238	SVEA 64 Semi-Peripheral	57 and 279	KWU 9x9-9B	98 and 320	SVEA 64 Central
17 and 239	SVEA 64 Semi-Peripheral	58 and 280	SVEA 64 Central	99 and 321	KWU 9x9-9A
18 and 240	SVEA 64 Semi-Peripheral	59 and 281	ATRIUM 10	100 and 322	KWU 9x9-9B
19 and 241	SVEA 64 Semi-Peripheral	60 and 282	KWU 9x9-9B	101 and 323	SVEA 64 Central
20 and 242	SVEA 64 Semi-Peripheral	61 and 283	SVEA 64 Central	102 and 324	KWU 9x9-9B
21 and 243	SVEA 64 Semi-Peripheral	62 and 284	ATRIUM 10	103 and 325	KWU 9x9-9B
22 and 244	SVEA 64 Semi-Peripheral	63 and 285	SVEA 64 Central	104 and 326	SVEA 64 Central
23 and 245	SVEA 64 Semi-Peripheral	64 and 286	SVEA 64 Central	105 and 327	KWU 9x9-9A
24 and 246	SVEA 64 Semi-Peripheral	65 and 287	KWU 9x9-9A	106 and 328	SVEA 64 Central
25 and 247	SVEA 64 Semi-Peripheral	66 and 288	KWU 9x9-9A	107 and 329	KWU 9x9-9B
26 and 248	SVEA 64 Semi-Peripheral	67 and 289	SVEA 64 Semi-Peripheral	108 and 330	ATRIUM 10
27 and 249	SVEA 64 Semi-Peripheral	68 and 290	SVEA 64 Peripheral	109 and 331	SVEA 64 Central
28 and 250	SVEA 64 Semi-Peripheral	69 and 291	SVEA 64 Peripheral	110 and 332	KWU 9x9-9B
29 and 251	SVEA 64 Semi-Peripheral	70 and 292	SVEA 64 Semi-Peripheral	111 and 333	SVEA 64 Semi-Peripheral
30 and 252	SVEA 64 Peripheral	71 and 293	KWU 9x9-9A	112 and 334	SVEA 64 Peripheral
31 and 253	SVEA 64 Peripheral	72 and 294	KWU 9x9-9A	113 and 335	SVEA 64 Peripheral
32 and 254	SVEA 64 Semi-Peripheral	73 and 295	SVEA 64 Central	114 and 336	SVEA 64 Semi-Peripheral
33 and 255	SVEA 64 Central	74 and 296	ATRIUM 10	115 and 337	SVEA 64 Central
34 and 256	KWU 9x9-9B	75 and 297	KWU 9x9-9A	116 and 338	KWU 9x9-9A
35 and 257	SVEA 64 Central	76 and 298	SVEA 64 Central	117 and 339	KWU 9x9-9B
36 and 258	KWU 9x9-9A	77 and 299	KWU 9x9-9B	118 and 340	SVEA 64 Central
37 and 259	KWU 9x9-9A	78 and 300	KWU 9x9-9A	119 and 341	ATRIUM 10
38 and 260	SVEA 64 Central	79 and 301	KWU 9x9-9B	120 and 342	KWU 9x9-9A
39 and 261	KWU 9x9-9A	80 and 302	SVEA 64 Central	121 and 343	KWU 9x9-9A
40 and 262	KWU 9x9-9A	81 and 303	SVEA 64 Central	122 and 344	KWU 9x9-9A
41 and 263	KWU 9x9-9A	82 and 304	KWU 9x9-9B	123 and 345	KWU 9x9-9A

Table A-1. ID and channel type in TRACE Model (cont.)

124 and 346	KWU 9x9-9A
125 and 347	KWU 9x9-9A
126 and 348	SVEA 64 Central
127 and 349	SVEA 64 Central
128 and 350	KWU 9x9-9B
129 and 351	SVEA 64 Central
130 and 352	KWU 9x9-9A
131 and 353	KWU 9x9-9B
132 and 354	KWU 9x9-9A
133 and 355	SVEA 64 Semi-Peripheral
134 and 356	SVEA 64 Peripheral
135 and 357	SVEA 64 Peripheral
136 and 358	SVEA 64 Semi-Peripheral
137 and 359	GE 12
138 and 360	ATRIUM 10
139 and 361	SVEA 64 Central
140 and 362	KWU 9x9-9B
141 and 363	SVEA 64 Central
142 and 364	KWU 9x9-9B
143 and 365	KWU 9x9-9A
144 and 366	KWU 9x9-9A
145 and 367	KWU 9x9-9A
146 and 368	KWU 9x9-9B
147 and 369	KWU 9x9-9B
148 and 370	SVEA 64 Central
149 and 371	KWU 9x9-9B
150 and 372	SVEA 64 Central
151 and 373	KWU 9x9-9B
152 and 374	SVEA 64 Central
153 and 375	ATRIUM 10
154 and 376	KWU 9x9-9A
155 and 377	SVEA 64 Semi-Peripheral
156 and 378	SVEA 64 Peripheral
157 and 379	SVEA 64 Peripheral
158 and 380	SVEA 64 Semi-Peripheral
159 and 381	GE 12
160 and 382	SVEA 64 Central
161 and 383	KWU 9x9-9B
162 and 384	KWU 9x9-9A
163 and 385	KWU 9x9-9B
164 and 386	SVEA 64 Central
165 and 387	SVEA 64 Central
166 and 388	SVEA 64 Central
167 and 389	KWU 9x9-9B
168 and 390	KWU 9x9-9A
169 and 391	KWU 9x9-9A
170 and 392	KWU 9x9-9A
171 and 393	KWU 9x9-9A
172 and 394	KWU 9x9-9A
173 and 395	KWU 9x9-9A
174 and 396	KWU 9x9-9A
175 and 397	SVEA 64 Central
176 and 398	KWU 9x9-9A
177 and 399	SVEA 64 Semi-Peripheral
178 and 400	SVEA 64 Peripheral
179 and 401	SVEA 64 Peripheral
180 and 402	SVEA 64 Semi-Peripheral
181 and 403	SVEA 64 Central
182 and 404	KWU 9x9-9A
183 and 405	SVEA 64 Central
184 and 406	KWU 9x9-9B
185 and 407	SVEA 64 Central
186 and 408	KWU 9x9-9B
187 and 409	KWU 9x9-9A
188 and 410	KWU 9x9-9B
189 and 411	KWU 9x9-9A
190 and 412	KWU 9x9-9A
191 and 413	KWU 9x9-9B
192 and 414	KWU 9x9-9B
193 and 415	KWU 9x9-9A
194 and 416	KWU 9x9-9A
195 and 417	KWU 9x9-9B
196 and 418	SVEA 64 Central
197 and 419	KWU 9x9-9B
198 and 420	KWU 9x9-9A
199 and 421	SVEA 64 Semi-Peripheral
200 and 422	SVEA 64 Peripheral
201 and 423	SVEA 64 Peripheral
202 and 424	SVEA 64 Semi-Peripheral
203 and 425	SVEA 64 Central
204 and 426	ATRIUM 10
205 and 427	SVEA 64 Central
206 and 428	KWU 9x9-9B
207 and 429	SVEA 64 Central
208 and 430	KWU 9x9-9B
209 and 431	KWU 9x9-9B
210 and 432	KWU 9x9-9A
211 and 433	KWU 9x9-9A
212 and 434	KWU 9x9-9A
213 and 435	KWU 9x9-9A
214 and 436	KWU 9x9-9A
215 and 437	SVEA 64 Central
216 and 438	SVEA 64 Central
217 and 439	SVEA 64 Central
218 and 440	KWU 9x9-9B
219 and 441	SVEA 64 Central
220 and 442	KWU 9x9-9A
221 and 443	SVEA 64 Semi-Peripheral
222 and 444	SVEA 64 Peripheral